

Dissertation zur Erlangung des Doktorgrades
der Fakultät für Chemie und Pharmazie
der Ludwig-Maximilians-Universität München

**Structural biochemistry of the INO80 chromatin
remodeler reveals an unexpected function
of its two subunits Arp4 and Arp8**



Sebastian Fenn
aus
Fürth in Bayern

2011

Erklärung

Diese Dissertation wurde im Sinne von § 13 Abs. 3 bzw. 4 der Promotionsordnung vom 29. Januar 1998 (in der Fassung der vierten Änderungssatzung vom 26. November 2004) von Herrn Prof. Dr. Karl-Peter Hopfner betreut.

Ehrenwörtliche Versicherung

Diese Dissertation wurde selbständig, ohne unerlaubte Hilfe erarbeitet.

München, den 15.04.2011

.....

Sebastian Fenn

Dissertation eingereicht am 15.04.2011

1. Gutachter: Herr Prof. Dr. Karl-Peter Hopfner
2. Gutachter: Herr Prof. Dr. Roland Beckmann

Mündliche Prüfung am 06.06.2011

This thesis has been prepared from April 2007 to April 2011 in the laboratory of Prof. Dr. Karl-Peter Hopfner at the Gene Center of the Ludwig-Maximilians-University of Munich (LMU).

Parts of this thesis have been published:

Fenn S, Breitsprecher D, Gerhold CB, Witte G, Faix J, Hopfner KP (2011): Structural biochemistry of nuclear actin-related proteins 4 and 8 reveals their interaction with actin. EMBOJ; advance online publication: 15 April 2011; doi: 10.1038/emboj.2011.118

Parts of this thesis have been presented at an international conference:

Poster presentation at the 3rd SFB TR5 Symposium: Chromatin Assembly and Inheritance of Functional States, October 06-08, 2010 in Munich, Germany

1. INTRODUCTION.....	1
1.1 CHROMATIN	1
1.2 CHROMATIN REMODELING	2
1.2.1 Chromatin remodeling by histone modifications.....	2
1.2.2 ATP dependent chromatin remodeling	2
1.3 INO80 FAMILY CHROMATIN REMODELERS	4
1.3.1 The INO80 complex	5
1.3.2 Subunits of the INO80 complex.....	7
1.4 ACTIN BIOCHEMISTRY	9
1.5 THE ROLE OF NUCLEAR ACTIN	12
1.6 ACTIN RELATED PROTEINS	14
1.7 AIMS OF THE PROJECT	16
2. MATERIALS AND METHODS	17
2.1 MATERIALS	17
2.1.1 Chemicals.....	17
2.1.2 Bacterial strains and insect cell lines	17
2.1.3 Plasmids	18
2.1.4 Media and supplements.....	18
2.1.5 Buffers and solutions	19
2.2 METHODS.....	20
2.2.1 Bioinformatic methods.....	20
2.2.1.1 Homology searches and alignments	20
2.2.1.2 Determination of protein parameters	20
2.2.1.3 Structure visualization and analysis.....	20
2.2.2 Molecular biology methods	20
2.2.2.1 Molecular cloning.....	21
2.2.2.2 Oligonucleotides.....	22
2.2.3 Protein biochemistry methods.....	23
2.2.3.1 Generation of virus for protein expression in insect cells.....	23
2.2.3.2 Protein expression in <i>E. coli</i> and insect cells.....	24

2.2.3.3 Protein Purification.....	25
2.2.3.4 Analytical size exclusion chromatography	27
2.2.3.5 Surface plasmon resonance	28
2.2.4 Structural methods	29
2.2.4.1 X-ray crystallography	29
2.2.4.1.1 Protein crystallization	29
2.2.4.1.2 Theory of X-ray diffraction	30
2.2.4.1.3 Electron density calculation and the phase problem	30
2.2.4.1.4 Molecular replacement	32
2.2.4.2 Small angle X-ray scattering (SAXS).....	33
2.2.5 Structural studies on <i>S. cerevisiae</i> Arp4	36
2.2.5.1 Protein crystallization	36
2.2.5.2 Crystal structure determination.....	37
2.2.5.3 Solution structure of Arp4.....	37
2.2.6 Structural studies on <i>S. cerevisiae</i> Arp8	38
2.2.7 Structural studies on <i>S. cerevisiae</i> Rvb1-Rvb2	38
2.2.8 Structural studies on the entire <i>S. cerevisiae</i> INO80 complex	38
2.2.9 Actin biochemistry methods	39
2.2.9.1 Pyrene actin assays.....	39
2.2.9.2 <i>In vitro</i> TIRF microscopy	40
2.2.9.3 Critical concentration assay.....	41
2.2.9.4 Sedimentation assay	41
2.2.9.5 Pointed end elongation assay.....	41
3. RESULTS	42
3.1 STRUCTURAL STUDIES ON THE INO80 HOLO-COMPLEX.....	42
3.2 PURIFICATION OF INDIVIDUAL INO80 COMPONENTS.....	44
3.3 IDENTIFICATION OF NEW INTERMOLECULAR INTERACTIONS WITHIN THE INO80 COMPLEX	47
3.3.1 Interaction between Nhp10 and Ies5.....	48
3.3.2 Interaction between Arp5 and Ies6	50
3.4 SOLUTION STRUCTURES OF INO80 SUBCOMPLEXES	52

3.5 PURIFICATION AND CRYSTALLIZATION OF THE RVB1-RVB2 SUBCOMPLEX.....	55
3.6 STRUCTURAL STUDIES OF ARP4 AND ARP8	57
3.6.1 Sequence alignments between actin, Arp4 and Arp8 respectively.....	57
3.6.2 Purification of Arp4 and Arp8	59
3.6.3 Crystallization and structure determination of Arp4.....	61
3.6.4 Crystal structure of Arp4 reveals characteristic loop insertions and deletions within the actin fold.....	64
3.6.5 Solution structures of Arp4 and Arp8	66
3.6.6 ATP is tightly bound to Arp4.....	70
3.6.7 The structure of Arp4 explains why it is unable to form actin like filaments	72
3.7 BIOCHEMICAL STUDIES OF ARP4 AND ARP8.....	76
3.7.1 Arp4 inhibits actin polymerization by binding to monomers.....	76
3.7.2 Arp4 preferentially interacts with the barbed end of actin monomers	80
3.7.3 Arp4 depolymerizes actin filaments.....	83
3.7.4 Effects of Arp4 on the equilibrium of G- and F-actin depends on the nucleotide state	84
3.7.5 Arp8 does not inhibit actin polymerization but sequesters ADP-actin	86
3.7.6 Arp4 and Arp8 synergistically inhibit actin polymerization	90
3.7.7 Model for the actin-Arp4 interaction	92
<u>4. DISCUSSION.....</u>	<u>96</u>
4.1 STRUCTURE AND FUNCTION OF THE INO80 COMPLEX.....	97
4.2 AN UNEXPECTED ROLE FOR THE ACTIN RELATED PROTEINS ARP4 AND ARP8.....	101
<u>5. SUMMARY.....</u>	<u>107</u>
<u>6. REFERENCES.....</u>	<u>109</u>
<u>7. APPENDIX.....</u>	<u>120</u>
7.1 EXPRESSION AND PURIFICATION TRIALS OF INO80 COMPLEX COMPONENTS.....	120
7.2 ABBREVIATIONS.....	121
<u>8. CURRICULUM VITAE.....</u>	<u>124</u>
<u>9. ACKNOWLEDGEMENTS</u>	<u>125</u>

1. Introduction

1.1 Chromatin

Each nucleus of a human cell contains DNA which, if extended reaches a length of nearly 2 m. Packaging this large amount of nucleic acids into cell nuclei with diameters of approximately 10 μm creates a significant topological challenge (Clapier & Cairns, 2009; Kinner et al, 2008). In eukaryotes, the naked DNA is therefore compacted into condensed chromatin fibers by a hierarchical scheme of folding. Different levels of compaction are achieved with the help of various proteins, including histones and structural maintenance of chromosomes (SMC) proteins (Luger, 2003).

The basic repeating structure in chromatin is the nucleosome core particle consisting of two tight superhelical turns of DNA wrapped around an octamer of two copies each of the four histone proteins H2A, H2B, H3 and H4 (Horn & Peterson, 2002). The linear progression of nucleosomes along the DNA called “beads on a string” is then further compacted into more complex structures, including a 30 nm fiber and less defined higher structural elements, ending at the most condensed entity, the metaphase chromosome (see Figure 1) (Felsenfeld & Groudine, 2003).

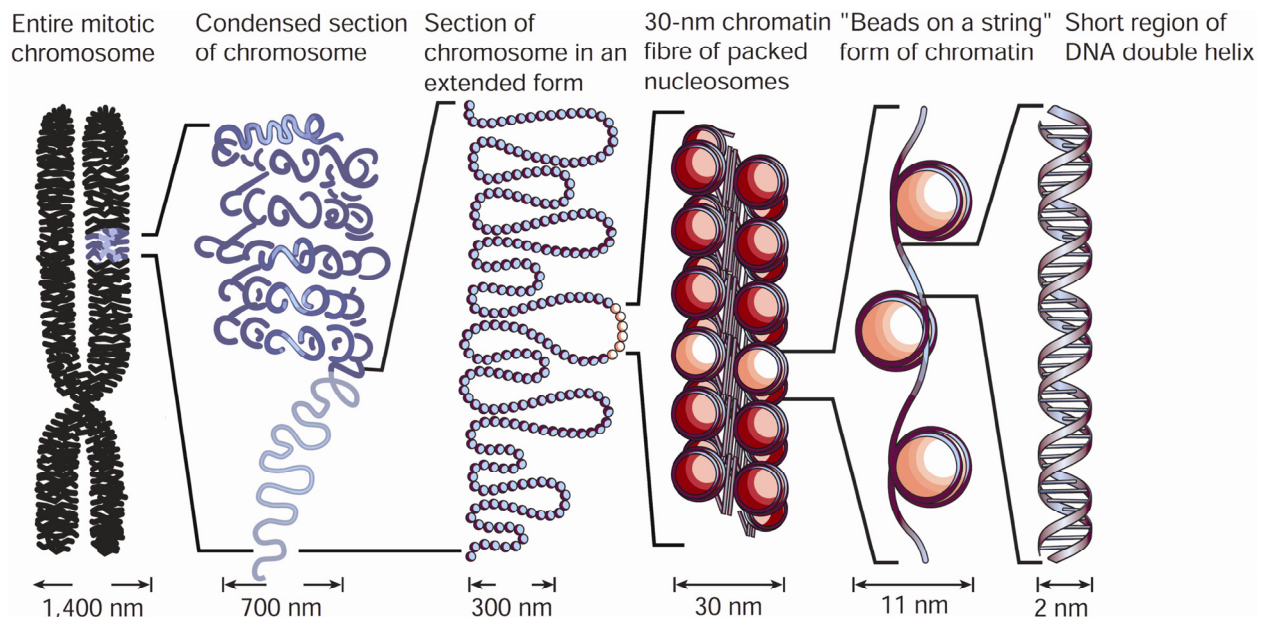


Figure 1: Hierarchical structure of chromatin

Different levels of DNA compaction are achieved with the help of histone proteins and additional proteins that stabilize higher order folding. Beyond the level of the 30 nm fiber structural knowledge about the exact arrangement of chromatin is scarce. Figure has been adapted from (Felsenfeld & Groudine, 2003).

It is immediately obvious that chromatin creates a natural barrier against processes that need access to DNA, like transcription, replication, repair and recombination. Therefore, a host of different mechanisms has to be present that ensures flexibility of chromatin, allowing for its loosening if DNA access is required (Vidanes et al, 2005).

1.2 Chromatin remodeling

1.2.1 Chromatin remodeling by histone modifications

Changes in the structure of chromatin have been mainly investigated in the context of gene transcription and comprise mechanisms like histone modification, histone variant incorporation and ATP dependent chromatin remodeling. Covalent modifications of histones include for example acetylation, methylation, or phosphorylation of specific histone residues (Campos & Reinberg, 2009). Acetylation is often carried out on lysines found at the N-terminal tails of histone proteins leading to a loss of positive charge, reduction in DNA binding strength and thereby a more open and accessible chromatin state (Narlikar et al, 2002). In contrast, repressive chromatin structure is commonly characterized by methylation (Paulsen & Ferguson-Smith, 2001). Phosphorylation of histones is an important signal in the DNA damage repair pathways where phosphorylation of histone H2AX, a variant of histone H2A leads to the recruitment of factors important for subsequent DNA damage repair (van Attikum & Gasser, 2009).

Alternatively, diverse combinations of histone modifications, also known as the “histone code” can provide signals that regulate various activities of other factors that mediate chromatin dynamics (Xu et al, 2009). Since these covalent modifications are reversible, they can act as chromatin-based "on/off" switches that regulate a multitude of DNA related processes.

1.2.2 ATP dependent chromatin remodeling

ATP dependent chromatin remodeling is a dynamic process where the energy created by ATP hydrolysis is used to reversibly alter contacts between histones and DNA (Lusser & Kadonaga, 2003). It is carried out by nuclear enzymes, which are usually part of larger, multifactorial complexes. Although the subunit composition, size and functionality of those complexes vary considerably, they all share a conserved motor subunit that belongs to the SWI2/SNF2 (switching defective/sucrose-non fermenting) family of ATPases.

Remodeler ATPases are highly similar to DNA translocases and crystal structures suggest that these enzymes travel along the minor groove of DNA, a process that can generate the torque or energy needed during the remodeling activity (Durr et al, 2005; Thoma et al, 2005). According to recent models, the remodeler binds to the nucleosome, and the ATPase domain responsible for translocation remains anchored at that fixed position from which it conducts directional DNA translocation. This can create a small DNA loop which then propagates around the nucleosome by one-dimensional diffusion, breaking histone DNA contacts (Clapier & Cairns, 2009; Racki & Narlikar, 2008). In turn, these processes then lead to a variety of different phenomena, including the shifting of nucleosome position or the complete eviction of nucleosomes at regulatory sites. In general, ATP dependent chromatin remodeling endows chromatin with dynamic properties that implement states of “plasticity” or “fluidity”, needed for the proper execution of cellular functions (Eberharter & Becker, 2004).

Despite their similarities, remodeling complexes can be grouped into subfamilies, based on domains present outside of the conserved ATPase domain (see Figure 2). The four subfamilies SWI/SNF, ISWI (imitation switch), CHD (chromo-ATPase–helicase–DNA-binding protein) and INO80 (inositol requiring mutant 80) constitute the best-studied examples (Bao & Shen, 2007).

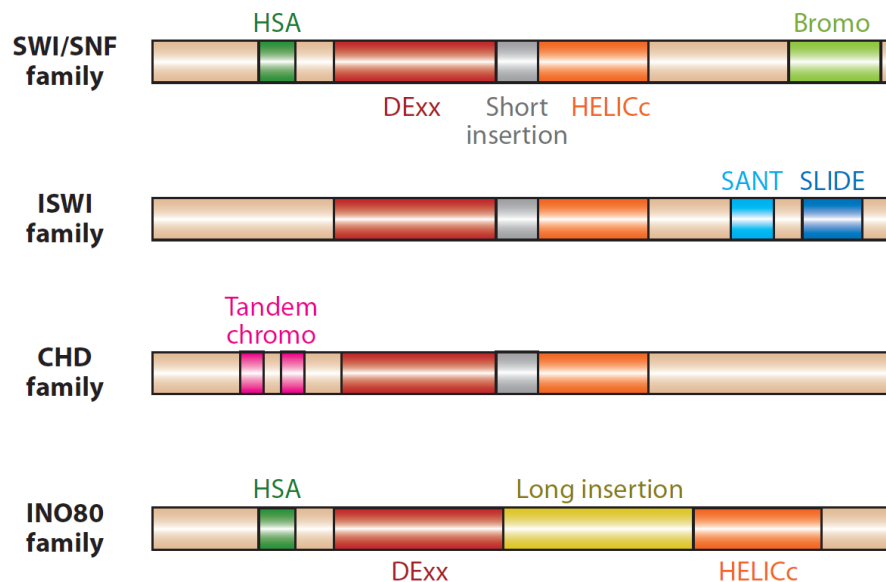


Figure 2: Core ATPase subunits of the four chromatin remodeler subfamilies

Chromatin remodelers are grouped into four families according to the domain organization of the central ATPase subunit. Besides the conserved ATPase domain consisting of a DExx and a HELICc part other specific domains are present in each remodeler, as indicated in the figure. The figure has been adapted from (Clapier & Cairns, 2009).

The SWI/SNF family remodelers were initially purified from *Saccharomyces cerevisiae* and are composed of 8 to 14 subunits, including a pair of actin related proteins (Arps). The catalytic ATPase contains a HSA (helicase-SANT) domain and a C-terminal bromodomain (Mohrmann & Verrijzer, 2005). They have diverse biological functions in processes like replication or transcription (Carey et al, 2006; Flanagan & Peterson, 1999).

The ISWI family remodelers contain 2 to 4 subunits and were initially purified from *Drosophila melanogaster*. Characteristic domains include a SANT domain (ySWI3, yADA2, hNCoR, hTFIIB) adjacent to a SLIDE domain (SANT-like ISWI) at the C-terminus of the ISWI ATPase (Corona & Tamkun, 2004). ISWI family complexes often optimize nucleosome spacing to promote chromatin assembly and the repression of transcription (Maier et al, 2008).

The CHD remodelers have 1 to 10 subunits and were first purified from *Xenopus laevis*. Characteristic features include two tandem chromodomains at the N-terminus of the catalytic subunit (Marfella & Imbalzano, 2007). Those domains may be involved in increasing functional variability of CHD family complexes, conferring both activating and repressing roles in transcription (Murawska et al, 2008; Sugiyama et al, 2007).

The INO80 class of remodelers and their diverse composition and functionality is described in more detail below.

1.3 INO80 family chromatin remodelers

The INO80 class of remodelers has more than 10 subunits and was initially purified from *Saccharomyces cerevisiae*. It has two members in yeast, the INO80 complex itself and the highly related SWR1 complex (Swi2/Snf2 related 1) (Krogan et al, 2003; Shen et al, 2000). Both complexes are conserved in higher eukaryotes with homologues in *Drosophila melanogaster* (Pho-dINO80 and Tip60) and human (hINO80 and TRRAP/Tip60) being experimentally verified (Jin et al, 2005; Klymenko et al, 2006). The hallmark feature of this family is a “split” ATPase domain which harbors a large insertion within its characteristic ATPase motifs (see Figure 2) (Bao & Shen, 2007; Conaway & Conaway, 2009).

Both the INO80 and SWR1 complex have subunits which are unique to the respective remodeler. The same holds true for the complexes of different species which have diverged in evolution leading to a unique set of individual components in each species. Nevertheless, the SWI2/SNF2 ATPase with its characteristic insert, two RuvB like proteins (Rvb1, Rvb2) which belong to the

family of AAA+ ATPases (ATPases associated with a variety of cellular activities), a set of actin related proteins (Arps) and actin itself constitute a conserved set of subunits which each member of the family shares.

1.3.1 The INO80 complex

The INO80 gene was first identified in a genetic screen for mutants affecting inositol biosynthesis (Ebbert et al, 1999). It was shown that the INO80 protein (INO80p) shares significant sequence homology to the SWI2/SNF2 family of DNA dependent ATPases and is part of a high molecular weight complex. The entire functional INO80 complex (INO80.com) from *S. cerevisiae* contains 15 principal subunits and has a molecular mass of over 1 MDa (Shen et al, 2000). The components of the yeast INO80 complex are INO80p, Rvb1, Rvb2, actin, Arp4, Arp5, Arp8, Nhp10 (nonhistone protein 10), Taf14 (transcription factor 14), Ies1 (INO eighty subunit 1), Ies2, Ies3, Ies4, Ies5 and Ies6. All proteins exhibit roughly equivalent stoichiometry compared to each other (see Figure 3). Only Rvb1 and Rvb2 show a 6:1 excess compared to the other polypeptides (Shen et al, 2000; Shen et al, 2003).

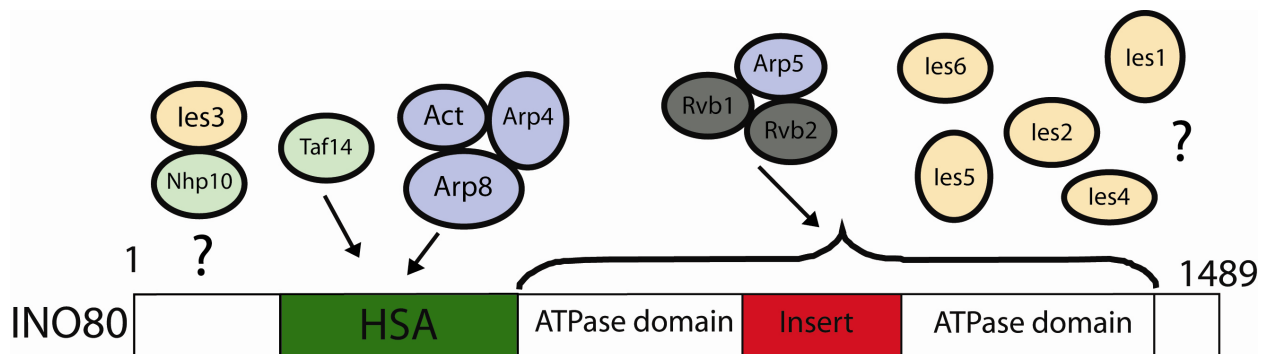


Figure 3: Current view of the architecture of the INO80 complex from *S. cerevisiae*

The 15 principal subunits are depicted with the INO80 protein acting as a scaffold to integrate them into the complex. The subunits are colored according to protein families: actin and actin related proteins (blue), Rvb1 and Rvb2 (grey), INO80 subunit proteins (orange) and other proteins (green). Different domains within the INO80 protein are labeled. The N-terminal HSA domain acts as a platform to assemble the Arp4-Arp8-actin module within the INO80 complex (Szerlong et al, 2008). The insert in the ATPase domain of INO80 integrates a Rvb1-Rvb2-Arp5 complex (Jonsson et al, 2004). Another known interaction exists between Nhp10 and Ies3 (Shen et al, 2003). For most of the other proteins, it is not known how they are bound in the complex and how they interact with each other (depicted by question marks). The figure has been modified from (Bao & Shen, 2007).

Biochemical studies indicate that the INO80 complex has DNA dependent ATPase activity, as well as 3'-5' helicase activity *in vitro*. Moreover, INO80.com is able to mobilize mononucleosomes in an ATP dependent manner (Shen et al, 2000; Shen et al, 2003).

In vivo the INO80 complex is involved in many nuclear processes. Several microarray studies have established a role of INO80.com mediated chromatin remodeling in transcriptional regulation. 150 out of 5602 yeast genes showed at least twofold change in mRNA level upon acute removal of the INO80 protein (Jonsson et al, 2004; Mizuguchi et al, 2004).

In addition to its function in transcriptional regulation, the INO80 complex has been shown to be directly involved in DNA damage responses. The phosphorylation of histone H2AX in response to DNA double strand breaks (DSBs) controls the recruitment of INO80 to the site of a DSB, thus establishing a link between chromatin remodeling and DNA repair. It has been shown that INO80.com facilitates the formation of single stranded DNA at the site of a DSB, a critical step during DNA repair by homologous recombination (van Attikum et al, 2004). Moreover, the INO80 remodeling activity is probably required for histone eviction near DSBs and defects in histone loss result in a delayed recruitment of the Rad51 repair protein (Tsukuda et al, 2005). Interestingly, Arp5 and Arp8 deletion mutants display hypersensitivity to DSB promoting agents, when the homologous recombination pathway is disrupted, suggesting an important role for INO80 in the non homologous end joining repair pathway as well (Morrison et al, 2004; van Attikum et al, 2004).

Moreover, it has been shown that INO80 localizes to replication forks and seems to exhibit a dual function during replication. On the one hand, the loss of INO80 chromatin remodeling activity perturbs the recruitment of cohesion establishment proteins to replication forks, giving INO80 a role in sister chromatid cohesion (Ogiwara et al, 2007). On the other hand, INO80 is important to facilitate the progression of stalled replication forks as indicated by compromised replisome integrity upon INO80 deletion (Papamichos-Chronakis & Peterson, 2008).

In addition to that INO80 is involved in the regulation of telomere structure and function as well as DNA damage checkpoint regulation (Morrison et al, 2007; Yu et al, 2007). Recently it has been found that INO80 exchanges the histone variant H2A.Z/H2B with free H2A/H2B dimers and thus has an antagonistic function to the SWR1 complex (Papamichos-Chronakis et al, 2011). It is very likely that new roles for the INO80 complex will continue to emerge in the future.

1.3.2 Subunits of the INO80 complex

Functional roles for individual subunits of the INO80 complex are quite elusive. This holds true also for the interaction network within the complex since it is largely unknown which subunits interact with each other. Clarification of those issues has been mainly sought by generating knockouts of individual components of the INO80 complex in yeast and subsequent probing of altered complex architecture and functionality. Those studies are hampered however by the fact that some subunits of INO80 are essential in yeast and knockout strains are not viable and therefore uninformative. Among those essential subunits are Rvb1, Rvb2, Arp4 and actin which are all part of other nuclear complexes as well.

Rvb1 and Rvb2 are part of INO80, SWR1 and NuA4 complexes (nucleosome acetyltransferase of histone H4) and are crucial for the chromatin remodeling activity of the entire INO80 complex (Jonsson et al, 2004). Within INO80 they most likely form a subcomplex together with Arp5, as the removal of temperature sensitive Rvb1 and Rvb2 mutants from the complex lead to a specific loss of Arp5. It was shown *in vitro* that this association is ATP dependent as it only occurs in the presence of non hydrolysable ATP (Jonsson et al, 2004; Shen et al, 2003).

Rvb1 and Rvb2 probably form hexamers as shown by the crystal structure of the human Rvb1 homologue RuvBL1 (Matias et al, 2006). Together they possibly build up a large dodecameric assembly which has been studied by electron microscopy (Gribun et al, 2008; Puri et al, 2007; Torreira et al, 2008). Their exact structure and stoichiometry however is unknown as no high resolution structure of the entire Rvb1-Rvb2 complex is available. Additionally, their exact functionality is controversial since several studies either prove or disprove both proteins to have ATPase and/or helicase activity (Jha & Dutta, 2009).

Nhp10 is a HMG-1 (high mobility group) like protein and its deletion leads to loss of Ies3 from the complex indicating an interaction between both proteins (Shen et al, 2003). Nhp10 has been further implied to specifically bind to DNA ends possibly helping to recruit the INO80 complex to the sites of DNA damage (Ray & Grove, 2009). Together with Ies3 it also seems to mediate the interaction with phosphorylated histone H2A further supporting its role in recruiting INO80 to the sites of a DNA double strand break (Morrison et al, 2004).

Taf14 is not only a subunit of the INO80 complex but also member of several transcription factors and the mediator complex. Its knockout leads to reduced transcriptional activity as well

as defects in actin organization (Welch & Drubin, 1994; Zhang et al, 2004). It contains a conserved YEATS domain (Yaf9, ENL, AF9, Taf14, Sas5) albeit with unknown function.

The INO80 subunit proteins Ies1 - Ies6 are, as the name implies unique to the INO80 complex. They are only loosely conserved between INO80 complexes of different species and little is known about their functionality. Ies2 and Ies6 are conserved between the yeast and human INO80 complex (Conaway & Conaway, 2009). The Ies4 subunit in the yeast INO80 complex seems to be responsible for cell cycle signaling since its phosphorylation by Mec1/Tel1 kinases leads to a modulation of the DNA damage checkpoint (Morrison et al, 2007).

Actin and actin related proteins are part of many chromatin remodeling complexes including INO80, SWR1, RSC, SWI/SNF and NuA4 in yeast (see Figure 4) (Dion et al, 2010). Whereas Arp5 and Arp8 are exclusively found in the INO80 complex, Arp4 is also part of other remodelers (Dion et al, 2010).

The ARP-containing remodeling complexes in budding yeast and humans				
Organism	Remodeling complex	Full name	Catalytic subunit	ARPs included
Budding Yeast	INO80.com	Inositol requiring mutant 80	Ino80	Actin, Arp4, Arp5, Arp8
	SWR1-C	Swi2/Snf2-Related 1 complex	Swr1	Actin, Arp4, Arp6
	RSC	Remodel the Structure of Chromatin	Sth1	Arp7, Arp9
	SWI/SNF	Switch/Sucrose Non-Fermentable	Snf2	Arp7, Arp9
	NuA4	Nucleosome Acetyltransferase of histone H4	Esa1	Actin, Arp4
Human	INO80	Inositol requiring mutant 80	hIno80	Actin, Baf53a, hArp5, hArp8
	SRCAP	SNF2-related CREB-activator protein	Srcap	Baf53a, hArp6
	BAF	Brahma (BRM) or Brahma related gene (BRG) associated factors	Brm1 or Brg1	Actin, Baf53a or b
	PBAF	Polybromo-associated BAF	Brg1	Actin, Baf53a or b
	TIP60/TRRAP	HIV-1 Tat interactive protein 60 kDa/transformation/transcription domain-associated protein	p400, Tip60	Actin Baf53a

Figure 4: Occurrence of actin related proteins in chromatin remodeling complexes

This list summarizes which Arps are found in different chromatin remodeling complexes of *S. cerevisiae* and human. The figure has been adapted from (Dion et al, 2010).

Arp5 and Arp8 knockouts have a similar phenotype as the knockout of the INO80 ATPase itself implying that both subunits are essential in the chromatin remodeling process of the entire INO80 complex (Shen et al, 2003). Arp4 has been connected with histone binding as it was shown to directly interact with phosphorylated histone H2A and possibly also with other histones (Galarneau et al, 2000; Harata et al, 1999; Sunada et al, 2005). Interestingly, Arp8 also interacts with histones, preferentially H3 and H4 (Shen et al, 2003) hinting at a role for actin related proteins as histone chaperones mediating histone contact during chromatin remodeling.

Arp8 seems to be important for the recruitment of Arp4 and actin into the complex since its knockout leads to a loss of those subunits (Shen et al, 2003). Specifically, Arp8 forms a discrete and stable subcomplex with Arp4, actin and an N-terminal part of INO80 the helicase-SANT-associated (HSA) domain (Szerlong et al, 2008). A subcomplex containing Arp4, actin and the HSA domain has been identified in the SWR1 complex and human BAF and PBAF complexes as well (Szerlong et al, 2008). This suggests that the complex of Arp4, actin and HSA is a conserved functional module, albeit with unknown function.

The occurrence of actin and actin related proteins in the nucleus and their functions in chromatin remodelers are still poorly understood and shall be addressed in the next paragraphs.

1.4 Actin biochemistry

Conventional actin is one of the most highly conserved and highly abundant proteins in eukaryotic cells (Galkin et al, 2002; Reisler & Egelman, 2007). Actin dynamics play a role in many cellular processes like formation of the cytoskeleton, intracellular motility, adhesion and locomotion (Schleicher & Jockusch, 2008). Its characteristic U-shaped fold, the “actin fold” consists of four subdomains arranged around a central nucleotide binding cleft (see Figure 5) (Kabsch et al, 1990). The molecule has two distinct ends, the “barbed”, or “plus” end constituted of subdomains 1 and 3 and the “pointed”, or “minus“ end made up of subdomains 2 and 4.

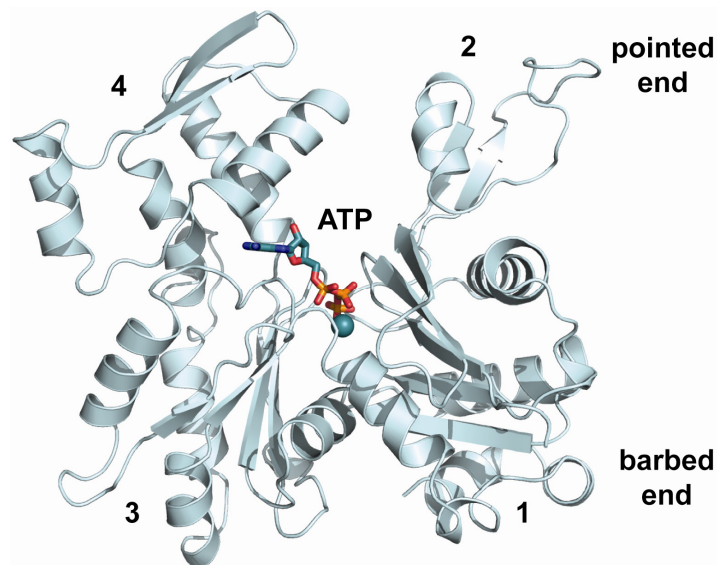


Figure 5: Structure of actin

Crystal structure of *S. cerevisiae* actin (pdb: 1YAG). The four subdomains are numbered, ATP is represented in sticks and the metal ion is displayed as a sphere.

Actin usually binds an ATP molecule together with a divalent metal ion in its highly conserved binding cleft. The bound nucleotide is essential for structural stability of the actin molecule as its removal, for example by the addition of EDTA, leads to unfolding (Altschuler et al, 2005). Nevertheless, actin is capable to hydrolyze ATP and subsequently exchange ADP by fresh ATP again. This process is important for actin dynamics as explained below.

The actin fold exposes several well defined interaction sites which allow it to interact with a large set of binding partners (Campellone & Welch, 2010; Dominguez, 2004). One very important interaction surface of actin lies at the barbed end, where a hydrophobic pocket is formed by the C-terminus of the molecule. This pocket is utilized by many actin binding proteins as a binding platform (Dominguez, 2004). Usually, an amphipathic helix is inserted into the groove with the hydrophobic residues pointing into the pocket. This binding mode is employed by proteins like cofilin or gelsolin and by proteins like WASP (Wiskott–Aldrich syndrome protein) containing WH2 (WASP homology) domains, which are specifically designed to interact with actin in this fashion (Dominguez, 2009).

Monomeric G-actin (globular-actin) is capable of assembling F-actin (filamentous-actin) by polymerization, a process which is highly dynamic and regulated by various actin binding proteins (Campellone & Welch, 2010). Structurally, the actin filament can be described as either a single left-handed short-pitch helix, with consecutive lateral subunits staggered with respect to one another by half a monomer length, or two right-handed long-pitch helices of head-to-tail bound actin subunits (see Figure 6) (Holmes et al, 1990; Oda et al, 2009). Actin monomers are incorporated into filaments preserving the same orientation. The generated filaments, just like the constituting monomers, thus possess two distinctly different ends: a barbed and a pointed end.

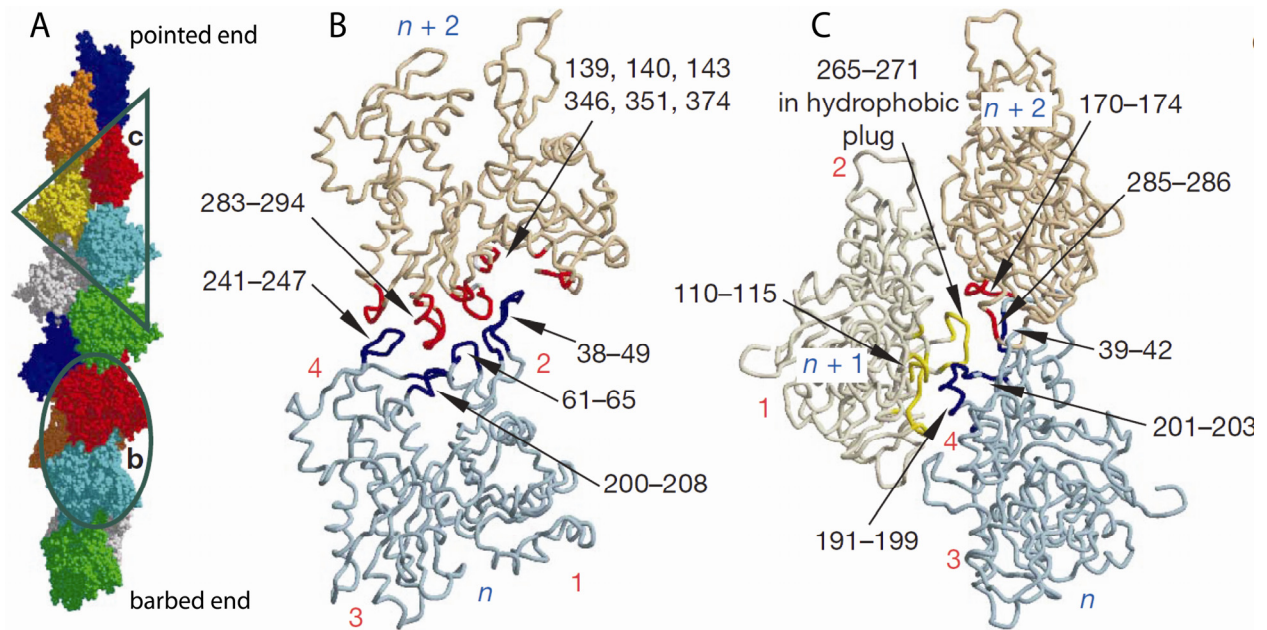


Figure 6: Structure of the actin filament

A) Atomic model of the two stranded actin filament obtained by fiber diffraction. Individual actin molecules within the filament are colored differently. The two subunits marked by the oval are enlarged in B. The three subunits marked by the triangle are enlarged in C.

B) Important residues for intra strand contact formation within the same filament are highlighted.

C) Important residues for inter strand contact formation within two adjacent filament strands are highlighted. The figure has been adapted from (Oda et al, 2009).

Actin monomers join the fast growing barbed end of the filament primarily in the ATP state. The incorporation into the filament leads to an about 40,000 fold increase of actins' ATPase activity (Blanchoin & Pollard, 2002). ATP hydrolysis takes place in the filament, and ADP-actin monomers dissociate again mainly from the pointed end. This creates an internal timing mechanism to discriminate between newly polymerized ATP-actin filaments and older ADP-actin containing filaments that are depolymerized again, leading to so called actin tread milling (see Figure 7) (Dominguez, 2009). The two ends of the filaments however, do not only exhibit different polymerization kinetics but also different affinities for actin monomers, as the barbed end has higher affinity for actin ($0.1 \mu\text{M}$) compared to the pointed end ($0.7 \mu\text{M}$) (Rickard & Sheterline, 1986).

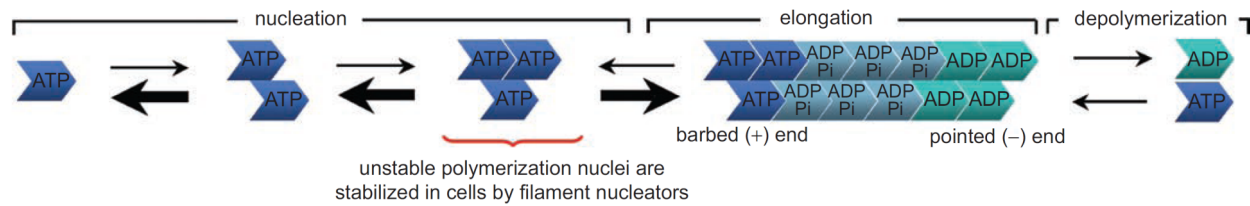


Figure 7: Actin filament dynamics

The rate limiting step of filament formation is the generation of small dimeric and trimeric filament nuclei. Only after such nuclei have been formed the fast addition of further actin monomers to the filament can take place. The nucleation step is therefore the most tightly controlled aspect of actin polymerization. It is influenced for example by filament nucleating proteins, or actin monomer sequestering proteins. The growing actin filament has two different ends. Polymerization takes place mainly by fast addition of ATP-actin to the barbed end of the filament. After ATP-hydrolysis within the filament ADP-actin mainly dissociates from the pointed end. The figure has been adapted from (Dominguez, 2009).

Since actin is such a crucial cellular protein its functionality is regulated on many different levels. Polymerization of actin for example, is no spontaneous process, as the formation of actin dimeric and trimeric ‘nuclei’ is kinetically unfavorable (Sept & McCammon, 2001). The cell therefore needs the help of actin nucleating factors like formins which stabilize actin polymerization nuclei and create a starting point for productive formation of actin filaments. Filament nucleating proteins thus present a means of regulating filament formation.

Another important actin binding and regulating protein is profilin. It is capable of providing a pool of monomeric actin for the ordered incorporation into actin filaments by preventing its premature polymerization. It does so by binding to the barbed end of actin monomers, thereby inhibiting nucleation and pointed end elongation, while having almost no effect on steady-state barbed end elongation (Paul & Pollard, 2009). Interestingly, profilin also stimulates the exchange of ADP to ATP in actin further bolstering the pool of polymerization competent actin (Witke, 2004).

1.5 The role of nuclear actin

Despite the first reports about the presence of actin in the nucleus more than 40 years ago it has still been under debate if actin occurs in the nucleus at all (Lane, 1969). Its presence in nuclear preparations has often been ruled down as cytoplasmic contamination by this highly abundant protein. It took until recent years to strongly establish a role of actin in various nuclear processes. As mentioned, actin has been identified as part of several chromatin remodeling complexes for

example the yeast INO80 complex (Shen et al, 2000), the mammalian BAF complex (Zhao et al, 1998), or the yeast SWR 1 complex (Krogan et al, 2003), implying an important role for actin in the turnover of chromatin. This is emphasized by the fact that actin seems to be involved in chromatin repositioning. Particularly, it has been observed that prevention of actin dynamics hampers long-range chromatin movement (Chuang et al, 2006). Furthermore, actin seems to play important roles in transcription (Miralles & Visa, 2006). It can bind transcription factors and influences their subcellular localization, it is required for optimal transcriptional activity of all three RNA polymerases (Franke, 2004) and it associates with hnRNP U a ribonucleoprotein involved in pre-mRNA processing, transport, and stability (Kukalev et al, 2005) giving rise to the assumption that actin plays important roles in mRNA maturation and export.

A very interesting question concerns the functional form of actin in the nucleus, namely its polymerization state. It has long been dismissed that filamentous actin exists within the nucleus. This was mainly because nuclear actin cannot be stained with phalloidin which recognizes actin filaments with at least seven subunits and is the most common method to detect actin filaments in the cytoplasm (Visegrady et al, 2005). Another argument that is raised against the existence of conventional actin filaments in the nucleus is based on different staining patterns obtained with various antibodies. Specifically, antibodies which stain monomeric actin, like antibodies raised against the profilin-actin complex (Gonsior et al, 1999), or antibodies against the “lower-dimer” of actin (Schoenenberger et al, 2005) have been found to give strong nuclear staining. On the other hand, antibodies against smooth-muscle α -actin give strong cytoplasmic staining but have never been found to stain nuclear actin (Milankov & De Boni, 1993). These findings indicate nuclear actin to be predominantly monomeric, or to adopt specialized conformations forming short oligomers for example, which are hard to detect by conventional methods.

However, there is mounting support that filamentous forms of actin do indeed play important roles in the nucleus. One line of evidence stems from studies with the actin monomer-sequestering drug latrunculin which binds to G-actin and blocks F-actin assembly. The addition of latrunculin to *X. laevis* egg extracts has been found to inhibit nuclear envelope assembly (Krauss et al, 2003) and other functions attributed to nuclear actin, like export of RNA and protein (Hofmann et al, 2001), or transcription (McDonald et al, 2006). The role of polymeric actin in transcription was also shown by expressing actin mutants in cells inhibited for RNA

polymerase I transcription by specific antibodies. Only actin mutants that stabilized polymeric actin could restore transcription (Ye et al, 2008).

With the help of fluorescence recovery after photo bleaching (FRAP) experiments a low mobility fraction of actin in the nucleus could be detected. This was then shown to correspond to polymerized actin (McDonald et al, 2006). Furthermore, phalloidin stainable actin filaments can be detected in the nuclei of certain cell types at least, for example the large *X. laevis* oocytes, which can even be destabilized by microinjection of the actin-specific transport receptor exportin 6 (Bohnsack et al, 2006). Additionally, certain stress conditions like dimethyl sulfoxide (DMSO) treatment (Fukui & Katsumaru, 1979), heat shock (Welch & Suhan, 1985), or cytoskeletal disruption and ATP depletion (Pendleton et al, 2003) lead to the formation of phalloidin stainable rod-like aggregates.

Although the conformation of nuclear actin filaments might be different from cytosolic ones it is still obvious that if nuclear filaments are indeed formed, proteins to regulate the formation, the productive use and the ordered disassembly of those filaments are needed.

1.6 Actin related proteins

One class of proteins which regulates actin dynamics in the cytoplasm and is also found in the nucleus is the previously mentioned group of actin related proteins (Dion et al, 2010). This family is structurally similar to actin, meaning that the core actin fold and the central nucleotide binding cleft are preserved (Muller et al, 2005). It has ten members in the yeast *S. cerevisiae* (Poch & Winsor, 1997), with Arp1 - Arp3 and Arp10 being predominantly cytoplasmic and Arp4 - Arp9 mainly nuclear.

One major player within the Arp family is the primarily cytosolic Arp2/3 complex. It is a stable complex of Arp2 and Arp3, supplemented with five additional subunits (ArpC1-ArpC5) and was the first major actin nucleator to be identified (Machesky et al, 1994). Among the known nucleators, the Arp2/3 complex is unique in its ability to both nucleate actin filament branches from the sides of pre-existing actin “mother” filaments and to organize them into branched networks (Pollard, 2007). Interestingly, it has also been demonstrated to play a role in nuclear actin regulation for example during transcription by RNA polymerase II (see Figure 8) (Wu et al, 2006; Yoo et al, 2007).

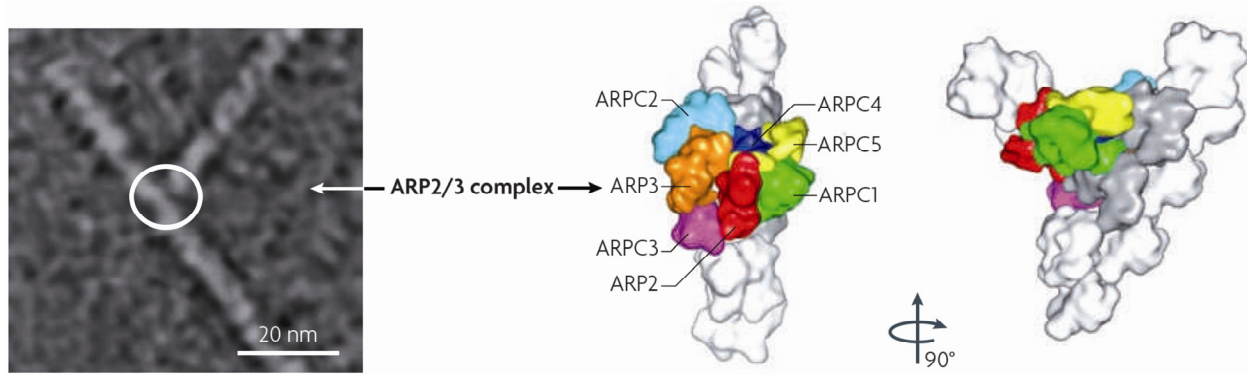


Figure 8: Structural model of the Arp2/3 complex at the branch points of actin filaments

The Arp2/3 complex consists of Arp2 and Arp3 plus the additional subunits ArpC1-ArpC5. Its structure has been solved in different nucleotide states (Nolen & Pollard, 2007). The morphology of an Arp2/3 branched actin filament is shown in the electron micrograph (left). The structural models are based on electron tomography (right). All seven subunits participate in binding to existing filaments and Arp2/Arp3 act as the first subunits of nascent filaments. Adapted from (Campellone & Welch, 2010).

The Arp2/3 complex and its effect on actin has been studied quite extensively which is not the case for many of the nuclear Arps. As previously mentioned, one well established role of nuclear Arps is their presence as integral part of several chromatin remodeling complexes, although their function within those complexes is largely unknown. Arps are often found as pairs within those complexes, for example Arp7/9 in yeast RSC and SWI/SNF complexes and the human homologue of Arp4 (Baf53) together with actin in human BAF, PBAF and Tip60 complexes (Clapier & Cairns, 2009).

Arp4 seems to be especially interesting since it is the most highly conserved, ‘primordial’ nuclear Arp and is found in the largest number of complexes (Dion et al, 2010). It is an essential gene in yeast (Harata et al, 1994) and a function of Arp4 has been established in histone binding (Galarneau et al, 2000). However, it not only seems to be part of higher molecular weight complexes but a lower molecular weight pool of free Arp4 was found in yeast cell extracts indicating a role of Arp4 independently of chromatin remodeling complexes (Sunada et al, 2005). Interestingly, temperature sensitive mutants of Arp4 have been shown to influence yeast cell shape leading to an increase in cell and nuclear size (Georgieva et al, 2008).

The same is true for Arp8 which has been mainly characterized as a subunit unique to the INO80 complex (Shen et al, 2000) but has now been found to have functions independently of chromatin remodeling complexes. Specifically, human Arp8 persists on chromatin during mitosis

and its depletion increases the fraction of misaligned chromosomes unlike the depletion of other components of the INO80 complex (Aoyama et al, 2008). Deletion of Arp8 in yeast leads to an abnormally increased cell volume and irregular, elongated cell morphology together with unusually elongated buds compared to wild type (Hibbs et al, 2007),(Watanabe et al, 2009).

Bearing the roles of cytoplasmic Arps in regulating actin turnover in mind and combine it with the fact that Arp4 is often found in a module together with actin, it could be possible that nuclear Arps are involved in regulating actin dynamics.

1.7 Aims of the project

Despite a still growing knowledge about biochemical and *in vivo* properties of the INO80 complex a structural framework for its action is still lacking. Neither the core ATPase INO80p, nor any of the complex components (except actin and the human homologue of Rvb1), nor the architecture of the entire complex have been structurally elucidated. The missing structural information causes a deficit of mechanistic understanding of the INO80 remodeling process, a problem which persists for chromatin remodelers in general. A similar lack of knowledge is true for the functional properties of the individual INO80 subunits. Either their exact activities are controversial as in the case of Rvb1 and Rvb2 or mostly unknown as in the case of actin and Arps. Another poorly understood property of the INO80 complex is the presence of so many ATP binding and possibly also ATP-hydrolyzing components besides the INO80 protein itself. Specifically, the complex contains actin, three actin related proteins and six or twelve subunits of the AAA+ ATPases Rvb1 and Rvb2. It is unclear, if all those proteins indeed bind to and hydrolyze ATP and how this ATP hydrolysis might contribute to the properties of the entire complex.

To tackle the demanding task of structurally and functionally characterizing the INO80 complex, a “divide and conquer” strategy was devised. First, the entire INO80 complex was purified endogenously from *S. cerevisiae* in order to analyze it by electron microscopy. Second, previously unknown stable subcomplexes which can be purified independently from the rest of the complex were identified and subsequently studied by X-ray crystallography, small angle X-ray scattering (SAXS) and functional assays. Third, individual subunits were studied structurally and functionally. A special emphasis was put on characterizing the actin related subunits of the INO80 complex and their interplay with actin.

2. Materials and Methods

2.1 Materials

2.1.1 Chemicals

All common chemicals were obtained from Merck (Darmstadt, Germany), Roth (Karlsruhe, Germany) and Sigma (Deisenhofen, Germany), unless otherwise stated. Crystallization screens and crystallization tools were from Hampton Research (Aliso Viejo, USA), Nextal Biotechnologies (Montreal, Canada; now QIAGEN, Hilden, Germany) or Jena Bioscience (Jena, Germany). RP-HPLC purified oligonucleotides were ordered from Thermo Electron Corporation (Ulm, Germany) and Eurofins MWG (Ebersberg, Germany), respectively. Enzymes and nucleotides for molecular biology were from Fermentas (St- Leon-Rot, Germany), or New England Bioscience (Frankfurt, Germany). Chromatographic media were purchased from GE Healthcare (Freiburg, Germany).

2.1.2 Bacterial strains and insect cell lines

Table 1: *Escherichia coli* strains

<i>E.coli</i> strain	Genotype	Source
XL1 Blue	recA1 endA1 gyrA96 thi-1 hsdR17 supE44 relA1 lac [F'proAB lacIqZΔM15 Tn10 (Tetr)]	Stratagene, Heidelberg
Rosetta (DE3)	F- <i>ompT hsdSB</i> (rB- mB-) <i>gal dcm</i> (DE3) pRARE2 (CamR)	Novagen, Madison USA
DH10MultiBac	not specified	Imre Berger (Berger et al, 2004)

Table 2: Insect cell lines

Cell line	Origin	Source
High Five insect cells	clonal isolate, derived from <i>Trichopulsia ni</i>	Invitrogen, Karlsruhe
Sf9 insect cells	clonal isolate, derived from <i>Spodoptera frugiperda</i>	Invitrogen, Karlsruhe
Sf21 insect cells	clonal isolate, derived from <i>Spodoptera frugiperda</i>	Invitrogen, Karlsruhe

2.1.3 Plasmids

Table 3: Utilized plasmids

Plasmid	Expression System	Source
pET21b(+)	<i>E.coli</i>	Novagen, Madison USA
pET28b(+)	<i>E.coli</i>	Novagen, Madison USA
pFBDM	Insect cells	Imre Berger (Berger et al, 2004)

2.1.4 Media and supplements

Luria Bertani (LB) liquid media, yeast extract peptone dextrose (YPD), as well as LB agar plates were prepared according to standard protocols (Sambrook et al, 2001). The media was supplemented with the respective antibiotics using stock solutions in 1:1000 dilutions.

Table 4: Antibiotic stock solutions

Antibiotic	Concentration (1000x)	Solvent
Ampicilin (Na-Salt)	100 mg/ml	water
Kanamycin	50 mg/ml	water
Chloramphenicol	50 mg/ml	ethanol
Tetracycline	12.5 mg/ml	ethanol
Genatmycin	10 mg/ml	water

Insect cell media powder (Express Five for High Five expression) was purchased from Invitrogen (Karlsruhe, Germany) and solubilized according to the manufacturer's protocol. Before use, the media was supplemented with gentamycin (10 µg/ml) and glutamine (final concentration 18 mM). Sf-900 III SFM liquid media (for Sf9 and Sf21 cells) and Sf-900 II methionine free medium was also purchased from Invitrogen (Karlsruhe, Germany) and supplemented with gentamycin (10 µg/ml).

2.1.5 Buffers and solutions

The following table contains general buffers and solutions which were used in this work. Buffers for specific protein purifications and biochemical assays are given separately in the corresponding part.

Table 5: Buffers, dyes and solutions

SDS-PAGE	
4x stacking gel buffer	0.5 M Tris, 0.4% (w/v) SDS, pH 6.8 (25°C)
4x separation gel buffer	3 M Tris, 0.4% (w/v) SDS, pH 8.9 (25°C)
Electrophoresis buffer, 1x TGS	190 mM glycine, 50 mM Tris, 0.1% (w/v) SDS
5x Loading dye	50% glycerol, 250 mM Tris/HCl pH 6.8 (25°C), 7.5% SDS, 5 mM EDTA, 10 mM DTT, 0.5% bromphenolblue
Coomassie staining solution	50% (v/v) ethanol, 7 % (v/v) acetic acid, 0.2% Coomassie Brilliant blue R-250
Gel electrophoresis of nucleic acids	
Electrophoresis buffer, 1x TAE	40 mM Tris, 20 mM acetic acid, 1 mM Na ₂ EDTA
6x Loading dye	1.5 g/l bromphenol blue, 1.5 g/l xylene cyanol, 50% (v/v) glycerol
Buffers for preparation of chemically competent cells	
TFB-1	30 mM KOAc, 50 mM MnCl ₂ , 100 mM KCl, 10 mM CaCl ₂ , 15% (v/v) glycerol, pH 5.8 (25°C)
TFB-2	10 mM MOPS, 10 mM KCl, 75 mM CaCl ₂ , 15% glycerol, pH 7.0 (25°C)

2.2 Methods

2.2.1 Bioinformatic methods

2.2.1.1 Homology searches and alignments

DNA and protein sequences were found in the NCBI database (<http://www.ncbi.nlm.nih.gov>). Homology searches were performed using the NCBI Basic Local Alignment Search Tool (BLAST) server (<http://www.ncbi.nlm.nih.gov/BLAST>). Multiple sequence alignments were performed with ClustalW (<http://align.genome.jp/>).

2.2.1.2 Determination of protein parameters

Theoretical physical and chemical parameters of the recombinant proteins (molecular weight, isoelectric point and extinction coefficients) were calculated with ProtParam (Gasteiger et al, 2003) from the ExPASy Proteomics Server (www.expasy.org/tools/protparam.html).

2.2.1.3 Structure visualization and analysis

Images of the crystal structures were prepared with PyMol from DeLano Scientific (Palo Alto, USA). Calculation of protein interaction surfaces was performed with pdbsum (Laskowski, 2009) (<http://www.ebi.ac.uk/pdbsum/>). Superposition of two homologous structures was performed with COOT (Emsley & Cowtan, 2004).

2.2.2 Molecular biology methods

Standard molecular biology procedures like polymerase chain reaction (PCR), restriction enzyme digestion, ligation of DNA fragments, preparation of competent *E. coli* cells, transformation, amplification of plasmid DNA and analysis by agarose gel were essentially performed according to standard protocols (Sambrook et al, 2001). In addition, plasmid DNA was prepared with a plasmid purification kit (Qiagen, Hilden, or Metabion, Martinsried, Germany) and isolation and purification of DNA fragments were performed using a gel extraction kit (Qiagen, Hilden, or Metabion, Martinsried, Germany) according to the manufacturer's instructions. DNA sequencing was done by Eurofins MWG (Ebersberg, Germany). Further standard methods for working with proteins like SDS-PAGE and determination of protein concentration were used as described (Sambrook et al, 2001).

2.2.2.1 Molecular cloning

In general, the Polymerase Chain Reaction (PCR) primers to amplify genes had a region complementary to the gene of interest of 20-25 nucleotides with a melting temperature (T_m) between 68-72°C. A restriction endonuclease site and in some cases a hexa His tag was attached to the gene of interest via the primers. An overhang of five adenines was also added to the primer to assure efficiency of restriction endonuclease cleavage. Components of the INO80 chromatin remodeler were amplified from yeast genomic DNA by PCR using Phusion Flash Master Mix (Finnzymes, Espoo, Finland). Primer concentration was 0.5 μ M each, and approximately 10-50 ng of template DNA was added to each reaction. Each thermocycling program used 30 cycles, with times and temperatures of denaturation, annealing and elongation adjusted to achieve optimal amplification of the respective gene. PCR products were purified from agarose gels using a Gel Extraction Kit (Qiagen, Hilden, or Metabion, Martinsried, Germany).

DNA was digested using restriction endonucleases and corresponding buffers as recommended by the manufacturer. Cleaved vector DNA was additionally treated with calf intestine alkaline phosphatase (Fast AP, Fermentas, St. Leon-Rot, Germany) to prevent re-ligation. For ligation, a threefold molar excess of the digested DNA fragment was incubated with linearized vector and T4 DNA ligase (Fermentas, St. Leon-Rot, Germany) according to the manufacturer's instructions. Incorporation of multiple genes into a single vector via the pFBDM multiplication module was performed as described (Berger et al, 2004).

Transformation of plasmid DNA was performed using chemically competent *E. coli* cells (Hanahan, 1983). Briefly, 100 μ l of competent cells were mixed with 10 μ l of the ligation reaction or 40-200 ng of purified plasmid DNA and incubated on ice for 5 min. In the case of double transformations with two different plasmids the amount of transformed plasmid was increased to 500-1000 ng each. Cells were heat-shocked at 42°C for 45 s and immediately chilled on ice. 800 μ l of fresh LB medium were added, followed by incubation at 37°C for 45 min in a shaking incubator. Cells were plated on LB agar plates containing the respective antibiotics and incubated at 37°C overnight. Plasmid DNA was isolated from a 5 ml overnight culture using a Plasmid Extraction Kit.

2.2.2.2 Oligonucleotides

Table 6: DNA oligonucleotides used for molecular cloning

Name	Sequence in 5' to 3' orientation	Purpose
Arp4_SalI_His6 _TAGzyme_for	AAAAAGTCGACATGAAACATCATCATCATCAT CATAAAATGTCCAATCTGCTTTGCAAGTT	Cloning of Arp4 into pFBDM MCS php
Arp4_NotI_ Stop_bac	AAAAAGCGGCCGCCTATCTA AACCTATCGTTAAGCAATCT	Cloning of Arp4 into pFBDM MCS php
Arp5_SalI_His6 _TAGzyme_for	AAAAAGTCGACATGAAACATCATCATCATAT CATAAAATGTCTAGCAGAGACGCCTCTTTT	Cloning of Arp5 into pFBDM MCS php
Arp5_NotI_ Stop_bac	AAAAAGCGGCCGCTTAGTCT TCAAATACTTCGTATTCCC	Cloning of Arp5 into pFBDM MCS php
Arp8_SalI_His6 _TAGzyme_for	AAAAAGTCGACATGAAACATCATCATCATCATCATA AAATGTCGCAAGAAGAAGCAGAATCCAGTATTATT	Cloning of Arp8 into pFBDM MCS php
Arp8_NotI_ Stop_bac	AAAAAGCGGCCGCCTAGTACGTGA AAATACATTTATATTGTAAGATTCT	Cloning of Arp8 into pFBDM MCS php
yIes4_NdeI_for	AAAAACATATGTCCCAAGAAAGTAGTGTTTTATCA	Cloning of Ies4 into pet28
yIes4_XhoI_ stop_bac	AAAAACTCGAGTTATGAGTCCAGTCCATCCTCTCC	Cloning of Ies4 into pet28
yIes5_NdeI_for	AAAAACATATGCCTAGTAAAGATCCAGAGAGC	Cloning of Ies5 into pet28
yIes5_XhoI_ stop_bac	AAAAACTCGAGTTATGGTGTG TGCGTATCATTATATAATAA	Cloning of Ies5 into pet28
yIes6_NdeI_for	AAAAACATATGAGCGGTAGTAGGGGCAATAGC	Cloning of Ies6 into pet28
yIes6_XhoI_ stop_bac	AAAAACTCGAGCTATTTTA GAACGAAGTTGGCCCTCT	Cloning of Ies6 into pet28
yIes3_XhoI_fw	AAAAACTCGAGATGAAGTTCGAAGACCTCTTGGC	Cloning of Ies3 into pFBDM MCS p10
yIes3_NheI_rv	AAAAAGCTAGCTTAAAGAATGTTTTCCAAAAGGCCG	Cloning of Ies3 into pFBDM MCS p10

Name	Sequence in 5' to 3' orientation	Purpose
Nhp10_SalI_ His8_f	AAAAAGTCGACATGAAACATCATCATCATCATC ATCATAAAATGTCAGTTGAAGAAAAAAGCGCAGAC	Cloning of Nhp10 into pFBDM MCS php
yNhp10_NdeI _for	AAAAACATATGATGTCAGTT GAAGAAAAAAGCGCAGAC	Cloning of Nhp10 into pet21/pet28
Nhp10_NotI_ Stop_bac	AAAAAGCGGCCGCTTAGTTA GAGGAAACTAACTTCCATC	Cloning of Nhp10 into pFBDM MCS php
Ies5_SalI_for	AAAAAGTCGACATGCCTAGTAAAGATCCAGAGAGC	Cloning of Ies5 into pFBDM MCS php
Ies5_NotI_ Stop_bac	AAAAAGCGGCCGCTTATGGTG TGTGCGTATCATTATATAATAA	Cloning of Ies5 into pFBDM MCS php
hArp5_NheI_ for_His	AAAAAAGCTAGCATGAAACATCATCATCATCAT CATCATCATAAAATGGCGGCGAACGTGTTCCC	Cloning of hArp5 into pFBDM MCS p10
hArp5_NsiI_rev	AAAAAATGCATCTATGCCTGCTCACCAGCACC	Cloning of hArp5 into pFBDM MCS p10
hIes6_SalI_for	AAAAAGTCGACATGGCGGCGCAAATTCCAATTGTG	Cloning of hIes6 into pFBDM MCS php
hIes6_NotI_bac	AAAAAGCGGCCGCTCAGGG AACGATGCTCGTGGCCTTCC	Cloning of hIes6 into pFBDM MCS php

2.2.3 Protein biochemistry methods

2.2.3.1 Generation of virus for protein expression in insect cells

Plasmid DNA of expression constructs (pFBDM vector) was transformed into chemically competent DH10MultiBac cells with a prolonged regeneration phase of 4 h at 37°C. Cells were plated on agar plates, containing the appropriate antibiotics (kanamycin, gentamycin, tetracyclin) plus X-Gal (100 µg/ml) and IPTG (40 µg/ml). Plates were incubated at 37°C for 48 h. Successful integration of the gene of interest into the bacmid was assessed by blue/white screening. White colonies were used to inoculate an overnight shaking culture of 100 ml LB plus respective antibiotics. Cells were harvested by centrifugation and the recombinant bacmid isolated using a

Midi-Prep Kit (Qiagen, Hilden, Germany), following the instructions provided by the manufacturer.

Freshly diluted Sf9 insect cells were seeded in a 6-well tissue culture plate (0.4×10^6 cells per well). Typically, cells were transfected with 2 μg of bacmid DNA mixed with 3 μl of FuGENE HD Transfection Reagent (Roche, Basel, Switzerland) according to the manufacturer's protocol. After incubation of the transfected cells for 48-60 h at 27.5°C , the supernatant (viral generation V_0) was collected. Virus was amplified by infecting 10 ml of freshly resuspended Sf9 insect cells (1×10^6 cells/ml) with 1 ml of V_0 . Cells were cultured for 72-96 h in 100 ml flasks at 27.5°C with shaking at 85 rpm. The supernatant (V_1) was harvested by centrifugation and used for a second round of viral amplification by infecting 100-500 ml of Sf9 cells (0.4×10^6 cells/ml) with 1 ml of V_1 . The supernatant (V_2) was harvested by centrifugation and stored as high titer virus at 4°C for subsequent protein expression.

2.2.3.2 Protein expression in *E. coli* and insect cells

For over expression of recombinant proteins, chemically competent *E. coli* Rosetta (DE3) cells (Hanahan, 1983) were transformed with plasmid DNA carrying the gene of interest. Cells were grown at 37°C in LB medium in the presence of the appropriate antibiotics. During the logarithmic growth phase a small amount of cells was removed, mixed with glycerol (10% v/v final concentration), flash frozen in liquid nitrogen and stored as a glycerol stock at -80°C for future protein expression. At an OD 600 of 0.6-0.8 cells were chilled on ice for 20 min and protein expression was induced by the addition of IPTG to a final concentration of 0.5 mM. After further growth overnight at 18°C , cells were harvested by centrifugation at 4°C . Cell pellets were flash frozen in liquid nitrogen and stored at -20°C .

Large scale expression in insect cells was performed by incubating 1 l of freshly resuspended High Five insect cells (cell density: 1.0×10^6 cells/ml) with 20-50 ml of V_2 generation virus. Cells were cultured in 5 l flasks at similar conditions as described for viral titer amplification. Cell growth was monitored using a Countess cell counting device (Invitrogen, Karlsruhe). 48 h after cell proliferation had ceased, cells were harvested by centrifugation, flash frozen in liquid nitrogen and stored at -20°C .

2.2.3.3 Protein Purification

All buffers and their components used for protein purification are listed in Table 7. For purification, cell pellets were resuspended in lysis buffer (LB) and disrupted by extensive sonication. Cell debris was removed by centrifugation (30 min in an SS34 rotor at 15000 rpm for *E. coli* expressed proteins and 2 times 30 min for insect cell expressed proteins). His-tagged constructs were purified using Ni-NTA agarose (Qiagen, Hilden, Germany) packed in a gravity flow cartridge (BIO-RAD, Munich, Germany). After loading of soluble extracts, the resin was washed with Ni-NTA washing buffer containing different amounts of imidazole (20-50 mM) and high salt buffer usually containing 1 M salt. Protein was then eluted by adding 200 mM imidazole to the cell lysis buffer. Most proteins were further purified using anion-exchange columns. The ion exchange column was equilibrated with low salt buffer and after loading, the protein was eluted with a gradient of 20 column volumes from low to high salt buffer. Peak fractions were pooled, concentrated with centrifugal devices (Amicon Ultra, Millipore, Billerica, USA) and loaded onto a Superdex S200 26/60 size exclusion chromatography column (GE Healthcare, Freiburg, Germany) previously equilibrated with gel filtration buffer. Peak fractions were concentrated, flash frozen in liquid nitrogen and stored at -80°C.

Table 7: Buffers used for protein purification

Protein	Lysis buffer (LB)	Ni wash buffer	Ion exchange low salt buffer	Ion exchange high salt buffer	Gel filtration buffer
Arp4	20 mM EPPS	LB +	20 mM EPPS	20 mM EPPS	20 mM EPPS
	pH 8.0 (NaOH)	20 mM	pH 8.0 (NaOH)	pH 8.0 (NaOH)	pH 8.0 (NaOH)
	200 mM NaCl	Imidazole	200 mM NaCl	1 M NaCl	200 mM NaCl
	5% Glycerol	LB +	or 80 mM NaCl	5% Glycerol	5% Glycerol
	5 mM β -Me	1 M NaCl	5% Glycerol	5 mM β -Me	5 mM β -Me
			5 mM β -Me		
Arp5	20 mM Tris	LB +	20 mM Tris	20 mM Tris	20 mM Tris
	pH 8.6 (HCl)	20 mM	pH 8.6 (HCl)	pH 8.6 (HCl)	pH 8.6 (HCl)
	100 mM NaCl	Imidazole	100 mM NaCl	1 M NaCl	100 mM NaCl
	5% Glycerol	-	5% Glycerol	5% Glycerol	5% Glycerol

Protein	Lysis buffer (LB)	Ni wash buffer	Ion exchange low salt buffer	Ion exchange high salt buffer	Gel filtration buffer
Arp8	20 mM EPPS	LB +	20 mM EPPS	20 mM EPPS	20 mM EPPS
	pH 8.0 (NaOH)	20 mM	pH 8.0 (NaOH)	pH 8.0 (NaOH)	pH 8.0 (NaOH)
	200 mM NaCl	Imidazole	200 mM NaCl	1 M NaCl	200 mM NaCl
	5% Glycerol	LB +	5% Glycerol	5% Glycerol	5% Glycerol
	5 mM β -Me	1 M NaCl	5 mM β -Me	5 mM β -Me	5 mM β -Me
Nhp10	20 mM MOPS	LB +			20 mM MOPS
	pH 6.5 (NaOH)	20 mM			pH 6.5 (NaOH)
	300 mM NaCl	Imidazole	-	-	300 mM NaCl
	5% Glycerol	LB +			5% Glycerol
		1 M NaCl			
Ies4	20 mM HEPES	LB + 50 mM			20 mM HEPES
	pH 7.5 (NaOH)	Imidazole	-	-	pH 7.5 (NaOH)
	200 mM NaCl	LB +			200 mM NaCl
	5% Glycerol	1 M NaCl			5% Glycerol
Ies5	20 mM Tris	LB + 50 mM	20 mM Tris	20 mM Tris	20 mM Tris
	pH 8.6 (HCl)	Imidazole	pH 8.6 (HCl)	pH 8.6 (HCl)	pH 8.6 (HCl)
	100 mM NaCl	LB +	100 mM NaCl	1 M NaCl	100 mM NaCl
	5% Glycerol	1 M NaCl	5% Glycerol	5% Glycerol	5% Glycerol
Ies6	20 mM Tris	LB +	20 mM Tris	20 mM Tris	20 mM Tris
	pH 7.6 (HCl)	30 mM	pH 7.6 (HCl)	pH 7.6 (HCl)	pH 7.6 (HCl)
	100 mM LiCl	Imidazole	100 mM LiCl	1 M LiCl	100 mM LiCl
	5% Glycerol		5% Glycerol	5% Glycerol	5% Glycerol
	5 mM β -Me	-	5 mM β -Me	5 mM β -Me	5 mM β -Me
Nhp10/ Ies5	20 mM Tris	LB +	20 mM Tris	20 mM Tris	20 mM Tris
	pH 8.6 (HCl)	40 mM	pH 8.6 (HCl)	pH 8.6 (HCl)	pH 8.6 (HCl)
	250 mM NaCl	Imidazole	150 mM NaCl	1 M NaCl	100 mM NaCl
	5% Glycerol	LB +	5% Glycerol	5% Glycerol	5% Glycerol
	1 M NaCl				

Protein	Lysis buffer (LB)	Ni wash buffer	Ion exchange low salt buffer	Ion exchange high salt buffer	Gel filtration buffer
Nhp10/ Ies3/ Ies5	20 mM Tris	LB +	20 mM Tris	20 mM Tris	20 mM Tris
	pH 8.3 (HCl)	40 mM	pH 8.3 (HCl)	pH 8.3 (HCl)	pH 8.3 (HCl)
	100 mM NaCl	Imidazole	100 mM NaCl	1 M NaCl	100 mM NaCl
	5% Glycerol	LB +	5% Glycerol	5% Glycerol	5% Glycerol
	2 mM β -Me	2 M NaCl	2 mM β -Me	2 mM β -Me	5 mM β -Me
hArp5/ hIes6	20 mM Tris	LB +	20 mM Tris	20 mM Tris	20 mM EPPS
	pH 8.0 (HCl)	40 mM	pH 8.0 (HCl)	pH 8.0 (HCl)	pH 8.0 (NaOH)
	200 mM NaCl	Imidazole	200 mM NaCl	1 M NaCl	200 mM NaCl
	5% Glycerol	LB +	5% Glycerol	5% Glycerol	5% Glycerol
	5 mM β -Me	2 M NaCl	5 mM β -Me	5 mM β -Me	5 mM β -Me
Rvb1/ Rvb2	20 mM EPPS	LB	20 mM EPPS	20 mM EPPS	20 mM EPPS
	pH 8.0 (NaOH)	+ 50 mM	pH 8.0 (NaOH)	pH 8.0 (NaOH)	pH 8.0 (NaOH)
	100 mM NaCl	Imidazole	100 mM NaCl	1 M NaCl	100 mM NaCl
	5% Glycerol	-	5% Glycerol	5% Glycerol	5% Glycerol
	5 mM β -Me	-	5 mM β -Me	5 mM β -Me	5 mM β -Me

2.2.3.4 Analytical size exclusion chromatography

The elution behavior of a protein on a gel filtration column is related to its hydrodynamic volume which in turn is related to the molecular mass of the protein. Usually, the elution point of a sample decreases linearly with the logarithm of the molecular volume and can be used to estimate the molecular mass of the sample. To this end, a gel filtration column is calibrated with a standard containing globular proteins of known molecular mass to generate a trend line. The trend line is then used to calculate the molecular mass of an unknown sample from its elution volume. Care has to be taken when analyzing samples that do not behave ideally, for example elongated or partially unfolded proteins. In this case the molecular weight determined by gel filtration does not correspond to the actual molecular weight.

Experimentally, the elution from a Superdex 200 26/60 gel filtration column, or a high resolution Superose 6 PC 3.2/30 column connected to an Ettan LC System (GE Healthcare, Freiburg, Germany) was used to estimate the molecular weight of a given sample. A gel filtration standard

containing thyroglobulin (670 kDa), bovine gamma-globulin (158 kDa), chicken ovalbumin (44 kDa), equine myoglobin (17 kDa) and vitamin B₁₂ (1.35 kDa) (Bio-Rad, Munich, Germany) was used to calibrate the columns.

2.2.3.5 Surface plasmon resonance

The phenomenon of surface plasmon resonance (SPR) can occur when a beam of light passes from a medium with high refractive index (e.g. glass) into a medium with low refractive index (e.g. water). If the angle of the incident beam is larger than a critical angle the light is completely reflected at the interface of both media leading to total internal reflection. This complete reflection is abolished however if the surface of the glass is coated with a thin film of metal, usually gold. In this case the incident beam can resonate with the electrons in the metal leading to the creation of an evanescent field that penetrates about 300 nm into the metal and the aqueous environment. This causes a loss of intensity in the reflected light which is maximal at a defined angle called the surface plasmon resonance angle. Most importantly the exact position of this angle is dependent on the refractive index of the aqueous medium which in turn can be altered by the addition of protein. As the evanescent field only enters a small distance into the medium the changes of the surface plasmon resonance angle are most sensitive to changes directly on the surface of the gold layer.

In the actual experiment, SPR can be used to monitor the binding event of two interactors for example two proteins or protein and DNA. One binding partner, usually the smaller one is coupled to the gold surface and the other partner passes over this surface. If binding occurs it changes the molecular mass present on the gold surface and in turn the refractive index leading to a positional shift of the surface plasmon resonance angle which can be measured very sensitively by the instrument. The change is usually quantified in resonance or response units (RUs). This allows for very sensitive measurements of binding affinities and even binding kinetics as the association and dissociation of the binding partners can be measured separately. For a comprehensive review of the SPR technique compare (Golemis & Adams, 2005).

The experiments were carried out on a Biacore X-100 machine (GE Healthcare, Freiburg, Germany). About 300 resonance units of actin were immobilized on the surface of a CM5 chip (GE Healthcare, Freiburg, Germany) by amine coupling at pH 5.0. Binding experiments were performed in a buffer of 10 mM EPPS pH 8.0, 150 mM NaCl and 5 mM β -ME at a flow rate of

10 $\mu\text{l}/\text{min}$ at 25°C . Functionality of the chip was tested by addition of DNaseI as a positive binding control and BSA as a negative control. Arp4 and Arp8 were passed over the chip in a concentration range of 1-60 μM and 0.01-10 μM respectively, and allowed to bind for 120 s. The change in surface plasmon resonance was measured and the sensograms recorded. The chips were regenerated after each successive round of binding by three alternate additions of running buffer containing 3 M NaCl and 0 M NaCl, respectively. This regeneration procedure did not alter the ability of the immobilized actin to bind protein in subsequent cycles. Analysis of the data was performed using the BIAevaluation software supplied with the instrument. The steady state binding response in the case of Arp4 was determined by averaging the response over 5 s at the end of the injection and was corrected for background binding. data were fitted to a 1:1 binding model.

2.2.4 Structural methods

2.2.4.1 X-ray crystallography

For a detailed description of protein crystallography and the theoretical background of structure determination by X-ray diffraction compare (Bergfors, 2009; Drenth & Mesters, 2007; Rhodes, 2006).

2.2.4.1.1 Protein crystallization

Protein crystals that diffract X-rays are the prerequisite for structure determination by X-ray crystallography. Crystals are repetitive and regular arrangements of molecules in a three dimensional lattice and are formed, when proteins “precipitate” very slowly from supersaturated solutions in an ordered manner. This thermodynamically driven process includes nucleation, growth of the crystal and growth termination, and is dependent on a variety of parameters, like pH, temperature, protein concentration, and nature of the precipitant. Many crystallization conditions have to be screened and optimized to find the most useful condition for the generation of good quality crystals. The most frequently used procedure for obtaining protein crystals is the vapor diffusion method (sitting drop or hanging drop). In this case, a buffered protein solution is mixed with precipitant solution and kept in a sealed chamber with a reservoir that contains a more concentrated precipitant solution. Equilibrium between the drop and the reservoir is slowly reached through vapor diffusion. The precipitant concentration in the drop is increased by loss of

water to the reservoir. Once the saturation point is reached, and other conditions such as pH and temperature are chosen correctly, protein crystals will form in the drop, which might be suitable for X-ray diffraction experiments.

2.2.4.1.2 Theory of X-ray diffraction

X-rays are electromagnetic waves with a wavelength in the range of atomic distances (ca. 10^{-10} m = 1 Å). They are capable of interacting with the electrons of atoms in the protein crystal, causing dipole oscillation of the electrons at the X-ray frequency. The oscillating electrons then emit X-rays with the same wavelength as the incident beam in every direction, a phenomenon that is called elastic scattering. As a crystal is composed of molecules which are periodically repeated in three dimensions, the emitted waves scattered from different atoms can interfere, normally cancelling each other out. Only if the light path of waves differ by $n\lambda$ (with n being an integer), constructive interference is observed. The difference in the light path is thereby dependent on the distance between the scattering atoms. Thus, scattering can be described as reflection at imaginary lattice planes. The lattice planes pervade the crystal lattice and its lattice points. Intersections with the unit cell axes of the crystal lattice are termed Miller Indices (h,k,l), which describe the orientation of and the spacing between a set of parallel lattice planes. The conditions for constructive interference are given by Bragg's Law:

$$n \cdot \lambda = 2 \cdot d \cdot \sin \theta$$

Only if the distance d between parallel lattice planes and the angle θ between the lattice planes and the incident beam follow Bragg's Law, a reflection (h,k,l) is observed. The intensity of each reflection (h,k,l) represents the overall scattering from a particular set of parallel lattice planes (h,k,l). According to Friedel's Law, reflections (h,k,l) and (-h,-k,-l) have the same magnitude, but opposite signs for phase angles (Friedel mates).

2.2.4.1.3 Electron density calculation and the phase problem

Electrons around atom nuclei are delocalized and their positions are described as a three dimensional distribution, the so called electron density distribution ρ . As crystals are periodic assemblies of molecules, the electron density of a crystal resembles a periodic function. Thus, a Fourier Transformation (Fourier-Summation) can be applied to calculate the electron density for each point (x, y, z) in a crystal:

$$\rho(x, y, z) = \frac{1}{V} \sum_{hkl} F(h, k, l) e^{-2\pi i(hx+ky+lz)}$$

This formula represents the summation over all structure factors $F(h,k,l)$ for each position (x,y,z) in a normalized unit cell $(1/V)$.

The structure factor $F(h,k,l)$ (the Fourier coefficient) is the sum of scattering contribution of all atoms j in a unit cell, with (x,y,z) as fractional coordinates, to a reflection (h,k,l) , and can be derived from the following equation.

$$F(h, k, l) = \sum_{j=1}^N f_j \cdot e^{[2\pi i(hx_j+ky_j+lz_j)]} \cdot e^{-B \cdot \sin^2 \frac{\theta}{\lambda^2}}$$

The atomic scattering factor (or form factor) f_j describes the scattering power of an atom j , which is dependent on the atom type and the diffraction angle (resolution) of the corresponding reflection. The Debye-Waller- or B-factor, the last term in this equation, represents the contribution of thermal disorder or “vibration” (isotropic/anisotropic).

The electron density ρ is related to $F(h,k,l)$ by a direct Fourier Transformation:

$$F(h, k, l) = V \cdot \int_{x=0}^a \int_{y=0}^b \int_{z=0}^c \rho(x, y, z) \cdot e^{[2\pi i(hx+ky+lz)]} dx dy dz$$

Thus, the structure factor $F(h,k,l)$ can be easily calculated from a known structure.

In contrast, *de novo* structure determination deals with the inverse problem. $F(h,k,l)$ is a complex number, which is formed by the amplitude $|F(h,k,l)|$ and the phase $\alpha(h,k,l)$ of a scattered wave:

$$F(h, k, l) = |F(h, k, l)| e^{[i \cdot \alpha(h,k,l)]}$$

The already mentioned inverse Fourier Transformation can be written so that the phase term $\alpha(h,k,l)$ becomes evident.

$$\rho(x, y, z) = \frac{1}{V} \sum_{hkl} |F(h, k, l)| \cdot e^{[-2\pi i(hx+ky+lz-\alpha(h,k,l))]}$$

Whereas the amplitude $|F(h,k,l)|$ of a scattered wave is proportional to the square root of the measured intensity ($I = |F|^2$) for each reflection (h,k,l) , and is directly available from the

diffraction pattern, the phase information is lost during measurement and thus accounts for the unknown component of the complex number $F(h,k,l)$. This is the so called “phase problem” in crystallography.

To overcome the phase problem in *de novo* structure determination, several approaches are applied including isomorphous replacement and anomalous scattering techniques, or a combination of both methods. This usually requires the binding of a heavy atom and/or the presence of anomalous scattering atoms, to the protein in the crystal. However, if parts of the structure or the structure of a close homologue are known, phases can be obtained by molecular replacement. In this thesis, molecular replacement techniques were used to obtain phases and will be described briefly in the following part.

The Patterson function is an important tool to obtain phase angles in *de novo* structure determination. It is a Fourier Transformation of the measured intensities (its squared reflection amplitudes $|F|^2$), which do not depend on phases (phase angle = 0°):

$$P(u, v, w) = \frac{1}{V} \sum_{hkl} |F(h, k, l)|^2 \cos[2\pi(hu + kv + lw)]$$

The Patterson unit cell is given in (u,v,w) , and has identical dimensions as the real unit cell (x,y,z) . The Patterson function results in a map (Patterson map) of interatomic distance vectors. The endpoints of the vectors represent the multiplied electron density, and thus their height depends on the electron number of the respective atoms, which makes it useful to determine the relative position of heavy atoms in a unit cell.

2.2.4.1.4 Molecular replacement

Molecular replacement is possible when parts of a protein structure or the structure of a close structural homologue of a protein are already known. The phase angles of the unknown structure are thereby obtained from the known structure. For this, the known model has to be rotated and translated into the electron density of the unknown structure. The replacement is a 6-dimensional search problem (or two 3 dimensional searches), which can be solved with the Patterson function. During translation and rotation search, the Patterson maps of the model structure and of the crystal diffraction data are compared. The intramolecular vectors depend only on the orientation of the molecule and are used for the rotation search. The radius of the unit cell

thereby limits the length of the included vectors. The translation search uses intermolecular cross vectors, which depend on both the orientation and the position of the molecule. The derived coordinates of the molecules in the unit cell then allow the calculation of new structure factor amplitudes $|F_{\text{calc}}|$ and an estimation of the respective phase angles α_{calc} . The following equation then allows the calculation of an electron density for the new crystal structure with the help of the experimentally derived structure factor amplitudes $|F_{\text{obs}}|$:

$$F(\mathbf{h}) = (|F_{\text{obs}}| - |F_{\text{calc}}(\mathbf{h})|) \cdot e^{i\alpha_{\text{calc}}(\mathbf{h})}$$

The calculated F_o - F_c density is useful for finding corrections between the new and the known model. But it has always a bias towards the model structure, from which the phase angles were derived. To minimize model bias, usually the following equation is used:

$$F(\mathbf{h}) = (2|F_{\text{obs}}| - |F_{\text{calc}}(\mathbf{h})|) \cdot e^{i\alpha_{\text{calc}}(\mathbf{h})}$$

This $2F_o$ - F_c electron density is used to build in the new structure or to change variations, to find a closer agreement between the calculated and observed structure factors. In the refinement procedure a reliability factor, the so called R-factor, is used to monitor the quality of the model.

2.2.4.2 Small angle X-ray scattering (SAXS)

Small angle X-ray scattering allows gathering of structural information about proteins and other biomolecules in solution. In contrast to crystallography, which is no solution method it can be performed in a buffer of choice and is thus closer to the actual conditions in which proteins occur *in vivo*. Unlike NMR spectroscopy which can be used to determine the structure of small proteins in solution, SAXS has no limitations in terms of protein size that can be studied. The structures obtained from SAXS data by *ab initio* modeling however are of relatively low resolution and not always unambiguously defined.

It is thus beneficial to compare SAXS structures with existing high resolution data such as partial crystal structures to further evaluate the obtained model. Through this combination with X-ray crystallography SAXS is a powerful tool which may provide more accurate and complete models of protein structures, conformation, interactions and assemblies in solution (Putnam et al, 2007). This is especially true for proteins, or protein complexes that are too large and flexible to be studied by X-ray crystallography.

SAXS has been the topic of excellent reviews and the theoretic background will be described only briefly (Koch et al, 2003; Putnam et al, 2007). In a SAXS experiment the incident X-ray wave is scattered by the electrons surrounding the atoms of the examined biomolecule as well as the electrons present in the solvent. As the contribution of the solvent scattering is relatively high, SAXS is a contrast method that relies on a difference in electron density between the scattering biomolecule and the surrounding solvent. Because of that SAXS experiments are very sensitive to changes in the buffer and always require accurate measurements of a buffer control which is then subtracted from the actual sample measurement to create the final scattering curve. Since the scattering molecules are spatially averaged in solution the scattered waves are averaged as well and do not add up to a defined diffraction pattern as in X-ray crystallography. Still the scattering can be recorded as a function of the scattering angle and structural information can be extracted. The scattering image is usually recorded as a function of the momentum transfer $s = \frac{4\pi \sin \theta}{\lambda}$ where 2θ is the scattering angle.

At the lowest resolution, SAXS scattering is dictated by a single size parameter, the radius of gyration (R_G). The R_G is the square root of the average squared distances of each scatterer from the center of the particle that is scattering X-rays and therefore a measure for the size of the particle. For well-behaving samples with no inter-particle interference or aggregation the scattering can be related by the Guinier approximation where I_0 is the intensity at the scattering amplitude $s = 0$.

$$I(s) \cong I_0 \cdot e^{-\frac{1}{3}R_G^2 s^2}$$

The Guinier plot, where $\ln(I(s))$ is plotted versus s^2 should give a linear function with I_0 as intercept and a slope that can be used to calculate R_G . Only very homogenous samples with low intermolecular attractive forces will give a linear Guinier plot. Therefore, it is a useful tool to test sample quality.

Whereas analysis of low s -values gives information about the particle dimension, analysis of high s -values yields details regarding the molecular shape. For a folded macromolecule the intensity of the scattering falls off with Porod's law:

$$I(s) \propto s^{-4}$$

The Kratky plot $s^2I(s)$ as a function of s , which is deduced from Porod's law and which can be calculated directly from the scattering curve, provides an excellent tool for evaluating the folding state of a sample. For folded domains, which have intensities that fall off proportional to s^{-4} , the Kratky plot yields a peak roughly shaped like a parabola. Unfolded peptides lack the characteristic folded peak and are linear in the large s regions (see Figure 9).

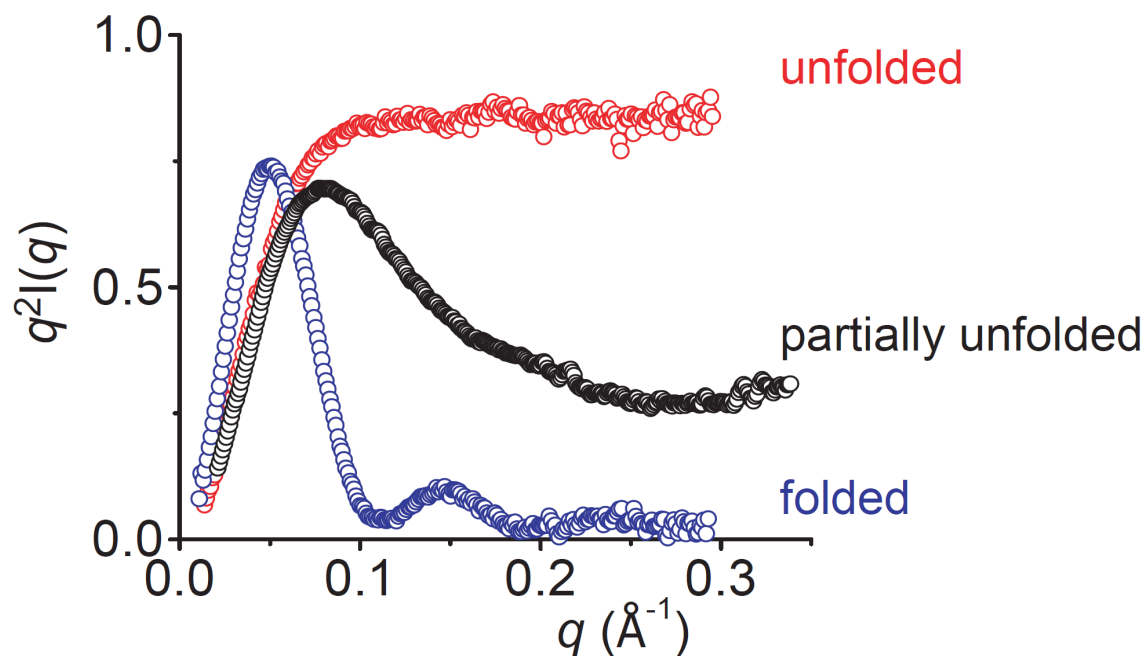


Figure 9: Kratky plots of typical protein samples

Globular macromolecules such as most properly folded proteins have bell-shaped curves. Extended molecules such as unfolded proteins lack a defined peak and have a plateau in the larger s range. Figure has been taken from (Putnam et al, 2007).

After the quality of the protein sample has been critically assessed, the scattering profile $I(s)$ is Fourier transformed into the pair distribution function according to the following equation:

$$p(r) = \frac{r^2}{2\pi^2} \int_0^{\infty} s^2 I(s) \frac{\sin sr}{sr} dr$$

The pair distribution function can be understood as a two-dimensional Patterson function that illustrates the frequency with which vectors of the length r connect two volume elements within the molecule. The pair distribution function is a real space representation and therefore much more intuitive than the primary scattering curve. The shape of the pair distribution function

provides information about the shape of the molecule. Theoretically, the $p(r)$ is zero at $r = 0$ and at $r \geq D_{\max}$, where D_{\max} corresponds to the maximum linear dimension of the scattering particle. D_{\max} cannot be directly calculated from the scattering data but must be estimated for a given molecule. In practice an iterative process is used, with multiple D_{\max} values chosen and the resulting $p(r)$ functions evaluated for their fit to the experimental data.

As described above, parameters like R_G , D_{\max} , or the folding state of the sample can be derived in a straightforward manner directly from the scattering data. In a computationally more demanding step the three dimensional reconstruction of the particle from the two-dimensional scattering curve is also feasible. Fitting the data leads to a multidimensional minimization problem that can be solved numerically. To achieve reasonable models it is helpful to add physical restraints, like imposing a uniform density on the interior of the molecule. The program GASBOR models a protein structure by comparing thousands of configurations of a chain of dummy residues where each dummy correspond to a single amino acid in the protein of interest (Konarev et al, 2006). The structure is approximated by iterative rounds of simulated annealing with additional penalties for non-protein-like density. To improve model quality the results of several individual GASBOR runs are then aligned and averaged to obtain a final shape. Through comparison of different models and assessment of their uniformity, an evaluation of the reliability of the final model is possible. In a perfect monodisperse system all runs should converge on a similar structure.

2.2.5 Structural studies on *S. cerevisiae* Arp4

2.2.5.1 Protein crystallization

For protein crystallization purified Arp4 was reductively methylated according to a standard protocol (Kim et al, 2008). After complete methylation the protein was again subjected to gel filtration on Superdex 200 (GE Healthcare) and freshly concentrated to about 8 mg/ml. Crystallization was performed by hanging drop vapor diffusion against 27% w/v PEG2000MME, 0.1 M HEPES-NaOH pH 7.0, 6% w/v D+-trehalose, 50 mM glycine at 20°C. Rod shaped crystals in space group $P6_1$ grew to useful sizes in about 2-3 weeks and were frozen in liquid nitrogen with 20% v/v glycerol in the mother liquor as cryo protectant.

2.2.5.2 Crystal structure determination

Diffraction data to a limiting resolution of 3.4 Å were collected on a single crystal at 100 K with a wavelength of 1.0 Å at beam line X06SA (Swiss Light Source, Villigen, Switzerland). The data set was processed and scaled using XDS (Kabsch, 1993). A molecular replacement model was generated from the structure of yeast actin (pdb: 1YAG) using CHAINSAW (Stein, 2008). All side chains of non identical residues between actin and Arp4 were truncated at the β carbon and up to ten residues N-terminal and C-terminal of insertions were deleted. Molecular replacement was carried out with PHASER (McCoy et al, 2007) and four molecules per asymmetric unit were found. The model was optimized by cyclic rounds of manual model building using COOT (Emsley & Cowtan, 2004) and refinement with PHENIX (Adams et al, 2010) applying NCS restraints for all chains. The stereochemistry of the refined structure was analyzed by Procheck (Laskowski et al, 1993) with 86.8%, 12.4%, 0.8% and 0% of residues in the most favored, additionally allowed, generously allowed and disallowed regions of the Ramachandran plot, respectively. Coordinates have been deposited in the protein data bank (accession code 3QB0).

2.2.5.3 Solution structure of Arp4

Arp4 protein samples for SAXS measurements were purified by preparative size-exclusion chromatography (in 20 mM EPPS pH 8.0, 100 mM NaCl, 2% v/v glycerol and 5 mM β-ME). As a buffer reference for the measurements the flow through of the concentration step was used. SAXS data were collected at beam line X33, EMBL/DESY (Hamburg, Germany) at a cell temperature of 20°C. Molecular weight estimation of Arp4 samples in solution, was performed by comparison of the corresponding $I(o)$ -values from Guinier approximation with BSA (66 kDa) and Porod-volume analysis (Putnam et al, 2007). Arp4 was measured at protein concentrations of 2.1, 4.7 and 7.2 mg/ml. Data were processed using the ATSAS package (Konarev et al, 2006). A set of 10 independent *ab initio* structures was calculated using GASBOR without any prior symmetry information. Models were aligned and averaged using DAMAVER (Volkov & Svergun, 2003). For representation purposes the bead models were transformed to an electron density using the SITUS package (Wriggers & Chacon, 2001). Docking of structures into these densities was done using UCSF Chimera (Pettersen et al, 2004). Comparison between measured scattering data and theoretical scattering data from the existing structure was done using CRY SOL (Svergun et al, 1995).

2.2.6 Structural studies on *S. cerevisiae* Arp8

Two different *S. cerevisiae* Arp8 constructs were generated to derive solution structures by SAXS measurements. Full length Arp8 and a truncated Arp8 missing the N-terminal 244 amino acids were purified by preparative size exclusion chromatography (in 20 mM EPPS pH 8.0, 100 mM NaCl, 2% v/v glycerol and 5 mM β -ME) using a Superdex-200 (GE Healthcare). Measurements and data analysis were carried out like in the case of Arp4. The proteins were measured at concentrations of 1.4, 4.3, and 8.1 mg/ml, respectively.

2.2.7 Structural studies on *S. cerevisiae* Rvb1-Rvb2

The Rvb1-Rvb2 complex was purified using a bicistronic expression construct containing the ATPase dead mutants of Rvb1 (E312Q and E391G) and Rvb2 (E297Q) which was created by Harald Dürr in the laboratory of Prof. Karl-Peter Hopfner. During the purification of Rvb1-Rvb2 complex, the final gel filtration revealed that two species are present in the preparation. Both species, which might correspond to a “6mer” and a “12mer”, respectively were concentrated separately and subsequently used for crystallization setups.

Crystallization of purified Rvb1-Rvb2 complex (ATPase mutants) was carried out by hanging drop vapor diffusion at concentrations of about 10 mg/ml (monomer concentration). The two species derived after gel filtration (“6mer” and “12mer”) were crystallized separately. Additionally, both Rvb1-Rvb2 complexes were reductively methylated and subjected to crystal screening (Kim et al, 2008). Final crystal conditions used were 1.2 M ammonium tartrate dibasic pH 7.8, 0.1 M HEPES-NaOH pH 7.0 (for the methylated 6mer peak) and 0.5 M ammonium dihydrogen phosphate, 0.1 M tri-sodium citrate pH 5.5, 0.25 M lithium sulfate (both for the unmethylated “6mer” and “12mer” peaks). Crystals grew to final sizes within several days and were frozen in liquid nitrogen with different cryoprotectants. Diffraction was tested at different beam lines at the ESRF and SLS.

2.2.8 Structural studies on the entire *S. cerevisiae* INO80 complex

The intact INO80 complex can be purified endogenously from *S. cerevisiae* using a strain expressing a FLAG-tag on the scaffold protein INO80 (Shen, 2004; Shen et al, 2000). Purification was carried out as published (Shen, 2004) with the additional final purification step of size exclusion chromatography using an analytical Superose 6 PC 3.2/30 column (GE

Healthcare). Gel filtration was performed in 25 mM HEPES pH 7.5, 100 mM KCl, 5% v/v glycerol, 2 mM MgCl₂, 1 mM EDTA, 2 mM DTT without detergent. Peak fractions were pooled and concentrated to be analyzed by negative stain electron microscopy.

For electron microscopic studies, carbon coated copper grids were glow discharged in vacuum for 45 s to provide a negatively charged surface. Typically, 3.5 µl of a 0.2 mg/ml solution of INO80 complex was applied to the charged grids and incubated for 45 s. Grids were washed with water and negatively stained by 2% w/v uranyl acetate. The microscopic analysis was performed on a 120 kV Spirit electron microscope equipped with a 2K CCD camera (FEI, Hillsboro, USA).

2.2.9 Actin biochemistry methods

All experiments concerning the effect of Arp8 on actin dynamics were carried out using the truncated version of Arp8 lacking the N-terminal 244 amino acids. This Arp8 variant that contains the actin fold of Arp8 was confirmed to be properly folded by SAXS experiments (see section 3.6.5).

2.2.9.1 Pyrene actin assays

Actin was purified from rabbit muscle and labeled with pyrene according to standard protocols (Hertzog & Carlier, 2005). Prior to the experiments, Ca²⁺-ATP-actin was converted to Mg²⁺-ATP-actin by addition of 10x Mg-exchange buffer (20 mM Tris pH 8.0, 2 mM ATP, 1 mM MgCl₂, and 0.5 mM DTT). For assembly assays, dilutions of proteins were prepared in storage buffer (20 mM EPPS pH 8.0, 100 mM KCl, 5 mM β-ME, 2% v/v glycerol,) and 10x low salt KMEI buffer was added (250 mM KCl, 10 mM MgCl₂, 10 mM EGTA, and 100 mM imidazole pH 7.3). Anti-foam 204 (Sigma) and KCl were added to reach final concentrations of 0.005% v/v, and 50 mM, respectively. 18 µl of a 40 µM solution of 10% pyrene labeled Mg²⁺-ATP-G-actin (in 2 mM Tris, pH 8.0, 0.2 mM ATP, 0.1 mM CaCl₂, and 0.5 mM DTT) were placed in an 8-well microtiter assembly strip (Thermo Scientific). The assembly reaction was initiated by transferring 162 µl of the protein solution to 18 µl of pyrene labeled actin. The polymerization of actin was followed by measuring the fluorescence increase of pyrene actin (excitation at 364 nm and emission at 407 nm) in a Fluoroskan II plate reader (Thermo Scientific) for at least 1500 s. For polymerization experiments with Mg²⁺-ADP-actin monomers, ATP was replaced by ADP in all buffers. The relative polymerization rate was derived by measuring the slopes from the points

where 10–50% of the actin had assembled. The amount of F-actin at steady state was obtained by measuring pyrene fluorescence after 16 h incubation of the reaction at 4°C.

For analysis of the effects of Arp4 and Arp8 on F-actin, 40 μM Mg^{2+} -ATP-actin (15% pyrene labeled) was polymerized over night in KMEI-buffer. The assays were performed by rapidly mixing 10 μl of different Arp4 and Arp8 concentrations in KMEI buffer with 90 μl of a solution of 2.2 μM F-actin. Pyrene fluorescence decrease was monitored with a Jasco FP-6500 fluorimeter. For depolymerization experiments in ADP containing buffer, ATP was hydrolyzed by adding 10 U/ml hexokinase (Sigma) and 20 mM glucose to the mixture.

2.2.9.2 *In vitro* TIRF microscopy

Total internal reflection fluorescence microscopy (TIRFM) is an optical technique with resemblance to surface plasmon resonance. A laser beam passes a medium of high refractive index (immersion oil) to reach a medium of low refractive index, the aqueous solution to be studied. The incident angle of the beam is chosen so that the light is totally reflected at the interface of both media. The consequence is the creation of an evanescent wave which permeates into the medium of lower refractive index albeit only about 200 nm. As a result only fluorophores close to the interface of both media are excited and thus unwanted background fluorescence is largely avoided (Breitsprecher et al, 2009). Using fluorescently labeled actin, this allows for the study of nucleation and growth of single actin filaments.

Time-lapse TIRFM on Oregon-Green-(OG)-labeled actin was essentially performed as described (Breitsprecher et al, 2008). Briefly, images from an Olympus IX-81 inverted microscope were captured every 5 s with exposures of 200 ms with a Hamamatsu Orca-R2 CCD camera (Hamamatsu Corp., Bridgewater, NJ). The pixel size corresponded to 0.11 μm . Reactions in TIRF-assays contained 1.3 μM actin (30% OG-labeled). Prior to the experiments, Ca^{2+} -ATP actin was converted to Mg^{2+} -ATP actin by addition of 10x Mg-exchange buffer. Polymerization experiments were performed in TIRF buffer (10 mM imidazole, 50 mM KCl, 1 mM MgCl_2 , 1 mM EGTA, 0.2 mM ATP, 10 mM DTT, 15 mM glucose, 20 $\mu\text{g/ml}$ catalase, 100 $\mu\text{g/ml}$ glucose oxidase, and 0.5% methylcellulose (4000 cP) pH 7.4). The elongation rates of filaments were calculated with ImageJ software using the plugins MtrackJ and Manual Tracking. Each experiment was repeated at least 3 times. For each polymerization measurement, at least 15 barbed ends of individual filaments were manually tracked. The average number of actin

filaments was obtained by counting them in an area of 100x140 μm at 200 s after initiation of the polymerization reaction.

2.2.9.3 Critical concentration assay

For determination of the critical concentration (C_{crit}) of F-actin in the presence of Arp4 and Arp8, 20 μM of the respective protein were mixed with pre-polymerized F-actin (20% pyrene labeled) in a concentration range from 5 nM to 10 μM in KMEI- and Mg-exchange buffer and incubated at room temperature in the dark. After 16 h, pyrene fluorescence was detected in a Fluoroskan II plate reader (Thermo Scientific). C_{crit} was derived from plots of fluorescence versus actin concentration as intercept of the linear regressions of filamentous and monomeric actin signals. Dissociation constants were derived using the following equation (Hertzog & Carlier, 2005):

$$K_D = ([\text{Arp}] - [C_{\text{critArp}}] + [C_{\text{critCapped}}]) * [C_{\text{critCapped}}] / ([C_{\text{critArp}}] - [C_{\text{critCapped}}])$$

$[\text{Arp}]$ is the total concentration of Arp4 or Arp8, respectively. $[C_{\text{critArp}}]$ is the concentration of unpolymerized actin given by the intercept of the linear regression lines of the signals for filamentous and monomeric actin in the presence of Arp and capping protein. $[C_{\text{critCapped}}]$ is the critical concentration for polymerization determined as the intercept of the regression lines for filamentous and monomeric actin in the absence of Arp and presence of capping protein.

2.2.9.4 Sedimentation assay

100 μl of a solution of 5 μM Mg^{2+} -ATP-actin were polymerized either alone or in presence of Arp4 and Arp8 by addition of 1x KMEI-buffer and incubated for 5 h at room temperature. F-actin was sedimented by centrifugation for 30 min at 120,000 g. Subsequently, pellets and supernatants were analyzed by SDS-PAGE, and the band intensities were quantified using the profile plotting tool implemented in the ImageJ software.

2.2.9.5 Pointed end elongation assay

F-actin (20% pyrene labeled) was used at an assay concentration of 20 nM capped by 3 nM CapZ to seed pointed end elongation in the presence of different Arp4 concentrations. Monomeric actin (20% pyrene labeled) was added to polymerize from the pointed end and fluorescence was monitored as a signal for polymerization.

3. Results

3.1 Structural studies on the INO80 holo-complex

Structural knowledge about the architecture and the interplay between different subunits of the INO80 complex is scarce. To get an idea about the structure of the entire INO80 complex, it was attempted to obtain a low resolution shape of the intact complex from negative stain electron microscopy (EM) data. The resulting three dimensional model could subsequently serve as a template to place high resolution structures of single components or subcomplexes of INO80, obtained with other structural methods, with respect to each other. This hybrid approach could lead to a detailed picture of the assembly of the INO80 complex.

To this end, a FLAG tagged INO80 complex was purified endogenously from *S. cerevisiae* in amounts and purity suitable for electron microscopy. About 100 g of wet cell pellet was obtained by growing 12 l of a yeast strain with chromosomally FLAG tagged INO80 protein in shaking flasks and used as starting material to purify the complex. FLAG affinity purification (Shen, 2004) was followed by gel filtration on an analytical Superose 6 PC 3.2/30 column with a void volume of 0.8 ml. The protein complex eluted at a volume of about 1.12 ml which according to the column calibration corresponds to a molecular mass of about 4.5 MDa. This is considerably more than the theoretical complex mass of about 1.2 MDa (see Figure 10). The mass determination with the help of gel filtration is highly inaccurate for such large complexes however, as the mass of the complex is in the upper region of the separation range of the column and the gel filtration standard used to calibrate the column contains thyroglobulin (670 kDa) as the largest component.

After the last purification step about 55 μ g of pure complex could be obtained from 100 g of yeast cell pellet. This material was used for subsequent electron microscopy studies at concentrations of about 0.2 mg/ml (see Figure 10).

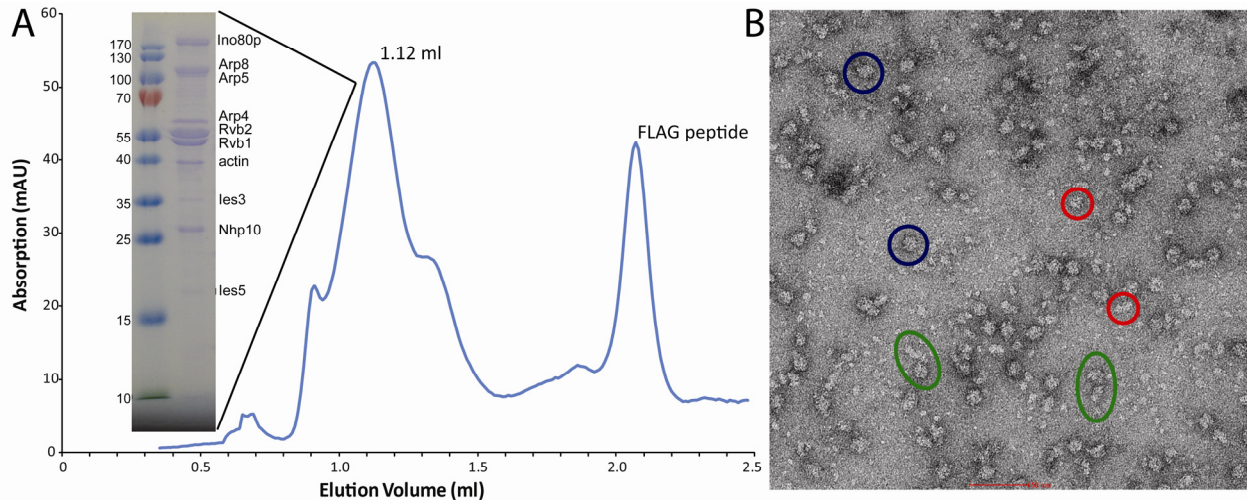


Figure 10: Purification and electron microscopic studies of the yeast INO80 complex

A) Typical elution profile of the INO80 complex after FLAG purification from a Superose 6 size exclusion. The first large peak (1.12 ml) contains the INO80 complex, whereas the second peak corresponds to free FLAG peptide. The central fractions of the INO80 peak were combined and concentrated. The inset depicts a Coomassie stained SDS gel with concentrated peak fractions containing the INO80 complex. Labeled proteins have been identified by mass spectrometry.

B) Representative micrograph of uranyl acetate stained INO80 complex. As indicated by the differently colored circles, the preparation contains multiple species. The green circles might indicate intact INO80 complexes, the blue circles might correspond to dodecameric complexes of Rvb1-Rvb2 and the red circles probably show smaller fragments of the complex which have dissociated during sample preparation or staining of the grids.

As obvious from the micrograph, the preparation of the INO80 complex seems to be heterogeneous and contain different species. At least three distinctly different entities can be identified, as marked in Figure 10. They might correspond to the intact complex (green circles), isolated Rvb1-Rvb2 complex (blue circles) and smaller particles possibly representing dissociated parts of the INO80 complex (red circles).

The reference free reconstruction of a low resolution structural model from EM data however, is not trivial. In addition to sophisticated data collection methods such as the random conical tilt, or the orthogonal tilt method (Llorca, 2007) it requires a very clean and homogeneous sample. The heterogeneity of the sample thus precludes the further analysis of the electron microscopic data, especially since no reference structure is available which might help to identify the actual particles and their orientation.

3.2 Purification of individual INO80 components

To make ideal use of a possible low resolution structure obtained from EM, which can be hard to interpret and to get an idea about the structure and functionality of the different INO80 subunits several of them were structurally characterized in an isolated form. To this end, all principal members of the *S. cerevisiae* INO80 complex, except actin and Taf14 were expressed and purified individually. If purification was successful, the proteins were subjected to crystallization screening and if appropriate functional testing. Soluble and pure protein could be obtained for seven of the 15 INO80 components. An overview of all expression and purification trials performed on different INO80 components can be found in the appendix (see section 7.1).

The three actin related proteins Arp4, Arp5 and Arp8 could only be expressed in insect cells, since they were either insoluble (Arp4 and Arp5) or not expressed (Arp8) in *E. coli*. Structural and functional studies on Arp4 and Arp8 will be discussed in detail in section 3.6.

Arp5 was only expressed at a relatively low level resulting in a low yield (1-2 mg of pure protein per liter of insect cell culture) and was substantially degraded during purification, despite the use of protease inhibitors (see Figure 11).

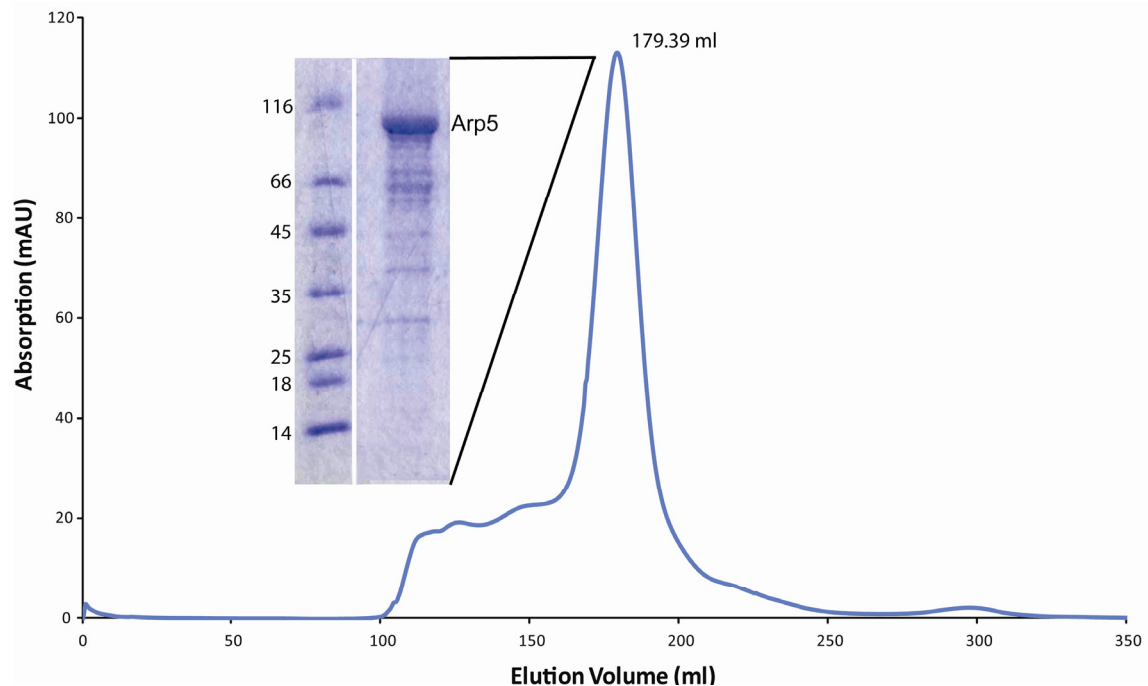


Figure 11: Purification of yeast Arp5

Elution profile of Arp5 from a S200 26/60 size exclusion after Ni-affinity and ion exchange chromatography. The central fractions of the peak were combined. The concentrated protein is depicted on a Coomassie stained SDS gel. Note the different degradation products present in the preparation.

Parts of the protein are likely degraded because of flexibility and lack of structure which allows for an easy access by proteases. It was not possible to optimize the purification strategy to minimize the observed degradation. The protein eluted from an S200 26/60 gel filtration column at a volume of about 179.4 ml which according to the column calibration corresponds to a molecular mass of about 135 kDa. This is slightly higher than the actual mass of an Arp5 monomer of 88 kDa and might be due to partially unfolded parts of the Arp5 protein. The screening of several hundred crystallization conditions with the partially degraded protein did not yield any promising hits.

The three INO80 subunit proteins Ies4, Ies5 and Ies6 could be expressed solubly in *E. coli*. Ies4 and Ies5 were expressed in a comparable yield (ca. 6.5 mg of pure protein per liter of shaking culture) and purification was possible without problems.

Ies5 was soluble but displayed a defined and very strong degradation band. The degradation product of Ies5 could be removed by ion exchange chromatography but tended to reappear in the final protein sample. The pure protein eluted from an S200 26/60 gel filtration column at a volume of about 199.5 ml (see Figure 12).

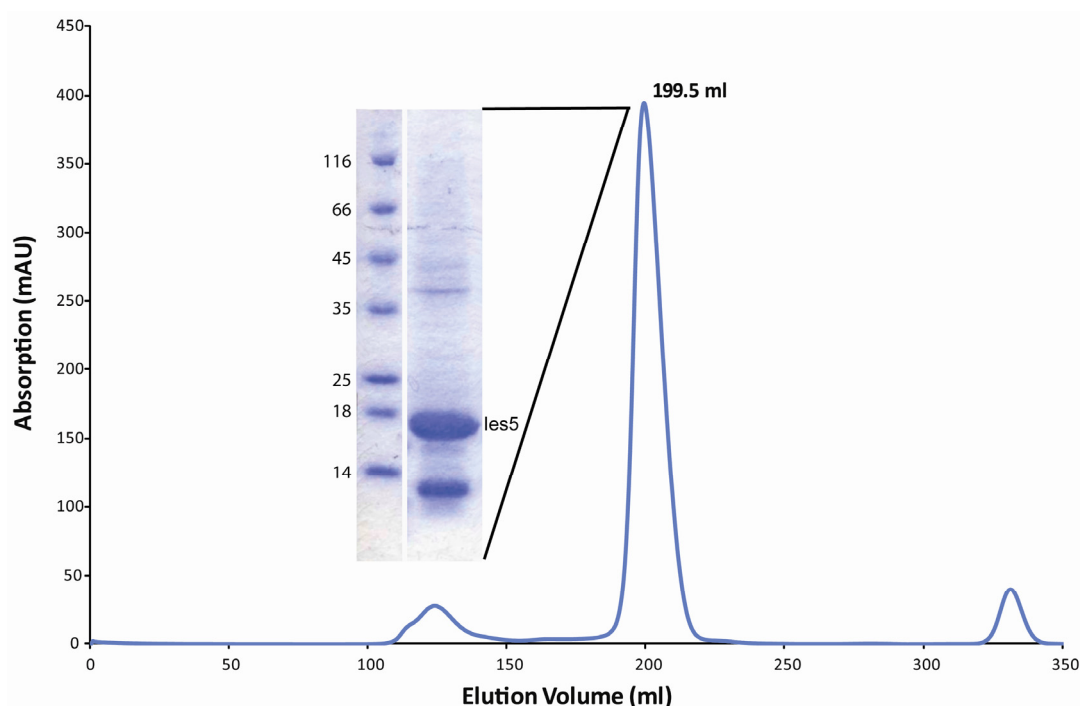


Figure 12: Purification of yeast Ies5

Elution profile of Ies5 from a S200 26/60 size exclusion after Ni-affinity and ion exchange chromatography. The central fractions of the peak were combined. The concentrated protein is depicted on a Coomassie stained SDS gel. Note the strong degradation band of Ies5 below 14 kDa.

According to the column calibration the elution volume corresponds to a molecular mass of about 66 kDa. This is substantially higher than the actual mass of an Ies5 monomer of 14.3 kDa and might either indicate oligomerization of Ies5, or non ideal behavior in gel filtration due to unfolding, or a very elongated shape. Nevertheless, large amounts of pure protein were obtained and used to screen for crystallization conditions at different protein concentrations. So far, promising crystal conditions could not be identified.

Ies4 had a tendency to aggregate during purification and despite good expression only very small amounts of non aggregated protein could be obtained after final gel filtration. The final amount of protein was not sufficient to conduct large scale crystallization trials.

Ies6 was expressed at low yield and heavily degraded during purification, so only a small amount of pure protein could be obtained (less than 0.3 mg of protein per liter of shaking culture) which was not enough to perform extensive crystallization experiments (see Figure 13).

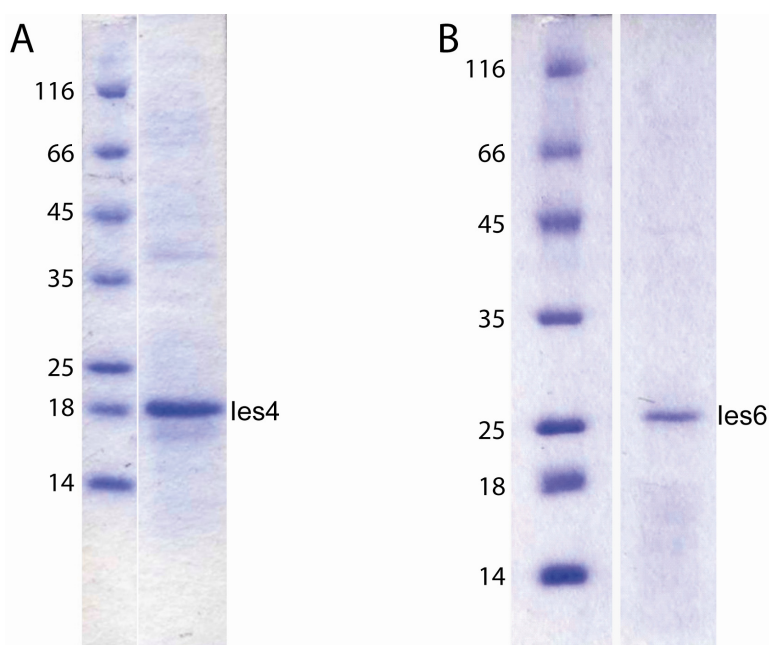


Figure 13: Purification of yeast Ies4 and Ies6

A) Coomassie stained SDS gel of concentrated Ies4 before gel filtration.

B) Coomassie stained SDS gel of concentrated Ies6 before gel filtration.

The fact that all three Ies proteins either showed degradation or aggregation during purification indicates that they most likely lack some interaction partners from the INO80 complex to either stabilize flexible parts or mask hydrophobic patches. As a result no crystals could be obtained with any of the three proteins.

Nhp10 was expressed and purified from *E. coli* as well. Like in the case of Ies4 the protein tended to aggregate during purification and only small amounts of pure and soluble protein could be obtained after purification (less than 1 mg of protein per liter of shaking culture) (see Figure 14). Nevertheless, crystal screening was performed with the pure protein but without being able to identify suitable conditions for crystal growth.

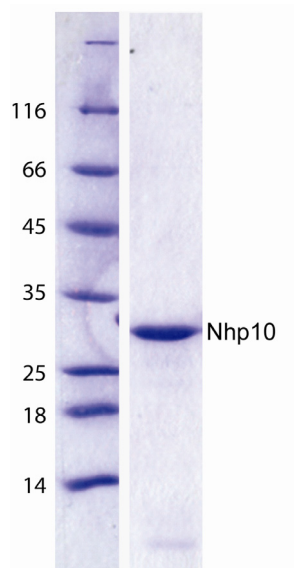


Figure 14: Purification of yeast Nhp10

Coomassie stained SDS gel of concentrated Nhp10 before gel filtration.

The other INO80 subunits could not be purified in substantial amounts due to different reasons. In the case of Ies1 and the INO80 protein itself no expression was detected, Ies3 expressed only insolubly and Ies2 was heavily degraded during purification. For Rvb1 and Rvb2 it is known that they form a complex (Jha & Dutta, 2009) and thus they were not expressed individually.

3.3 Identification of new intermolecular interactions within the INO80 complex

As mentioned in section 3.2, INO80 subunits that were expressed and purified in an isolated form often tended to aggregate, or displayed a lack of stability. To overcome those problems, the single proteins were expressed together with their interaction partners from the complex. This approach however was limited by the knowledge about the exact interaction network within the complex. Known interactions within INO80 include an interaction of Arp4 with Arp8 (Shen et al, 2003), an interaction of Arp4 and Arp8 with the HSA domain of the INO80 protein (Szerlong et al, 2008), the formation of a Rvb1-Rvb2 complex (Jha & Dutta, 2009), the interaction of the

Rvb1-Rvb2 complex with Arp5 (Jonsson et al, 2004) and an interaction of Nhp10 with Ies3 (Shen et al, 2003).

In order to identify new subcomplexes within the INO80 remodeler different co-expression experiments in *E. coli* were performed. One His-tagged and one untagged gene were transformed simultaneously into *E. coli* and pull down experiments were done to test if both proteins would co-purify. If initial pull downs indicated an interaction, large scale purification was performed to isolate stable complexes via three step purification and to test their stability during gel filtration. Two previously unknown interactions could be identified in this way. Nhp10 was found to interact with Ies5 and Arp5 to interact with Ies6.

3.3.1 Interaction between Nhp10 and Ies5

The complex of Nhp10 and Ies5 could be purified in large scale from *E. coli* (ca. 5 mg of pure protein complex per liter of shaking culture). The pure complex eluted from an S200 26/60 gel filtration column at a volume of about 184 ml which according to the column calibration corresponds to a molecular mass of about 116 kDa (see Figure 15). Like in the case of isolated Ies5 (see Figure 12) this is substantially higher than the expected mass of a monomeric 1:1 complex of Nhp10 and Ies5 which is 39 kDa. Again, this might either indicate that the Nhp10-Ies5 complex is larger than just a 1:1 assembly of both proteins, or that it does not behave ideally in gel filtration. Interestingly, the pure complex still contains the degradation band of Ies5 which is also found during the purification of isolated Ies5. This suggests that the part of Ies5 that binds to Nhp10 is different from the part that is degraded during purification. The successful purification of the Nhp10-Ies5 complex also demonstrates that it is possible to overcome the non ideal behavior of an isolated protein (in this case isolated Nhp10 which tends to aggregate on its own) by co-expression with its interaction partners. Although crystal screening with the complex was performed, no promising hits could be identified.

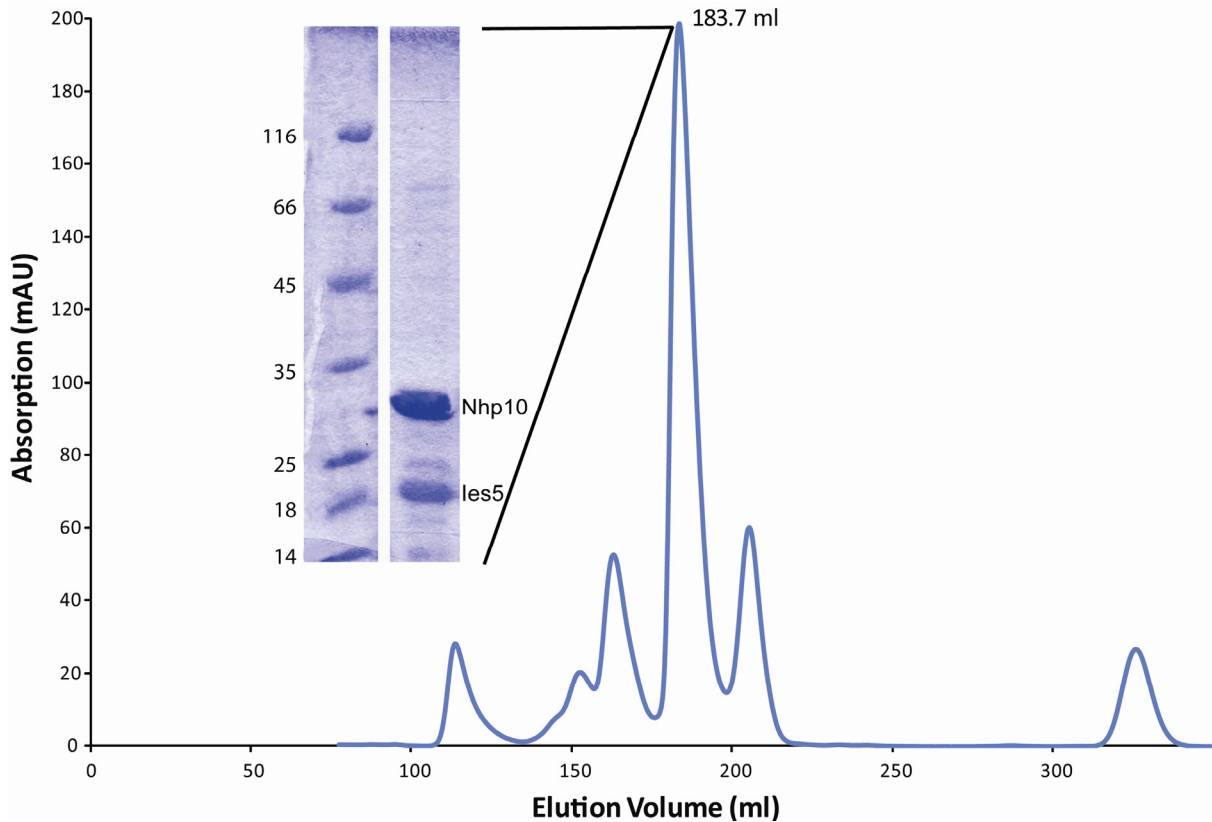


Figure 15: Purification of yeast Nhp10-Ies5 complex

Elution profile of the Nhp10-Ies5 complex from a S200 26/60 size exclusion after Ni-affinity and ion exchange chromatography. The central fractions of the peak were combined and concentrated. The inset depicts a Coomassie stained SDS gel with concentrated peak fractions containing Nhp10-Ies5.

Since an interaction between Ies3 and Nhp10 has been published in the literature (Shen et al, 2003) a complex between Nhp10, Ies3 and Ies5 was expressed in insect cells. Interestingly, isolated Ies3 is insoluble in *E. coli* as well as in insect cells. The trimeric complex however, can be purified without problems. Ies3 is thus solubilized by expressing it together with its interaction partners Ies5 and Nhp10. This further indicates that some of the INO80 subunits are only properly folded and stable in the context of their interaction partners from the complex. The trimeric complex of Nhp10, Ies3 and Ies5 can be expressed and purified at reasonable yields in insect cells (ca. 8 mg of pure protein per liter of shaking culture). The pure complex eluted from an S200 26/60 gel filtration column at a volume of about 160 ml which according to the column calibration corresponds to a molecular mass of about 270 kDa (see Figure 16). Again this is substantially higher than the actual mass of a monomeric 1:1:1 complex of Nhp10, Ies3 and Ies5 which is 67 kDa and might either indicate that the Nhp10-Ies3-Ies5 complex is larger than just a

1:1:1 assembly of the three proteins, or that it does not behave ideally on a gel filtration. A hint that it might be partially unfolded comes from SAXS studies described in section 3.4. Consequently, it was not possible to obtain crystals despite intensive screening efforts.

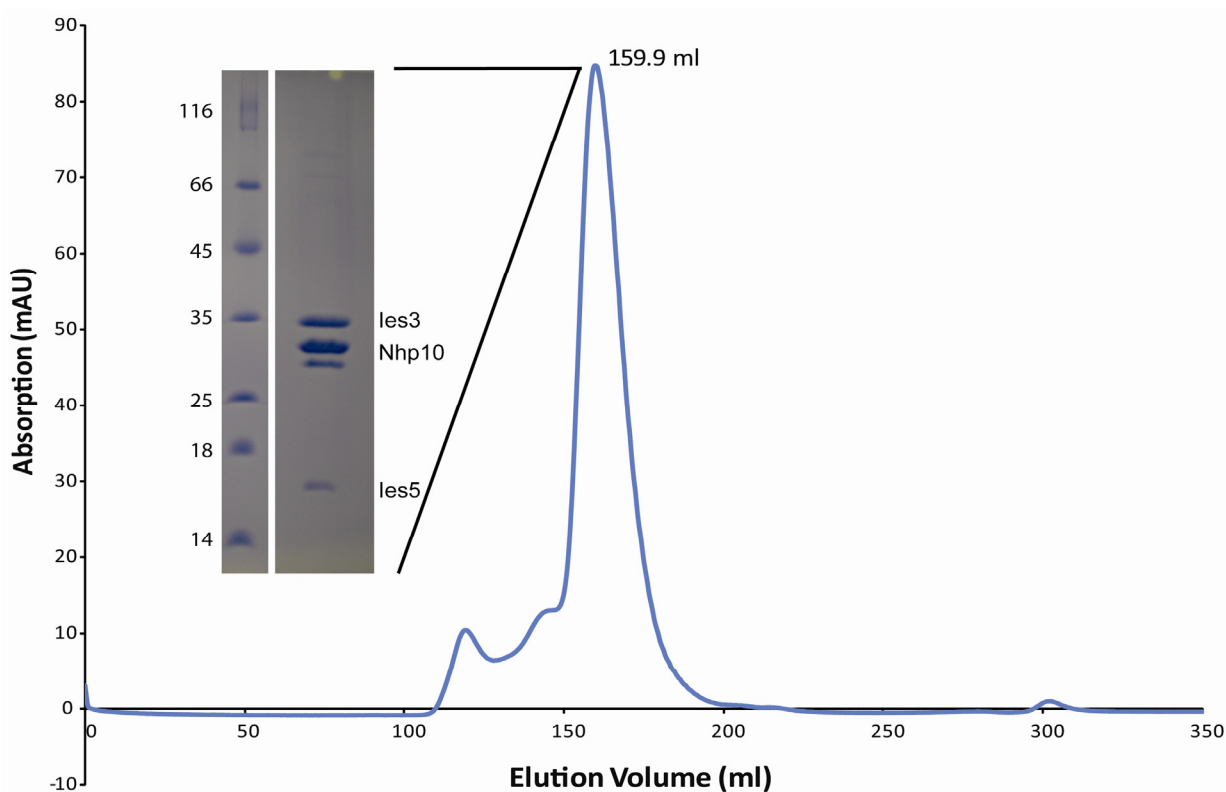


Figure 16: Purification of yeast Nhp10-Ies3-Ies5 complex

Elution profile of the Nhp10-Ies3-Ies5 complex from a S200 26/60 size exclusion after Ni-affinity and ion exchange chromatography. The central fractions of the peak were combined and concentrated. The inset depicts a Coomassie stained SDS gel with concentrated peak fractions containing Nhp10-Ies3-Ies5. Note: the weak staining of Ies5 is an intrinsic property of the protein and does not indicate substoichiometric binding to the complex.

3.3.2 Interaction between Arp5 and Ies6

As mentioned in section 3.2, isolated Arp5 from *S. cerevisiae* is heavily degraded during purification (see Figure 11). In order to be able to purify a stable complex between Arp5 and Ies6 it was chosen to switch to the human homologue of the complex as human Arp5 (68 kDa) is considerably smaller compared to its yeast counterpart (88 kDa).

The human Arp5-Ies6 complex was expressed and purified from insect cells (ca. 1-2 mg of pure protein per liter of shaking culture) and was found to be more stable than the yeast homologues. It eluted from an S200 26/60 gel filtration column at a volume of about 173 ml which according

to the column calibration corresponds to a molecular mass of about 169 kDa (see Figure 17). This is about double the actual molecular weight of the complex (89 kDa) and could hint at a dimerization, or partial unfolding of the two proteins (see SAXS studies described section 3.4). Crystallization attempts with the Arp5-Ies6 complex were not successful.

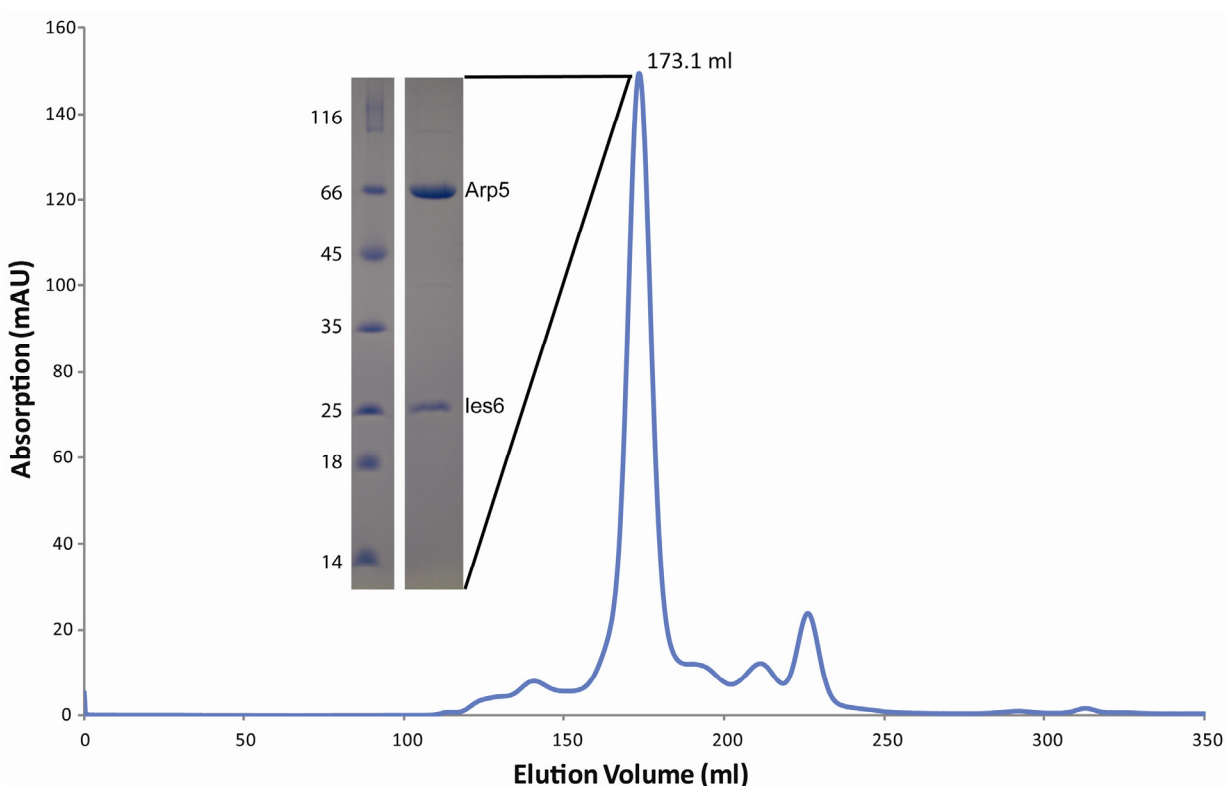


Figure 17: Purification of human Arp5-Ies6 complex

Elution profile of the Arp6-Ies6 complex from a S200 26/60 size exclusion after Ni-affinity and ion exchange chromatography. The central fractions of the peak were combined and concentrated. The inset depicts a Coomassie stained SDS gel with concentrated peak fractions containing Arp6-Ies6.

As described, an interaction between Arp5 and Rvb1-Rvb2 is published in the literature (Jonsson et al, 2004). An attempt to verify this interaction by co-expressing the Arp5-Ies6 complex together with Rvb1-Rvb2 in insect cells did in contrast not show an interaction between the proteins. Since this interaction seems to be ATP dependent (Jonsson et al, 2004), it would be advisable to supplement all buffers for cell lysis and purification with ATP and repeat the co expression experiment.

3.4 Solution structures of INO80 subcomplexes

As neither the Nhp10-Ies3-Ies5 complex nor the Arp5-Ies6 complex could be crystallized, SAXS measurements were performed with both complexes in order to get an idea about the general shape of those newly identified modules. The SAXS data were processed using GNOM. The sample quality of both complexes is not ideal as indicated by the increase of scattering intensity at very small angles (see Figure 18) and verified by the non linear behavior in the Guinier plot (data not shown).

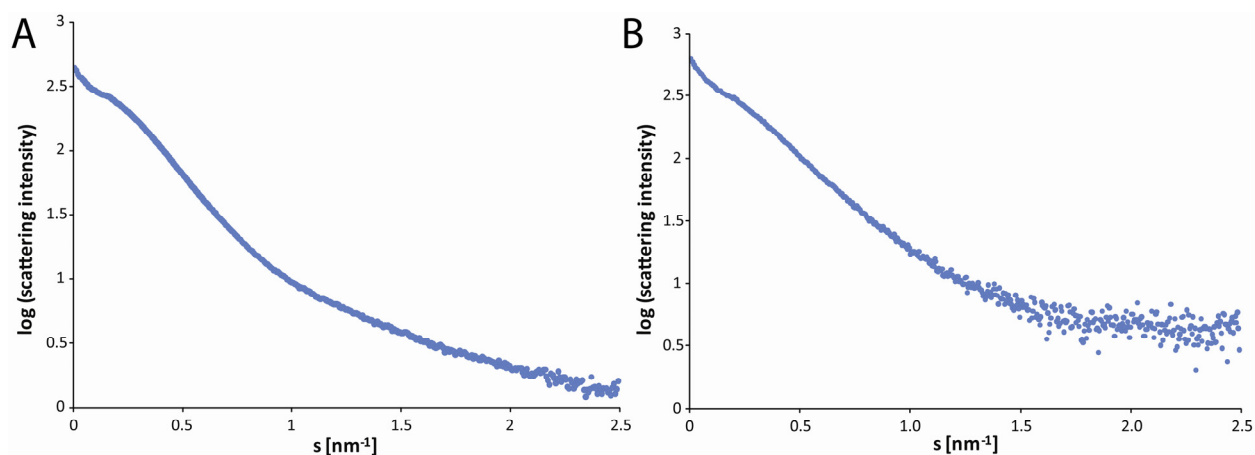


Figure 18: SAXS data of yeast Nhp10-Ies3-Ies5 and human Arp5-Ies6 complexes

A) Measured scattering curve of the Nhp10-Ies3-Ies5 complex after buffer correction.

B) Measured scattering curve of the Arp5-Ies6 complex after buffer correction.

Note the increase of intensity at very small scattering angles for both samples. This indicates that the complexes do not behave ideally but rather display slight aggregation.

Both subcomplexes seem to be slightly aggregated and the theoretical molecular weight determined from the scattering is higher than the actual value expected for monomeric complexes.

In the case of Arp5-Ies6 the molecular weight of a 1:1 monomeric complex is 89 kDa whereas the molecular weight determined from SAXS is 141 kDa.

A 1:1:1 monomeric complex of Nhp10-Ies3-Ies5 has an actual molecular weight of 67 kDa in contrast to the mass of 114 kDa determined by SAXS. Thus, the molecular weights derived from SAXS are lower than suggested by gel filtration (see section 3.3.1 and 3.3.2) and likely indicate that both complexes are partially unfolded causing slight aggregation.

Corresponding to the non ideal, aggregating behavior of both samples their Kratky plots indicate that the two complexes are indeed not completely folded (Putnam et al, 2007). This might show that parts of both complexes are unstructured possibly because they are still lacking further interaction partners like for example the INO80 protein which integrates them into the INO80 complex (see Figure 19).

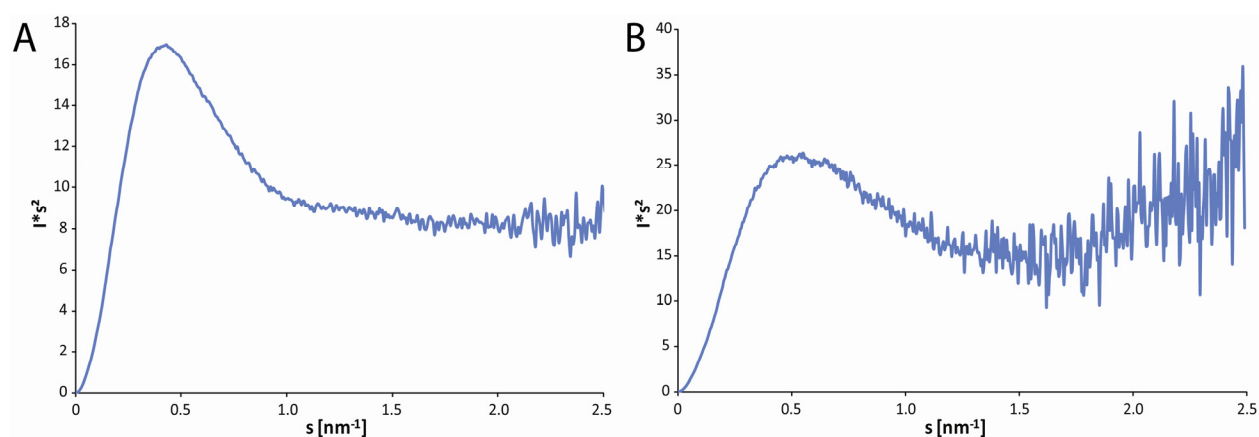


Figure 19: Kratky plot of yeast Nhp10-Ies3-Ies5 and human Arp5-Ies6 complexes

A) Plot of $I \cdot s^2$ versus s (Kratky-plot) for the Nhp10-Ies3-Ies5 complex.

B) Plot of $I \cdot s^2$ versus s (Kratky-plot) for the Arp5-Ies6 complex.

The not entirely bell-shaped curves indicate that both complexes are not completely folded (compare Figure 9). The Nhp10-Ies3-Ies5 complex however seems to behave slightly better as it reaches a stable plateau compared to Arp5-Ies6.

Nevertheless, *ab initio* structures of both complexes were calculated without symmetry constraints using GASBOR and averaged using DAMAVER (see Figure 20). In both cases, the obtained shapes are rather compact and slightly elongated and do not display any striking features. The interpretation of those SAXS structures will be only possible with the actual crystal structures of both complexes or at least single complex components in hand.

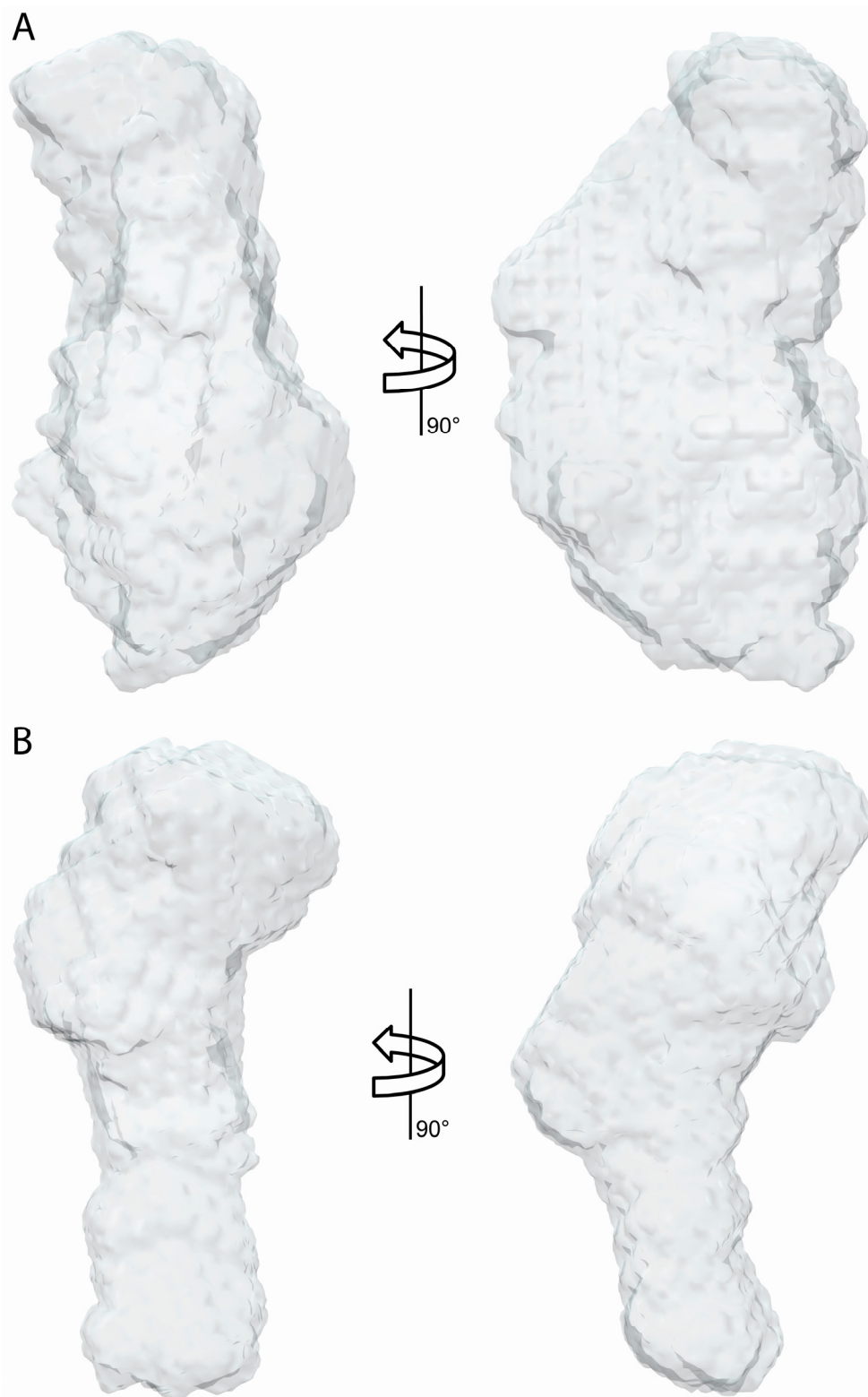


Figure 20: Ab initio shape reconstructions of Nhp10-Ies3-Ies5 and Arp5-Ies6 complexes

A) Final averaged *ab initio* shape reconstruction of Nhp10-Ies3-Ies5 represented by two different views.

B) Final averaged *ab initio* shape reconstruction of Arp5-Ies6 represented by two different views.

3.5 Purification and crystallization of the Rvb1-Rvb2 subcomplex

As mentioned, both Rvb proteins form a stable complex that has been reported to be a dodecameric assembly of six copies of Rvb1 and six copies of Rvb2 (Jha & Dutta, 2009). The complex could be expressed and purified from *E. coli* (a total of 7 mg of pure protein was obtained per liter of shaking culture). Interestingly, the final gel filtration on a S300 26/60 column revealed that apart from an aggregated protein fraction two distinct species are present in the preparation which might correspond to a “6mer” and a “12mer” complex, respectively (see Figure 21). Both species emerging from gel filtration contained Rvb1 as well as Rvb2 and were treated separately for all subsequent experiments.

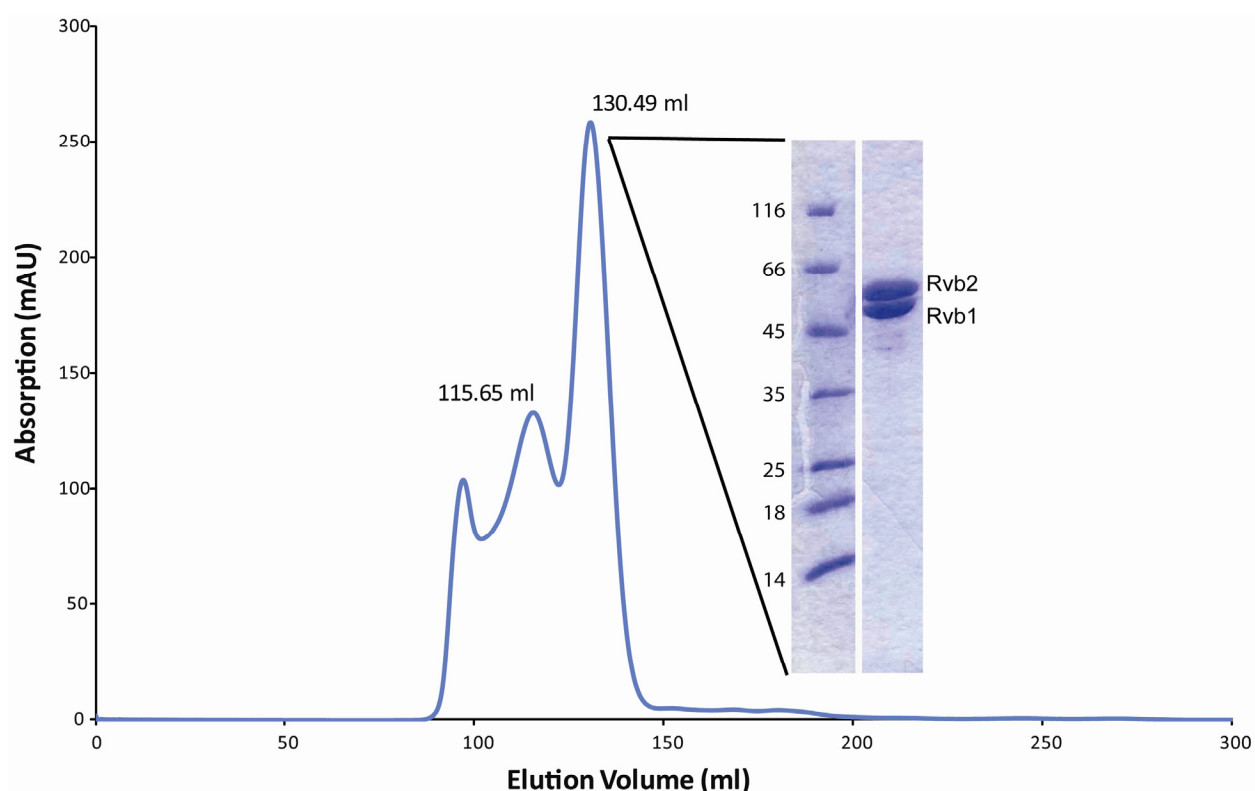


Figure 21: Purification of yeast Rvb1-Rvb2 complex

Typical elution profile of the Rvb1-Rvb2 complex from a Sephacryl 300 size exclusion reveals the presence of two different species. The first peak corresponds to the void volume of the column and contains aggregated protein. The middle peak (115.65 ml) is a higher molecular weight species of Rvb1-Rvb2, possibly a dodecamer. This peak is therefore termed the “12mer” fraction. The last peak (130.49 ml) is a lower molecular weight fraction of the Rvb1-Rvb2 complex, possibly a hexamer. This peak is therefore termed the “6mer” fraction. The inset depicts a Coomassie stained SDS gel of the concentrated “6mer” peak fractions of Rvb1-Rvb2. The molecular weight of the marker bands is indicated.

The concentrated samples were separately investigated by analytical gel filtration on a Superose 6 PC 3.2/30 column. The “6mer” fraction eluted at 1.44 ml which corresponds to a molecular weight of 437 kDa whereas the “12mer” fraction eluted at 1.30 ml corresponding to a molecular weight of 1.2 MDa (data not shown). In both cases this is larger than the expected molecular masses of 306 kDa for a 6mer and 612 kDa for a 12mer.

Both species could be crystallized separately and crystals were obtained in various conditions. Additionally, both complexes were reductively methylated according to a standard protocol to facilitate the formation of crystals (Kim et al, 2008). Indeed, the methylated derivatives of the Rvb1-Rvb2 complex crystallized in several conditions where the unmethylated proteins did not crystallize. In the end, growth of large single crystals was optimized mainly in two conditions, in one of which both the “12mer” and the “6mer” species yielded crystals (see Figure 22).



Figure 22: Crystals of Rvb1-Rvb2

A) Refined crystals of the unmethylated Rvb1-Rvb2 “6mer” in 0.5 M $(\text{NH}_4)_2\text{HPO}_4$, 0.1 M tri-sodium citrate pH 5.5 and 0.25 M Li_2SO_4 .

B) Crystals of the unmethylated Rvb1-Rvb2 “12mer” in 0.32 M $(\text{NH}_4)_2\text{HPO}_4$, 0.1 M tri-sodium citrate pH 5.5 and 0.28 M Li_2SO_4 .

C) Refined crystals of the reductively methylated Rvb1-Rvb2 “6mer” in 1.2 M ammonium tartrate dibasic pH 7.8 and 0.1 M HEPES pH 8.0.

Unfortunately, all crystals that were tested at synchrotron beam lines never showed diffraction beyond a resolution limit of 7-8 Å. The diffraction data did not allow to unambiguously determine the crystal lattice and unit cell dimensions of the tested crystals.

Diffraction could not be improved despite extensive optimization efforts. The largest crystals obtained had a dimension of about 0.2 x 0.2 x 0.4 mm and were taken to a beam line equipped with a free mounting system (Kiefersauer et al, 2000). This system can be used to change the humidity of a crystal in a defined manner usually reducing the water content within the crystal. If

successful, this leads to crystal shrinkage and more tightly packed molecules within the crystal sometimes accompanied by a change in crystal lattice which in turn can lead to an improvement in diffraction. In the case of the Rvb1-Rvb2 crystals, however, no change in diffraction for the better was observed during changes in humidity, neither by increasing nor decreasing the humidity of the crystals.

3.6 Structural studies of Arp4 and Arp8

As mentioned, the role of nuclear Arps as components of several chromatin remodeling enzymes is poorly understood. To shed light on the enigmatic structures and functions of nuclear Arps the crystal structure of *S. cerevisiae* Arp4, as well as the X-ray scattering solution structures of Arp4 and Arp8 were determined. The Arp4 structure can explain why the protein, in contrast to the highly related conventional actin, does not form filaments, and provides a testable model for formation of a distinct complex with actin.

To uncover the biochemical relationship of Arp4, Arp8 and actin, the effects of Arp4 and Arp8 on actin filament dynamics were biochemically analyzed. Strikingly, both affect the polymerization and depolymerization of actin albeit in different ways. While Arp4 appears to bind to the barbed end of monomeric actin, thereby preventing the nucleation of actin filaments, Arp8 efficiently sequesters actin monomers with slow kinetics by interaction with a region of the monomer distinct from the barbed end. Most notably, Arp4 and Arp8 cooperate in monomer sequestering, consistent with formation of a discrete Arp4-Arp8-actin module within the INO80 complex. In summary, Arp4 and Arp8 evidently stabilize monomeric actin within chromatin modifying complexes and have a potential function in the regulation of the state of nuclear actin.

3.6.1 Sequence alignments between actin, Arp4 and Arp8 respectively

A sequence alignment between *S. cerevisiae* Arp4 and actin reveals that both proteins have a high sequence similarity and share a conserved core of residues that constitutes the central actin fold. Apart from the conserved fold, three main differences between the two proteins can be identified: two large insertions in Arp4 compared to actin and one important deletion. The first insertion (Insertion I) is about 25 residues long and sits between amino acids 196 and 197 of actin. The second insertion (Insertion II) is about 80 residues long and is located at amino acid 271 of actin. The deletion of about five residues in Arp4 compared to actin concerns amino acids

42-47 of actin which are an important structural element of actin, the so called DNase I binding loop.

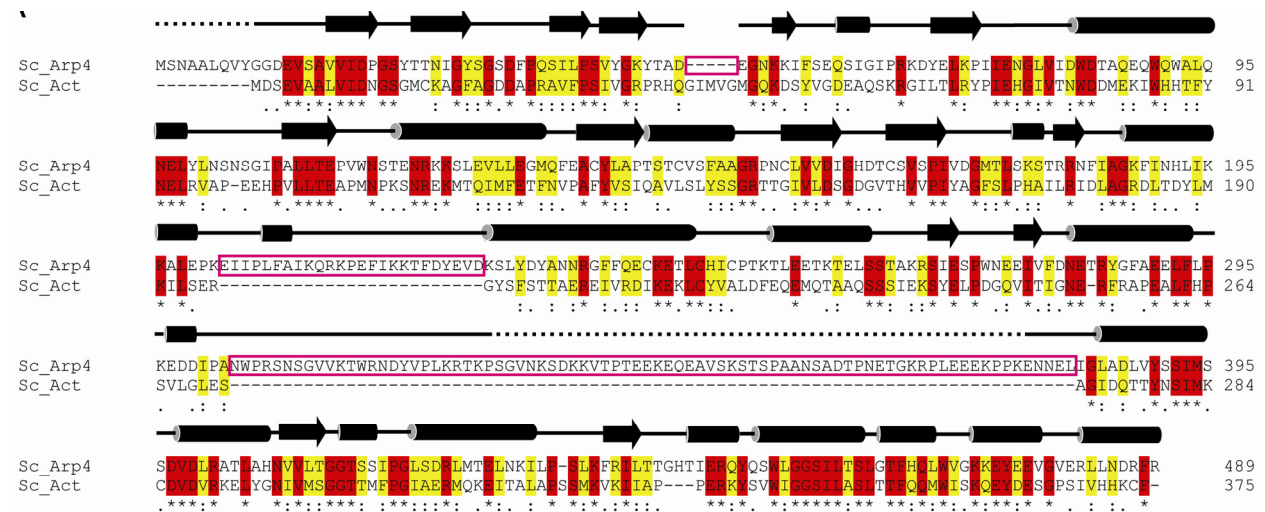


Figure 23: Sequence alignment of yeast Arp4 and yeast actin

Amino acid sequences of *S. cerevisiae* Arp4 (top) and actin (bottom) aligned to each other. Identical residues are shaded in red, similar residues in yellow. The main differences between the two proteins: shortening of the DNaseI loop, Insertion I (25 residues) and Insertion II (80 residues) are highlighted by pink boxes. The secondary structure of Arp4 based on the crystal structure (see section 3.6.4) is displayed on top of the alignment; residues missing in the electron density are depicted as dashed lines.

A sequence alignment between *S. cerevisiae* Arp8 and actin confirms the presence of the core actin fold within Arp8 as well (see Figure 24). Arp8 is more divergent from actin than Arp4 which is reflected by the presence of more and even longer insertions. Especially, the N-terminal 260 amino acids of Arp8 do not align with actin and contain a series of charged residues for which no secondary structure is predicted. They might represent an intrinsically unstructured part of the protein which is important to mediate protein protein interactions in the context of the INO80 complex for example with histones.

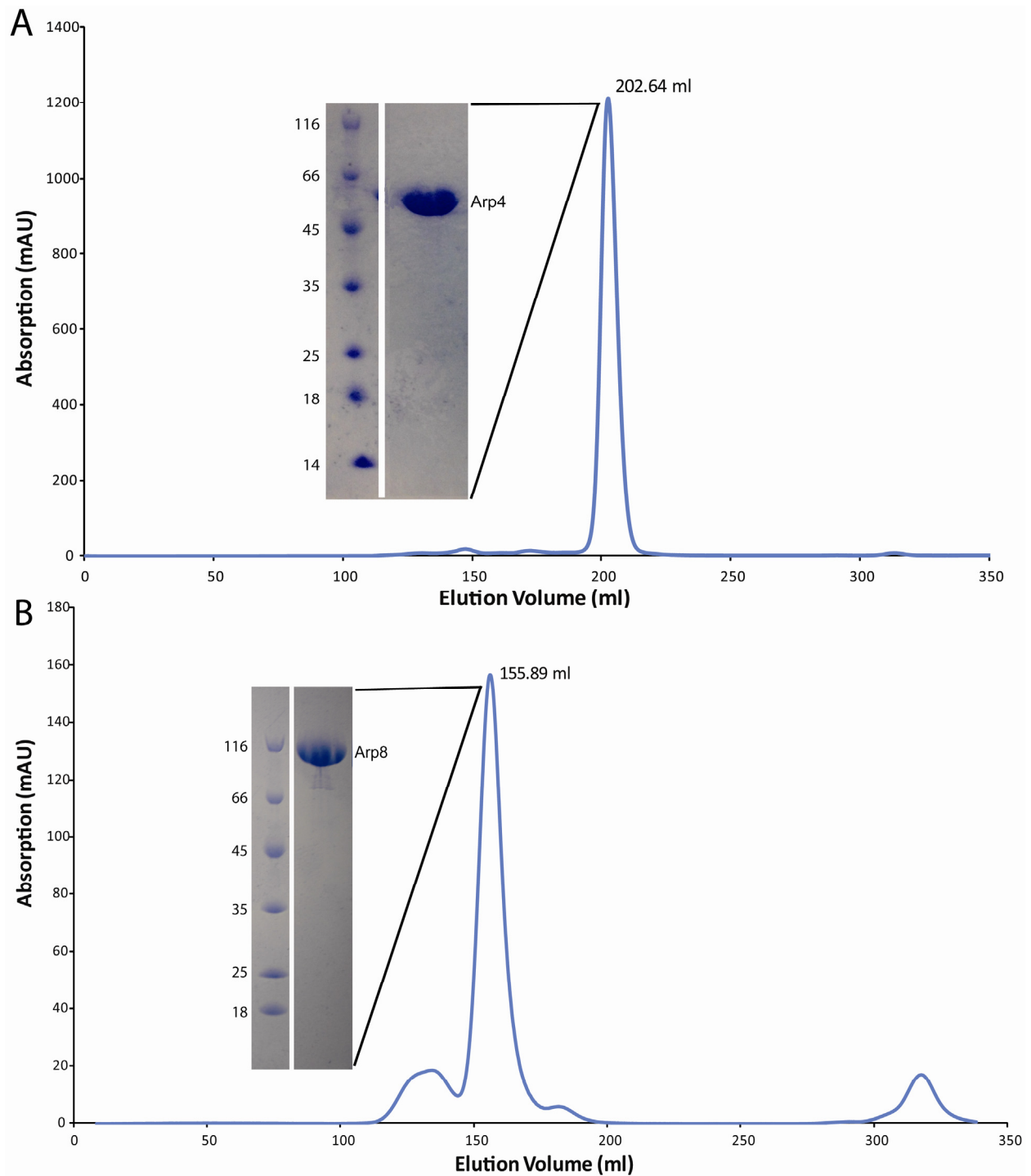


Figure 25: Purification of yeast Arp4 and Arp8

A) Elution profile of Arp4 from a S200 26/60 size exclusion after Ni-affinity and two ion exchange chromatographies. The central fractions of the peak were combined and concentrated. The inset depicts a Coomassie stained SDS gel with concentrated peak fractions containing Arp4.

B) Equivalent to A the elution profile of Arp8 and the pure protein is depicted.

Pure Arp4 eluted from an S200 26/60 gel filtration column at a volume of about 202.6 ml which according to the column calibration corresponds to a molecular mass of about 59 kDa. This agrees nicely with the actual mass of Arp4 which is 56 kDa and indicates that the protein is likely monomeric in solution. This is confirmed by SAXS experiments (see section 3.6.5). Arp8 on the other hand eluted from an S200 26/60 gel filtration column at a volume of about 155.9 ml which according to the column calibration corresponds to a molecular mass of about 311 kDa. This is about three times the actual mass of an Arp8 monomer which is 101 kDa. The SAXS measurements performed on Arp8 however indicate the protein to be monomeric but very elongated which might account for its elution behavior on gel filtration (see section 3.6.5).

3.6.3 Crystallization and structure determination of Arp4

Initial crystallization experiments were performed by sitting drop vapor diffusion with purified and reductively methylated *S. cerevisiae* Arp4 at a concentration of 8 mg/ml using commercially available screens from Hampton Research and Jena Bioscience. Only one crystallization condition of the ProComplex screen (condition A11: 25% w/v PEG2000MME, 0.1 M HEPES pH 7.5) yielded very small, almost one dimensional needle like crystals. The crystallization condition was refined to obtain larger three dimensional rod like crystals. Intensive additive screening resulted in the final optimal condition of 27% w/v PEG2000MME, 0.1 M HEPES-NaOH pH 7.0, 6% w/v D+-trehalose, 50 mM glycine. Arp4 crystallized in space group $P6_1$ and diffracted to 3.4 Å resolution (see Figure 26).

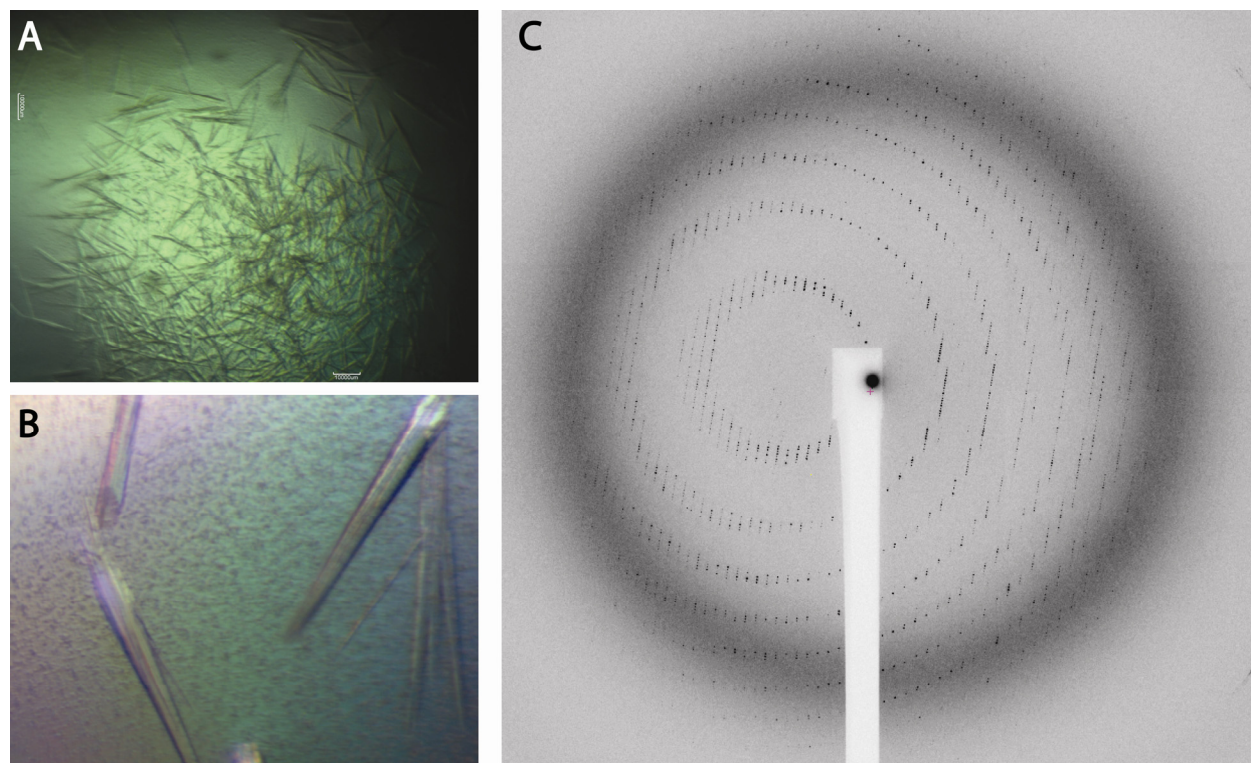


Figure 26: Crystals and diffraction pattern of yeast Arp4

A) Initial crystals that appeared in the crystallization screen.

B) Optimized crystals in the final condition.

C) Diffraction image of native Arp4 recorded at beamline X06SA (Swiss Light Source, Villigen, Switzerland). Crystals of Arp4 diffracted to 3.4 Å resolution.

The crystals contained four molecules per asymmetric unit and had unit cell dimensions of $a = b = 119.3 \text{ \AA}$, $c = 396.7 \text{ \AA}$ and $\alpha = \beta = 90.0^\circ$, $\gamma = 120.0^\circ$. For X-ray diffraction experiments, the crystals were transferred into the refined crystallization condition supplemented with 20% v/v glycerol and flash frozen in liquid nitrogen. Seleno-methionine derivatised Arp4 was produced by expressing the protein in insect cells grown in methionine free medium supplemented with Se-methionine. The labeled protein could be purified and crystallized under the same conditions as the native protein. The crystals however, only diffracted to around 7 Å with small anomalous signal which was not sufficient to solve the structure by an anomalous dispersion experiment.

Since experimental phasing was not possible, the structure was solved by molecular replacement using a search model generated from the structure of yeast actin in complex with gelsolin (pdb: 1YAG) with the program CHAINSAW (Stein, 2008). Four molecules were located in the asymmetric unit with the help of PHASER (McCoy et al, 2007) and the initial search model was

subsequently expanded and mutated into Arp4 by cyclic rounds of model building and refinement using COOT and PHENIX (Adams et al, 2010; Emsley & Cowtan, 2004). The structure was refined to an R-value of 19.2% (R-free 22.1%; see Table 8). The stereochemistry of the refined structure was analyzed by Procheck (Laskowski et al, 1993) with 86.8%, 12.4%, 0.8% and 0% of residues in the most favoured, additionally allowed, generously allowed and disallowed regions of the Ramachandran plot, respectively. The refined electron density map is surprisingly well defined for a 3.4 Å structure (see Figure 27).

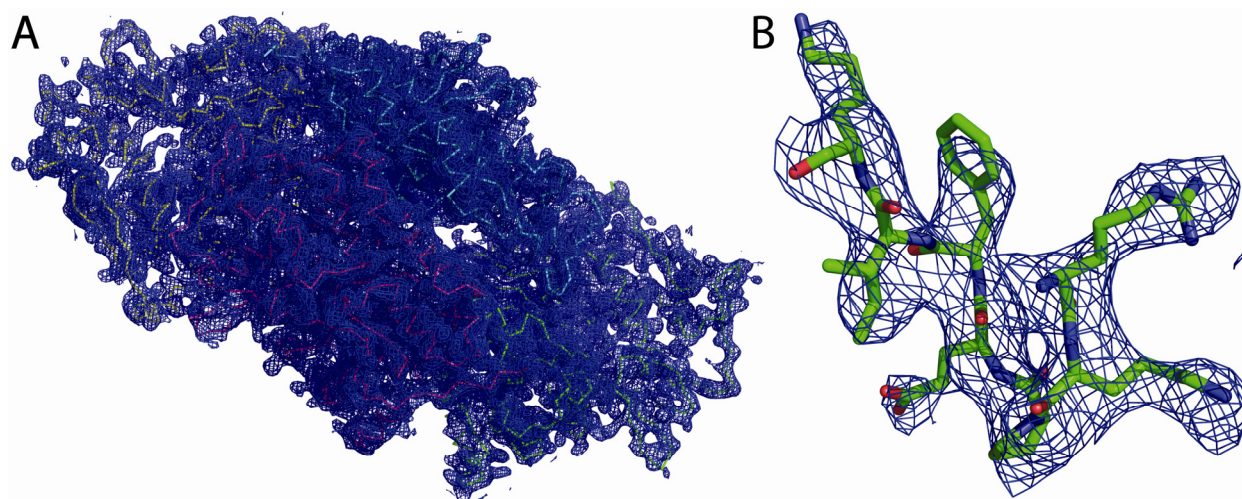


Figure 27: Electron density of the Arp4 structure

A) The four Arp4 molecules of the asymmetric unit (as Ca trace in different colors) placed in the final $2F_o-F_c$ density in blue contoured at 1σ .

B) Zoomed section of the electron density map showing amino acids 212-218 which are part of Insertion I of Arp4. This loop section was not part of the search model and shows that the density is well defined for a 3.4 Å resolution structure without extensive model bias.

In the end, the electron density was interpretable for the entire Arp4 polypeptide except the nine N-terminal amino acids and 49 amino acids within Insertion II of Arp4 (Ser328 – Lys377). Additional density was clearly visible in the center of the four subdomains and could be interpreted as a bound ATP molecule with one coordinated metal ion. A calcium ion was fitted into the structure as it better explained the electron density compared to a magnesium ion. This was judged by the reduction of difference electron density which favored the calcium ion.

Table 8: Data collection and refinement statistics

Data collection	
Space group	P6 ₁
Cell dimensions	
a, b, c (Å)	119.3, 119.3, 396.7
α , β , γ (°)	90.0, 90.0, 120.0
Resolution (Å)	50 – 3.4 (3.61 – 3.4) *
R_{merge} (%)	16.5 (38.6)
$I/I\sigma$	11.6 (4.4)
Completeness (%)	99.5 (99.0)
Redundancy	5.7 (5.3)
Refinement	
Resolution (Å)	50 – 3.4
No. reflections	43013
$R_{\text{work}} / R_{\text{free}}$ (%)	19.2 / 22.1
No. atoms	
Protein	13657
Ligand (ATP + metal)	124
Water	0
B-factors	
Protein	63.3
Ligand/ion	52.6
R.m.s. deviations	
Bond lengths (Å)	0.006
Bond angles (°)	0.805

*Values in parentheses are for the highest-resolution shell.

3.6.4 Crystal structure of Arp4 reveals characteristic loop insertions and deletions within the actin fold

The crystal structure of Arp4 represents the first atomic structure of a nuclear actin related protein and provides a structural framework to characterize similarities and key differences between *S. cerevisiae* Arp4 and actin. Arp4 displays the typical actin fold with a central nucleotide-binding cleft between subdomains one and two on one side and subdomains three and four on the other side (see Figure 28).

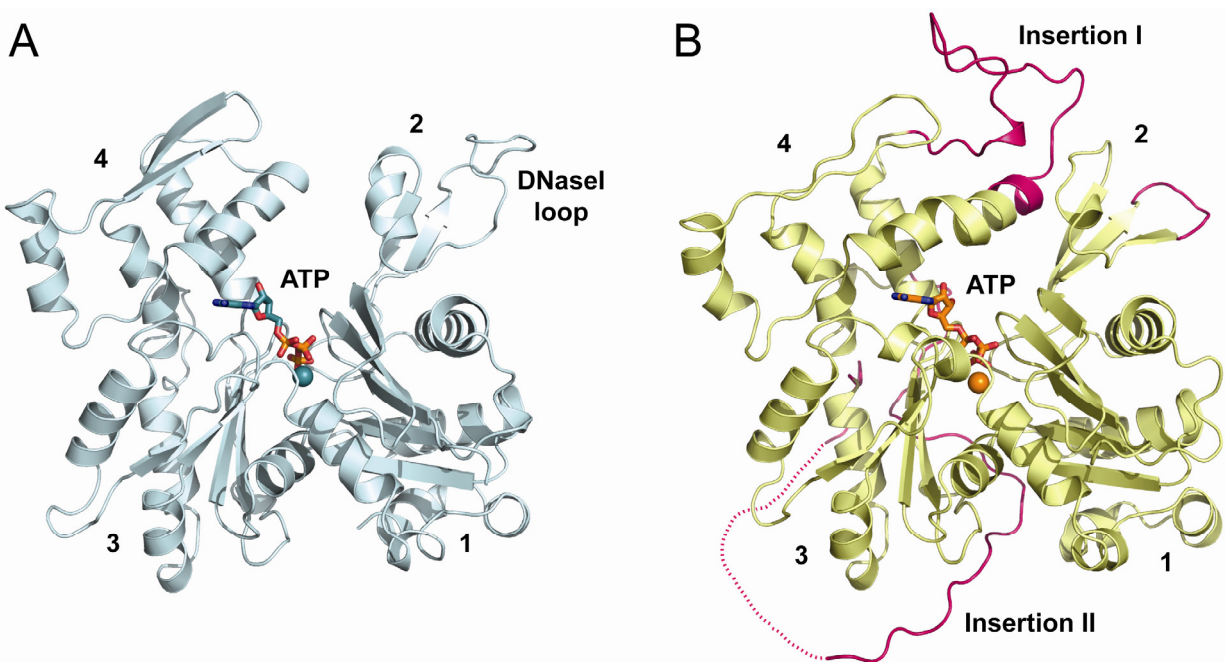


Figure 28: Comparison between actin and Arp4

A) Crystal structure of *S. cerevisiae* actin (pdb: 1YAG). The four subdomains are numbered and the DNaseI loop is labeled. ATP is represented in sticks and the metal ion is displayed as a sphere.

B) Crystal structure of *S. cerevisiae* Arp4 (pdb: 3QB0). The two insertions are labeled and shown in pink as is the shortened DNaseI loop. The 49 amino acids within Insertion II which are not visible in the electron density are indicated by the dashed line. The ATP molecule is represented in sticks and the metal ion is displayed as a sphere.

Despite its high overall structural similarity to conventional actin, the important differences on the level of primary structure, namely the two loop insertions and the deletion, lead to striking consequences in the tertiary structure and molecular surface of Arp4 compared to actin. The smaller Insertion I expands amino acids 196 to 203 in subdomain four of actin and the larger Insertion II between amino acids 268 and 272 bridges subdomains three and four of actin (see Figure 23). Insertion I lies mainly atop the pointed end of Arp4 whereas Insertion II winds itself around domain three on the backside of the Arp4 molecule (see Figure 28). Additionally, the DNaseI binding loop is substantially shorter in Arp4 compared to actin. As will be discussed in detail, all of these loops are placed at sites that are critical for actin polymerization and are likely responsible for a lack of polymerization capability of Arp4 (see section 3.6.7). Furthermore, significant differences between actin and Arp4 in the nucleotide-binding cleft could be identified. Those changes are consistent with stable ATP binding, but extremely slow or lacking ATP hydrolysis activity.

3.6.5 Solution structures of Arp4 and Arp8

The solution structures of Arp4 and Arp8 were determined by SAXS experiments in order to confirm the lack of polymerization and to verify the Arp4 crystal structure in solution. The theoretical SAXS curve of the Arp4 crystal structure calculated with CRY SOL is in good agreement with the experimental data, indicating that the crystal structure is similar to the structure in solution. The Kratky-plot of Arp4 displays a bell shaped curve showing that the protein is properly folded (see Figure 29).

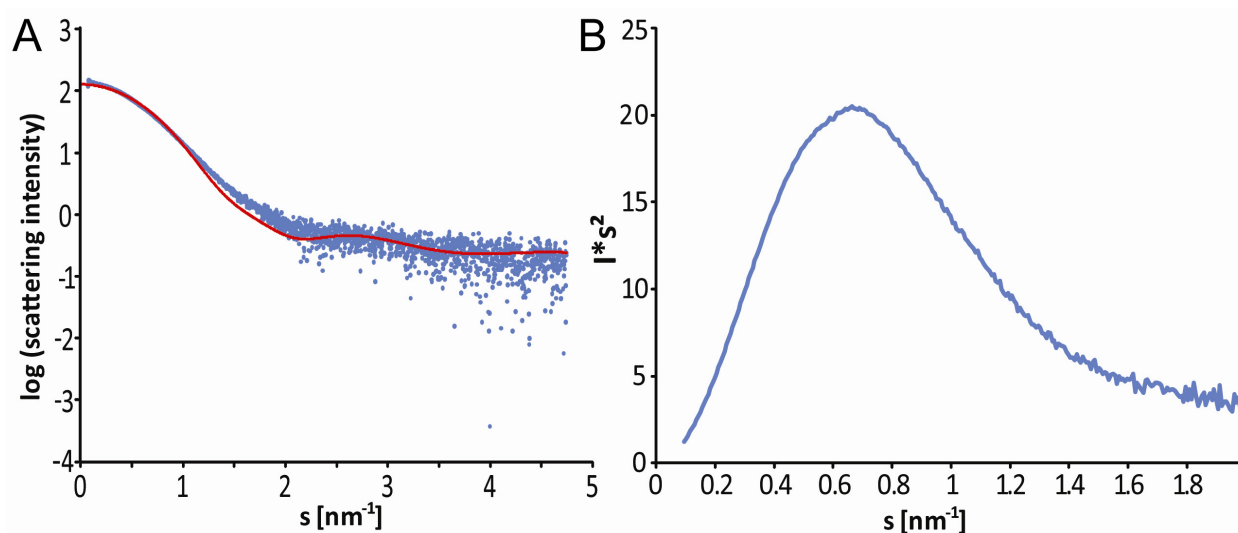


Figure 29: SAXS data of Arp4

A) Measured scattering curve of yArp4 after buffer correction (blue points) compared with the theoretical scattering curve of the yArp4-crystal structure calculated with CRY SOL (red line) (Svergun et al, 1995).
B) Kratky-plot ($I*s^2$ vs. s) of Arp4 has the typical bell shaped form of a completely folded protein (see Figure 9) (Putnam et al, 2007).

After processing the scattering data with GNOM, the modeling program GASBOR, was used to calculate the *ab initio* structure of Arp4. To obtain a final model, ten independent structures were calculated and averaged with DAMAVER. The models were constructed without symmetrical constraints being applied.

The *ab initio* shape reconstructions reveal a compact protein with a small protrusion. The reconstructed envelopes display the characteristic flatness typical for actin. The crystal structure can be nicely docked into the envelope with the additional protrusion allowing for the accommodation of the 49 unstructured amino acids of Insertion II which could not be located in the electron density (see Figure 30).

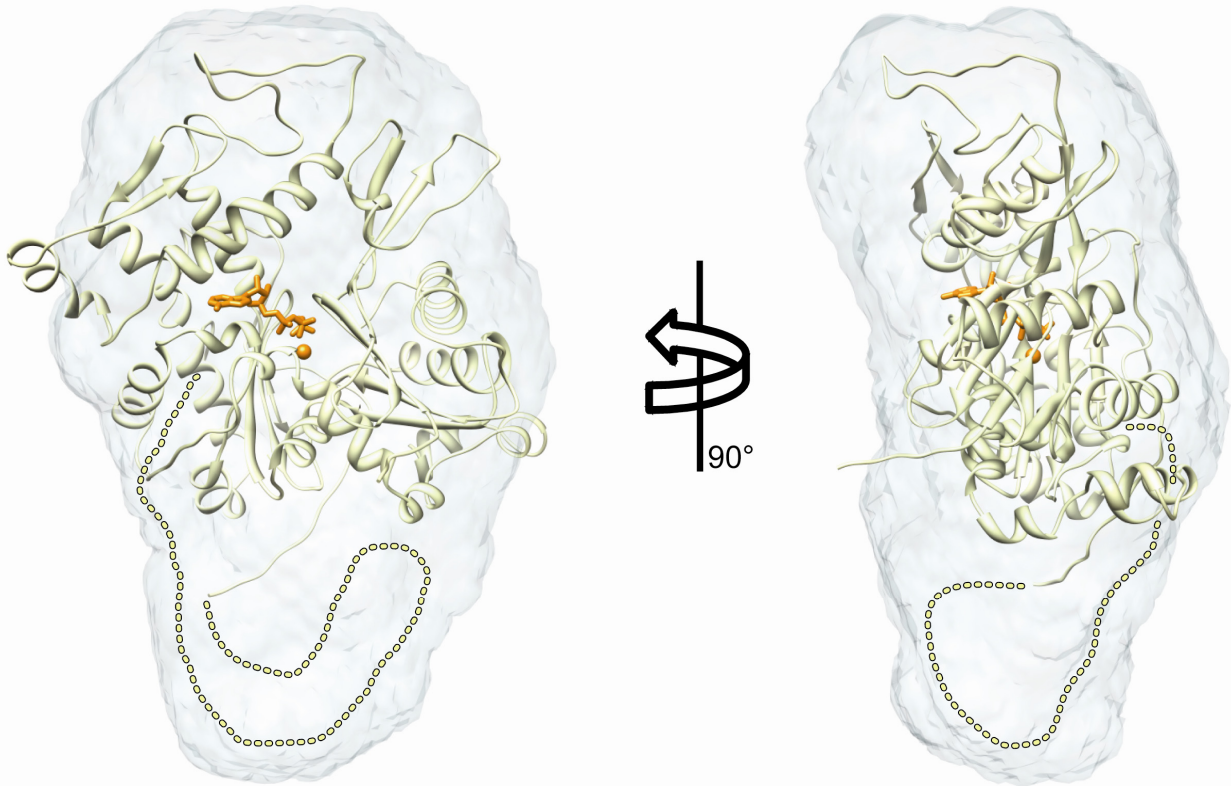


Figure 30: SAXS structure of Arp4

Overlay of the final averaged *ab initio* shape reconstruction of Arp4 derived by SAXS experiments (transparent envelope) with the docked crystal structure of Arp4 (yellow). Front and side views indicate a good fit between the crystal and the solution structure. The likely position of the disordered 49 amino acids of Insertion II within the solution structure is indicated by the dashed line.

The apparent molecular weight determined by SAXS is about 51 kDa, which corresponds well to the actual mass of an Arp4 monomer (56 kDa). This confirms the results from the gel filtration analysis. The protein concentrations in the SAXS measurements (up to 130 μM) lie well above the critical concentration, at which free actin monomers start to polymerize to form actin filaments which is about 0.1 μM and 0.7 μM at the barbed end and pointed end of a filament, respectively (Bonder et al, 1983). This indicates that ATP-Arp4 does not form actin like filaments at the tested conditions.

Next, the solution structure and oligomerization state of full length Arp8 and an N-terminally truncated Arp8 construct lacking the first 244 amino acids from *S. cerevisiae* were analyzed. The experimental scattering data could not be compared to a theoretical curve, since no crystal structure of Arp8 is available. However, no aggregation effects or changes in oligomerization at

higher concentrations (up to 80 μM) were detected for both constructs. The apparent molecular weight determined by SAXS was about 105 kDa for full length Arp8 and 76 kDa for the truncated version which corresponds well to the expected masses of an Arp8 monomer (101 kDa for full length and 73 kDa for the truncated version, respectively). This indicates that Arp8 is monomeric in solution and does not form polymers like actin. The Kratky-plot of full length Arp8 does not display a perfect parabola but rather ends in a plateau indicating that the protein is not entirely folded, whereas the shorter construct seems to be almost completely folded (see Figure 31).

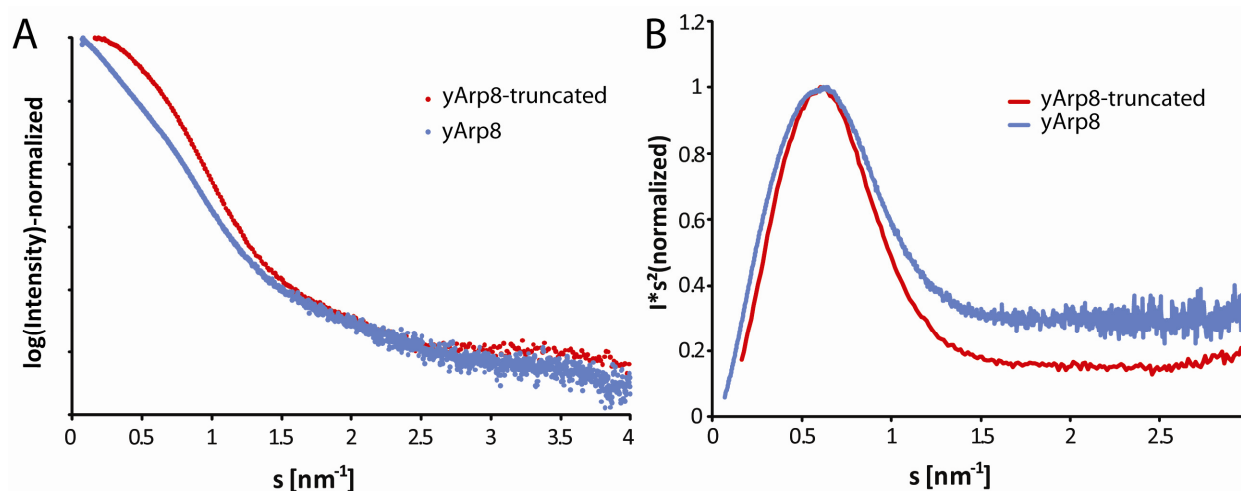


Figure 31: SAXS data of Arp8

A) Measured scattering curves of Arp8 (blue) and its truncated version lacking the first 245 amino acids (red).

B) Kratky-plots ($I*s^2$ vs s) for both proteins. The bell-shaped curves indicate that both full length Arp8 and truncated Arp8 are folded. Full length Arp8 however, seems to possess a higher degree of structural disorder.

Ab initio shape reconstructions reveal Arp8 to be more elongated than Arp4 in general. The compact part of the Arp8 SAXS structure however, is perfectly able to accommodate the actin fold present in Arp8 (see Figure 32). Interestingly, SAXS measurements of the N-terminally truncated Arp8 reveal a much more compact shape. This is consistent with the prediction that the first 244 amino acids of Arp8 are highly unstructured and indicates that the long extension found in the solution structure of full length Arp8 corresponds to the extended N-terminus (see Figure 24). It also confirms that the truncated version of Arp8 is properly folded (see Figure 32).

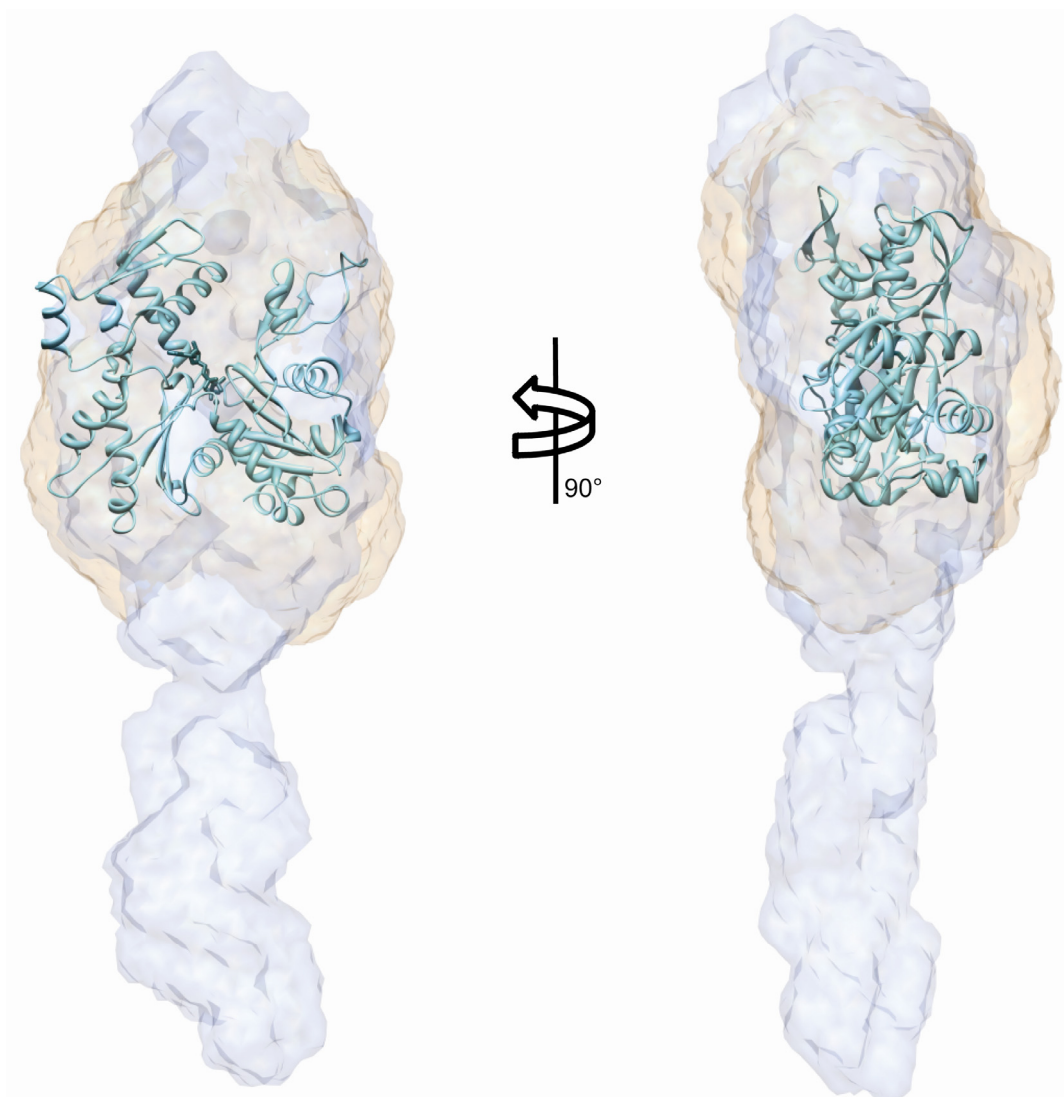


Figure 32: SAXS structures of Arp8

Overlay of the final averaged *ab initio* shape reconstruction of full length Arp8 (blue envelope) and N-terminally truncated Arp8 lacking the first 244 amino acids (red envelope) derived from SAXS experiments. The crystal structure of yeast actin (pdb: 1YAG, cyan) is docked into the envelopes for comparison. Front and side views indicate that the core actin fold fits into both solution structures of Arp8. Additional density can be attributed to insertions present in Arp8 compared to actin. The large N-terminus of Arp8 (amino acids 1-244) seems to form an extended protrusion consistent with the secondary structure prediction for it to be mainly unstructured.

In summary, SAXS data show that both Arp4 and Arp8 are monomeric under the tested conditions. This is consistent with the formation of an equal stoichiometric complex between Arp8, Arp4, actin and the HSA domain within the INO80 complex.

3.6.6 ATP is tightly bound to Arp4

ATP as well as a metal ion are clearly defined in the electron density in the nucleotide binding cleft of Arp4 (see Figure 33). This is consistent with previous biochemical observations that Arp4 binds to ATP and that the nucleotide state of Arp4 might play a role in its association to chromatin remodeling complexes (Sunada et al, 2005).

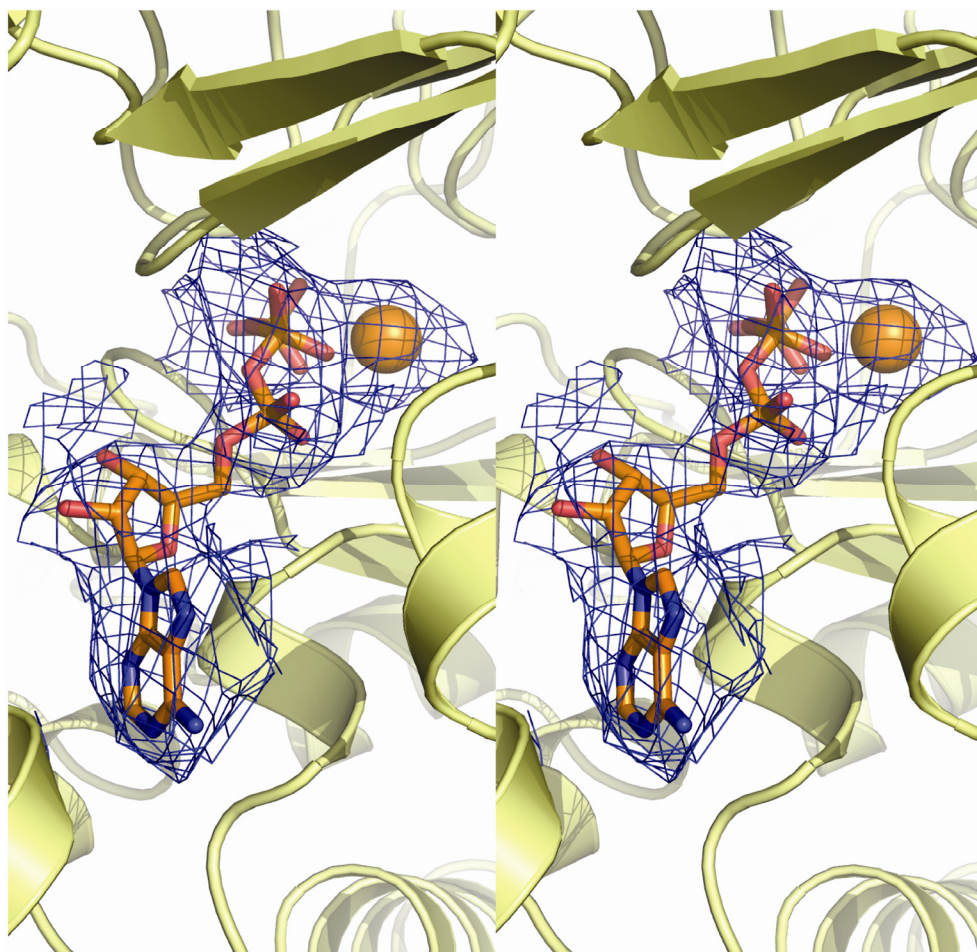


Figure 33: Electron density of the ATP molecule bound to Arp4

Stereo image of the simulated annealing difference omit map calculated for the ATP molecule and the metal ion using CNS. Electron density is clearly present between the four domains of Arp4 (yellow) indicating binding of the ATP and metal ligands (orange sticks and sphere). The map is displayed as blue mesh and contoured at 1.0 σ .

The presence of the nucleotide in the Arp4 structure is still somewhat surprising since neither ATP nor divalent metal ions were present during the purification process or the crystallization setups and must have been co-purified from the expression host. This argues not only for strong

ATP binding but also a lack of detectable ATPase activity of isolated Arp4 since the purification and crystallization process took about three weeks in total.

A comparison between the ATP binding modes of actin and Arp4 gives some hints how this tight binding might be achieved (see Figure 34).

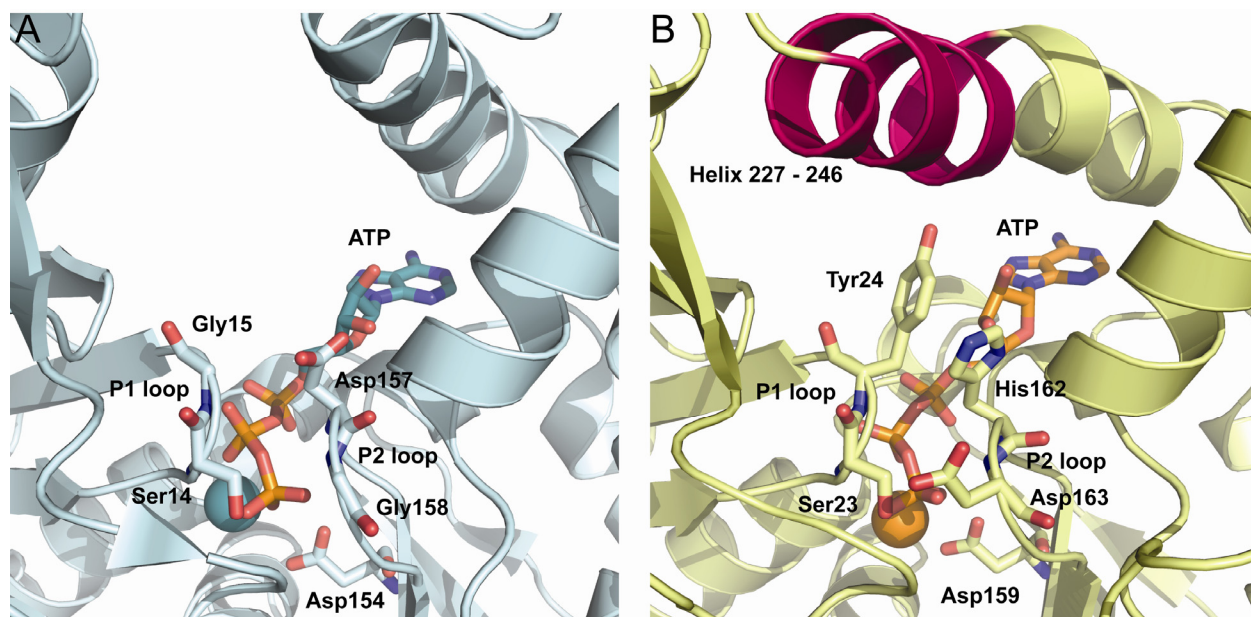


Figure 34: Comparison between ATP coordination of actin and Arp4

A) Detailed view of the ATP nucleotide bound by actin (pdb: 2HF4). The protein is displayed in cyan ribbon and important residues are represented as sticks and labeled. The ATP molecule and the metal ion are colored in a dark cyan.

B) Detailed view of the ATP nucleotide bound by Arp4 (in yellow). Important residues are represented as sticks and labeled. Note that Tyr 24 stacks on the ribose of ATP and Asp163 forms a hydrogen bond with Ser23 leading to tighter closure of the two nucleotide binding loops P1 and P2. Together with His162 and helix 227-246 (in pink) the nucleotide is more strongly shielded from the solvent as compared to actin.

The divalent cation is coordinated by the conserved Asp159^{Arp4} (corresponding to Asp154^{actin}). The side chain of Ser23^{Arp4} (corresponding to Ser14^{actin}) is rotated outward to accommodate the third phosphate moiety of ATP resulting in a conformation of the sensor loop (residues 75-77 in Arp4) similar to that observed in the structure of non-polymerizable ATP actin (Rould et al, 2006). Interestingly, Gly15^{actin} in the P1 nucleotide clamping loop of actin is substituted by Tyr24^{Arp4}. This tyrosine stacks on the ribose moiety of the bound ATP leading to an even tighter closure of the P1 loop around ATP in Arp4 as compared to actin. Accordingly, the P2 nucleotide clamping loop has Gly158^{actin} and Asp157^{actin} substituted by Asp163^{Arp4} and His162^{Arp4}, respectively. Asp163^{Arp4} forms a hydrogen bond with Ser23^{Arp4} leading to a tighter closure of the

P2 loop around the phosphate moieties in Arp4 (see Figure 34). Together with His162^{Arp4} the P1 and P2 nucleotide binding loops in Arp4 seem to shield the phosphate residues of the nucleotide more tightly from the environment compared to actin. Furthermore, an α -helix of Arp4 (residues 227-246 in Arp4) is longer by one and a half turns leading to a positional shift of this helix further closing the nucleotide binding cleft from the top.

The sequence comparison between actin and Arp4 (see Figure 23) additionally shows that His161^{actin} and Gln137^{actin} are substituted by Ser166^{Arp4} and Thr142^{Arp4}, respectively. According to mutational and structural studies, His161^{actin} takes part in the ATP hydrolysis cycle of actin by positioning a nucleophilic water (Martin et al, 2006; Vorobiev et al, 2003) and the mutation of Gln137^{actin} to alanine reduces the rate of ATP hydrolysis (Iwasa et al, 2008). Taken together, the absence of a catalytic histidine and glutamine and the tighter closure of the P1 and P2 nucleotide binding loops around the phosphate moieties of Arp4 lead to strong ATP binding and the apparent absence of ATPase activity of Arp4.

The intimate binding of ATP to Arp4 is further emphasized by the observation that ATP binding mutants (S23D^{Arp4}, D159G^{Arp4} and G161D^{Arp4}) were found to be insoluble upon expression in insect cells (data not shown). This is analogous to the instability of actin upon removal of the divalent cation and the nucleotide by EDTA (Altschuler et al, 2005) and indicates that ATP (or ADP) is required for proper folding of Arp4.

3.6.7 The structure of Arp4 explains why it is unable to form actin like filaments

The observation that Arp4 is apparently polymerization incompetent can be understood by analyzing its structure in the context of current models of F-actin obtained from fiber diffraction (see Figure 35) (Oda et al, 2009). In the filament, actin residues 283-294 at the barbed end of one monomer are enclosed by residues 61-65, 200-208 and 241-247 at the pointed end of the preceding monomer. Additionally, the DNaseI binding loop (residues 38-49 in actin) at the pointed end is extended to contact the hydrophobic groove between subdomains one and three at the barbed end of a following monomer (see Figure 35). On top of these intra-strand contacts of the two-stranded filament additional inter-strand contacts are formed. Most importantly, the C-terminus of the actin α -helix 191-199 contacts the amino terminus of the actin α -helix 110-115 in the neighboring strand and the so called hydrophobic plug (residues 265-271 in actin) contacts four regions in the opposite strand, including actin residues 201-203 and 39-42 of one subunit

and actin residues 170-174 and 285-286 of an adjacent subunit (see Figure 35 and compare Figure 6).

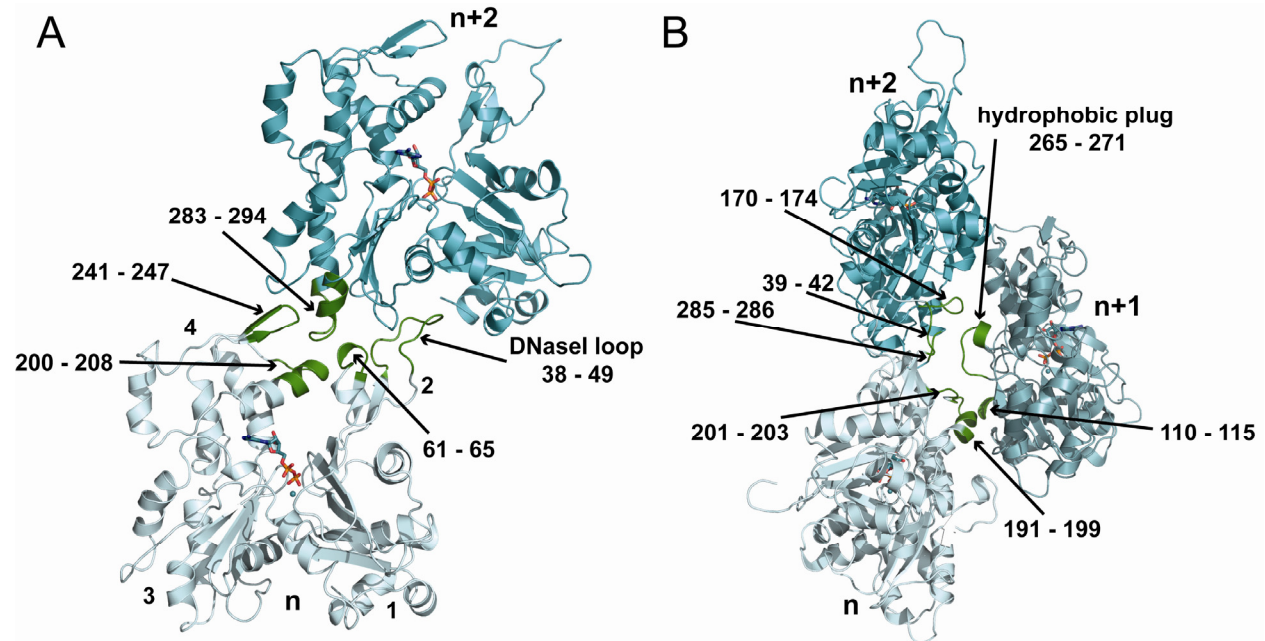


Figure 35: Contacts of adjacent actin monomers in the actin filament

A) Model of two intra-strand actin monomers (n and n+2) preceding each other within the actin filament (two shades of cyan) (Oda et al, 2009). Important residues for forming intra-strand contacts are highlighted in dark green and labeled. Note the extended DNaseI loop of the bottom monomer reaching into the hydrophobic groove between subdomains one and three of the following monomer.

B) Model of inter-strand interactions between two preceding actin monomers (n and n+2) with a third monomer from the second strand (n+1) of the double-stranded actin filament (three shades of cyan) (Oda et al, 2009). Important residues for forming inter-strand contacts are highlighted in dark green and labeled. Note the hydrophobic plug region extending from the n+1 monomer to contact both opposing actin monomers.

Taking a closer look at the corresponding regions in Arp4 readily reveals that most of the above mentioned contacts are not possible in Arp4 due to the presence of the Insertions I and II, as well as the shortening of the DNaseI loop. Insertion I (residues 199-226 in Arp4) forms a loop lacking secondary structure on top of the pointed end of Arp4. In addition to the inserted residues, α -helices at both ends of this loop differ in length in Arp4 as compared to actin (see Figure 28). Intriguingly, this insertion coincides with several stretches of amino acids which are important for forming contacts within the actin filament (Oda et al, 2009). Specifically, it masks regions 200-208 of actin by positioning part of the loop (residues 201-209 in Arp4) above of this region and by elongation of actin helix 202-216. Moreover, residues 241-247 of actin are also masked

by a stretch of this loop (residues 210-218 in Arp4) positioned above this interaction surface prohibiting it to form contacts with an adjacent actin monomer (see Figure 36).

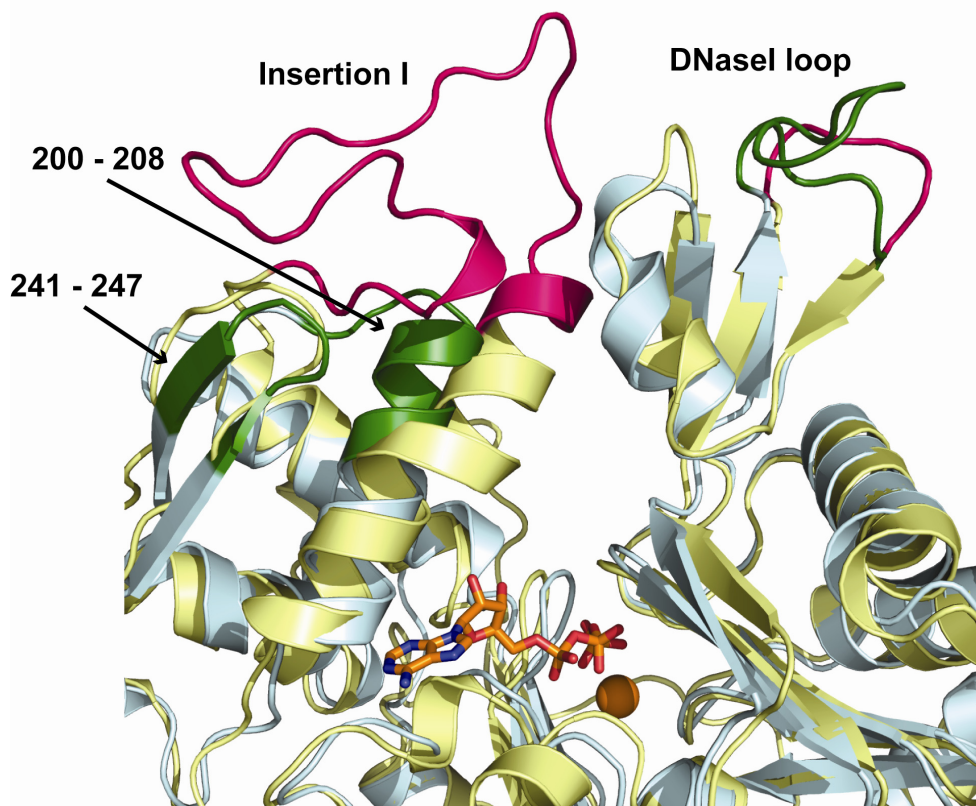


Figure 36: Pointed end of Arp4

Overlay between actin (cyan) and Arp4 (yellow) detailing differences at the pointed end. Highlighted in dark green and labeled are actin residues important for forming contacts within the actin filament (see Figure 35). In pink are changes present in Arp4 which render those contacts largely impossible (Insertion I and shortened DNaseI loop).

The next substantial difference at the pointed end of Arp4 compared to actin is the shortened DNaseI binding loop. This unstructured loop is implied to reach into the hydrophobic pocket present at the barbed end of an adjacent actin monomer. It is shorter by about five residues in Arp4 (residues 47-54 in Arp4) making it impossible to contact the barbed end on an adjacent monomer (see Figure 36).

Insertion II (amino acids 300-382 in Arp4) was partially disordered. Whereas residues 300-327 and 378-382 were ordered in the crystal, the position of residues 328-377 can be inferred from the SAXS envelope (see Figure 30). The loop emanates from domain 4 and packs on the “backside” of Arp4, mainly contacting domains three and four before it enters the actin fold

again in domain three (see Figure 37). It coincides with the hydrophobic plug region of actin (residues 265-274 in actin) which is predicted by the filament model (Oda et al, 2009) and mutational studies (Shvetsov et al, 2002) to be involved in inter-strand contacts. Very likely the expansion of this hydrophobic plug region in Arp4 compared to actin disturbs the ability to form the proper inter-strand interactions within actin filaments. In addition, Insertion II caps the amino terminus of the actin α -helix 110-115, another intra-strand interacting element, by stacking of Trp315^{Arp4} on top of that helix (see Figure 37).

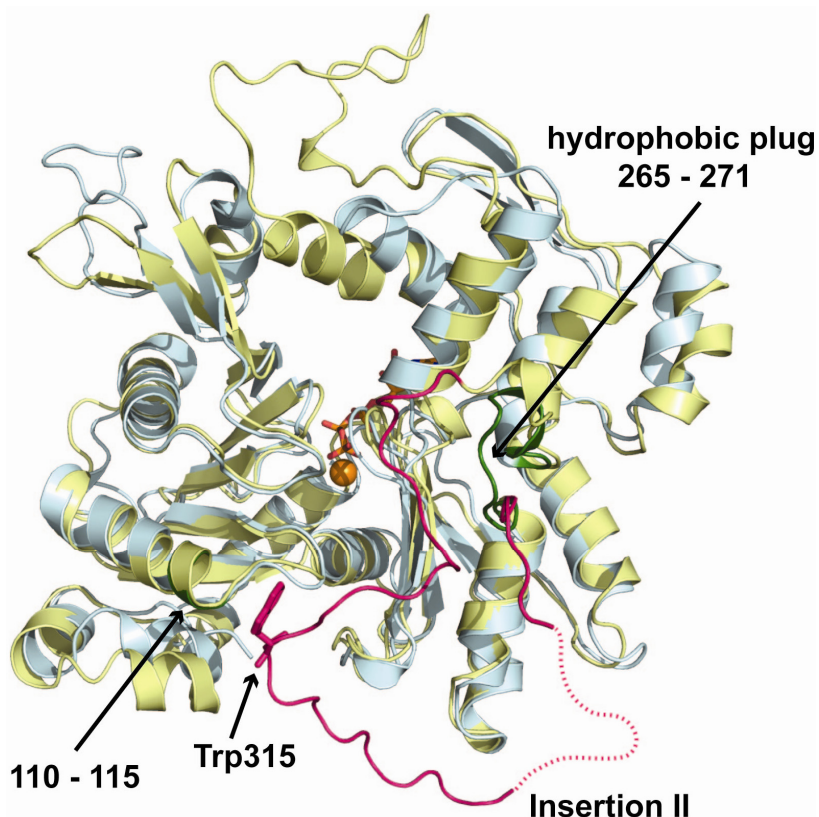


Figure 37: Insertion II of Arp4

View of the “backside” of actin (cyan) and Arp4 (yellow). The hydrophobic plug region of actin is colored in dark green and labeled. Insertion II (in pink; dashed line represents the unstructured 49 residues of Insertion II) expands this region in Arp4 and Trp315 (represented in sticks and labeled) caps α -helix 110-115 in actin, rendering important inter-strand contacts within the actin filament impossible (see Figure 35).

Taken together, the surface properties of Arp4 are very different as compared to actin. As a consequence, key interactions which are important for intra-strand filament contacts in actin are no longer possible. Additionally, crucial inter-strand interactions, especially through the hydrophobic plug region of actin are disturbed, nicely explaining why Arp4 itself is monomeric.

3.7 Biochemical studies of Arp4 and Arp8

3.7.1 Arp4 inhibits actin polymerization by binding to monomers

Given the possibility that nuclear Arps are involved in actin metabolism and that Arp4, Arp8 and actin form a complex within the INO80 chromatin remodeler (Szerlong et al, 2008) several assays were performed to address the question if and how Arp4 and Arp8 interact with F- and G-actin.

First, the spontaneous polymerization of monomeric, Mg^{2+} -ATP-actin in the presence of Arp4 was analyzed by conducting “pyrene assays” (“pyrene assays” were performed in collaboration with Dennis Breitsprecher from the group of Jan Faix at Hannover Medical School, Germany). This experiment is performed by using actin that has been fluorescently labeled by specific attachment of *N*-pyrenyliodoacetamide (pyrene) at the solvent accessible cysteine 374 (Hertzog & Carrier, 2005). The polymerization of this pyrene labeled actin is then induced by the addition of salt. Upon polymerization the environment of the fluorophore changes, as it gets buried within the filament leading to an increase in fluorescence which is used as a signal to measure the extent of polymerization. By subsequently adding a protein of interest it can be ascertained, if this protein has an influence on actin polymerization kinetics.

As seen in Figure 38, Arp4 decreased the initial polymerization rate of actin in a concentration dependent manner. If the reaction is continued for 16 h to measure the extent of polymerization at steady state it becomes evident that Arp4 did not markedly sequester actin monomers, as indicated by nearly constant levels of F-actin at steady-state. In other words, Arp4 does not form a polymerization incompetent complex with actin.

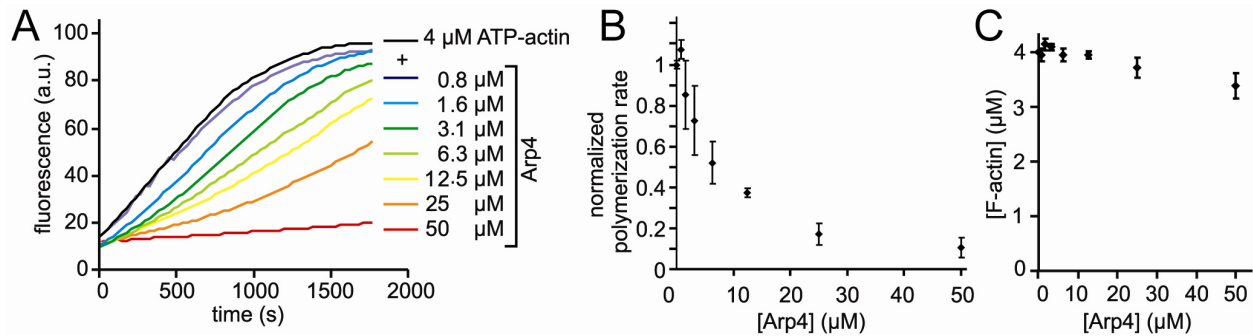


Figure 38: Influence of Arp4 on actin polymerization

A) Pyrene assays of actin polymerization. Mg^{2+} -ATP-actin was polymerized by addition of KMEI buffer and the Arp4 concentrations indicated, and the increase in pyrene fluorescence was detected over time. Arp4 markedly decreased the initial polymerization rates of actin.

B) Normalized polymerization rates derived from three independent experiments equivalent to (A) show a dose-dependent inhibition of polymerization.

C) Steady-state F-actin fluorescence from experiments equivalent to (A) is constant, independent of the Arp4 concentration and thus indicates that Arp4 does not sequester monomers.

To support this result, co-sedimentation spin down analyses of F-actin with Arp4 were performed (Co-sedimentation assays were performed by Dennis Breitsprecher from the group of Jan Faix at Hannover Medical School, Germany). In this case, actin is polymerized in the presence of Arp4 and then pelleted by extensive centrifugation. If the filaments are intact, the entire actin fraction will be found in the pellet, if Arp4 forms a polymerization incompetent complex with actin, parts of the actin fraction will be found in the supernatant. Finally, if the protein binds to actin filaments it will be found in the pellet together with actin. This experiment confirmed that Arp4 does not reduce the amount of actin filaments at steady state, and moreover showed that Arp4 does not tightly bind to actin filaments (see Figure 39).

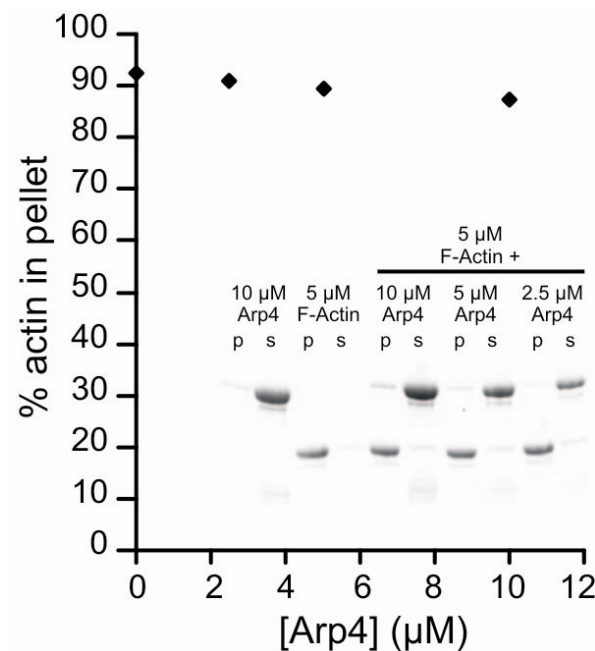


Figure 39: Spin down assays of Arp4 with actin filaments

Co-sedimentation assays of Mg^{2+} -ATP-actin polymerized in the presence of the indicated Arp4 concentrations show that Arp4 neither sequesters monomers nor binds to F-actin, as the entire actin fraction is found in the pellet whereas the entire Arp4 fraction is still in the supernatant.

This suggests that Arp4 interacts exclusively with actin monomers but without efficiently sequestering them, reminiscent of the G-actin binding protein profilin (Korenbaum et al, 1998). Profilin prevents premature actin polymerization by binding to the barbed end of actin monomers thereby inhibiting nucleation and pointed end elongation, while having almost no effect on steady-state barbed end elongation (see section 1.4) (Paul & Pollard, 2009).

To irrefutably verify the direct interaction of Arp4 with actin, surface plasmon resonance (SPR) experiments were performed to test the binding of Arp4 to actin immobilized on the surface of a sensor chip (see Figure 40). SPR clearly indicates that Arp4 specifically binds to monomeric actin and the K_D of the interaction can be estimated to be around 2 μ M.

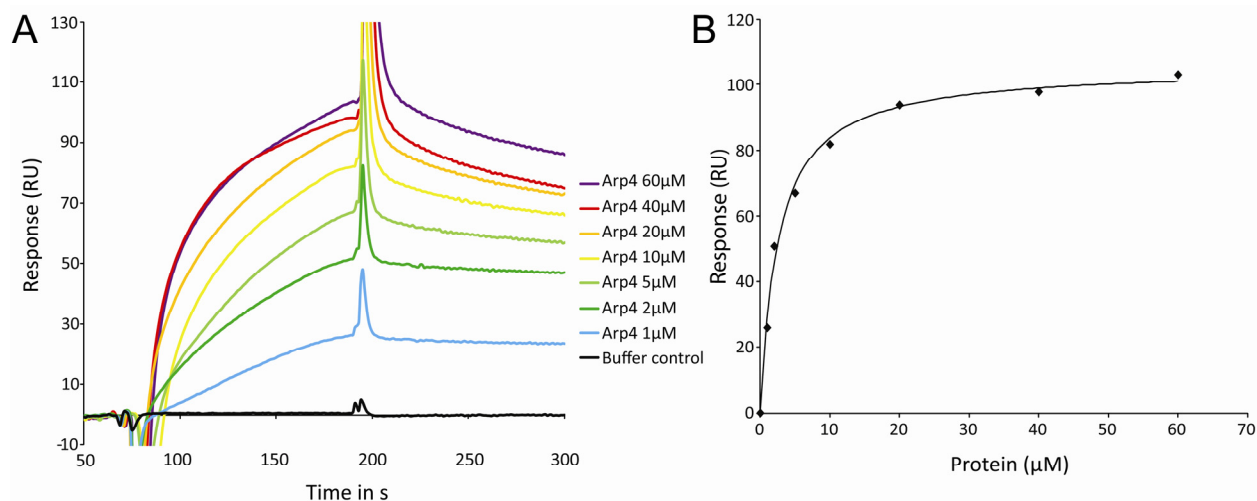


Figure 40: Surface plasmon resonance data of Arp4 binding to actin

A) Arp4 was passed over a sensor chip containing immobilized actin in a concentration range of 1-60 μM . Change in surface plasmon resonance was measured and the sensograms are depicted.

B) The corresponding binding curve of Arp4 and actin can be used to estimate the K_D . Three independent measurements were performed and a K_D of $1.6 \pm 0.8 \mu\text{M}$ was calculated.

In order to gain a more detailed picture of the inhibitory effects of Arp4 on actin assembly, *in vitro* TIRF microscopy on Oregon-Green (OG)-labeled, polymerizing actin filaments was employed (TIRF microscopy assays were performed by Dennis Breitsprecher from the group of Jan Faix at Hannover Medical School, Germany). In this assay, growing actin filaments can be directly observed in a fluorescence microscope, allowing the quantification of elongation speed and number of filaments. Interestingly, Arp4 decreased both the elongation rate of actin filament barbed ends as well as the total number of spontaneously formed filaments (see Figure 41). 5 μM Arp4 were already sufficient to reduce the number of growing filaments by 50%, while filament elongation rates were only slightly decreased. This effect indicates that Arp4 mainly inhibits filament nucleation leading to a strong reduction in the number of filaments whereas filament elongation is only slightly affected.

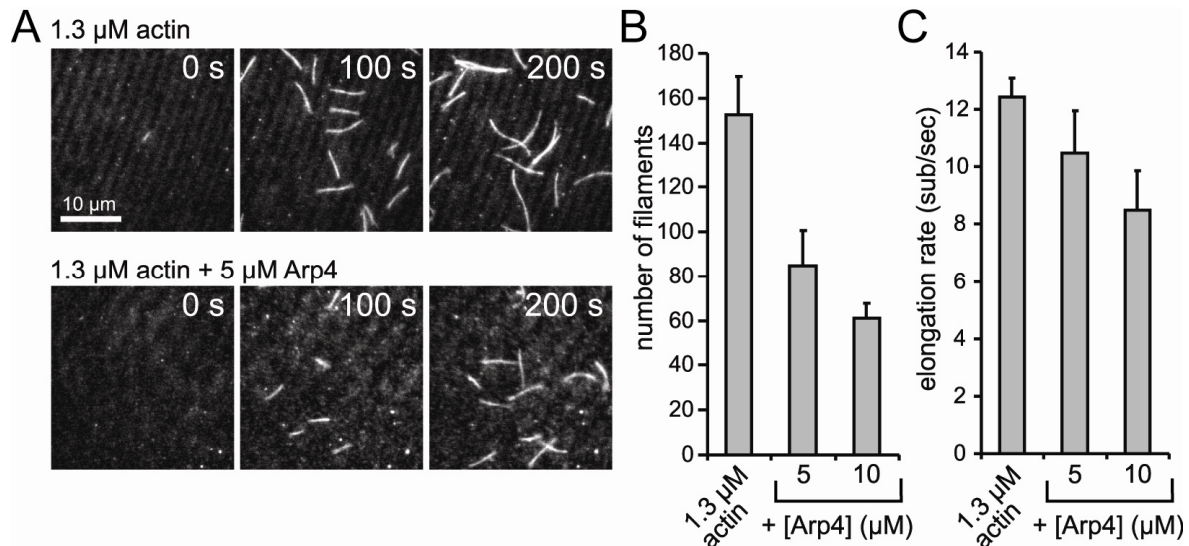


Figure 41: TIRF microscopic studies of the effect of Arp4 on actin polymerization

A) *In vitro* TIRF microscopy pictures of single actin filaments growing in the presence and absence of Arp4 at time points 0, 100 and 200 s.

B) Numbers of filaments were quantified after 200 s.

C) Filament elongation rates were quantified after 200 s.

Addition of Arp4 markedly decreases the number of growing filaments and has a slight effect on the elongation rate as well.

Again, this suggests that Arp4, like profilin interacts with monomeric actin and that this interaction inhibits primarily the formation of F-actin nuclei but without preventing the formation of actin filaments after nucleation has occurred.

3.7.2 Arp4 preferentially interacts with the barbed end of actin monomers

To further analyze the effects of Arp4 on the G-/F-actin equilibrium, the critical concentration of F-actin in the presence of Arp4 was determined (critical concentration assays were performed by Dennis Breitsprecher from the group of Jan Faix at Hannover Medical School, Germany). As mentioned, the critical concentration is defined as the concentration at which actin monomers start to spontaneously assemble to actin filaments. To measure it, different concentrations of actin are incubated in the presence of Arp4 until steady state is reached. The extent of polymerization is then judged by measuring pyrene fluorescence. The critical concentration is determined as the intercept of the linear regressions of the signals for filamentous and monomeric actin. To allow discrimination between the critical concentrations for barbed and pointed end polymerization which are inherently different for actin filaments (0.1 μM for barbed

end and $0.7 \mu\text{M}$ for pointed end) (Bonder et al, 1983), the experiment was performed both in the presence and in the absence of the barbed end capping protein CapZ. CapZ binds to barbed ends of filaments thereby blocking the exchange of actin subunits at these ends (Barron-Casella et al, 1995). Its presence in the critical concentration assay therefore allows the specific measurement of the critical concentration at the pointed end since the barbed end is blocked.

As expected, the critical concentration of F-actin alone, both in the absence of Arp4 and CapZ ($C_{\text{Crit}(\text{free})}$) was $0.1 \mu\text{M}$, while it was shifted to $0.6 \mu\text{M}$ when only the capping protein CapZ was present ($C_{\text{Crit}(\text{capped})}$) (see Figure 42). This corresponds nicely to the published values for both ends (see above). Interestingly, the presence of $20 \mu\text{M}$ Arp4 did not change $C_{\text{Crit}(\text{free})}$. This means that Arp4 does not interfere with the addition of actin monomers to the barbed end and is in line with the observation that Arp4 did not sequester monomers at steady state (see Figure 38 and Figure 39). On the other hand $C_{\text{Crit}(\text{capped})}$ was shifted to $\sim 2 \mu\text{M}$ in the presence of Arp4. This suggests that Arp4 interferes specifically with monomer addition to the pointed end possibly by blocking the barbed end of actin monomers (see Figure 42).

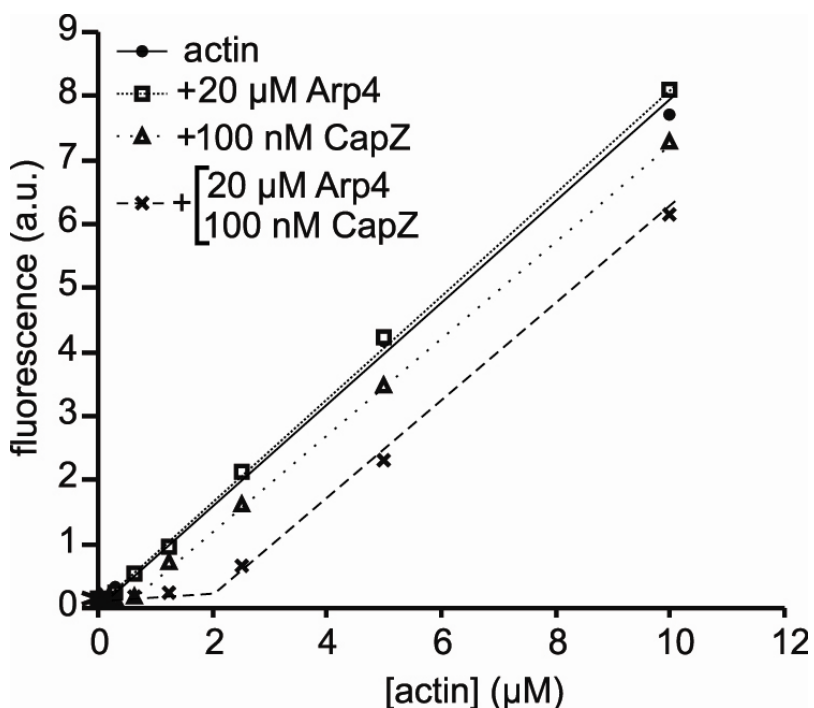


Figure 42: Effect of Arp4 on the critical concentration of actin polymerization

Critical concentration plot of F-actin in the presence and absence of Arp4 and CapZ. F-actin at different concentrations, either with free barbed ends or CapZ-capped barbed ends was incubated in the presence and absence of $20 \mu\text{M}$ Arp4. Arp4 only increases the critical concentration of capped filaments.

Moreover, these assays were instrumental to calculate the K_D for the Arp4/G-actin interaction to be ca. $8 \mu\text{M}$ (see section 2.2.9.3) (Hertzog & Carlier, 2005). This is in agreement with the value of $2 \mu\text{M}$ determined by SPR (see section 3.7.1).

Most notably, analogous effects on the critical concentration of free and capped filaments were again previously observed for the small G-actin binding protein profilin, which binds the barbed end of the monomer and thus prevents monomer addition to the pointed end of the filament when barbed ends are capped (Korenbaum et al, 1998).

To further investigate the effect of Arp4 on filament elongation, pyrene assays with CapZ-capped filaments were performed. Since the barbed end is blocked in this case, only pointed end elongation of the filaments is possible. A concentration dependent reduction of pointed end elongation through the addition of Arp4 could be monitored (see Figure 43), further supporting the results of the critical concentration assay (see Figure 42). Consequently, these results suggest that Arp4 directly interacts with the barbed end of the monomer.

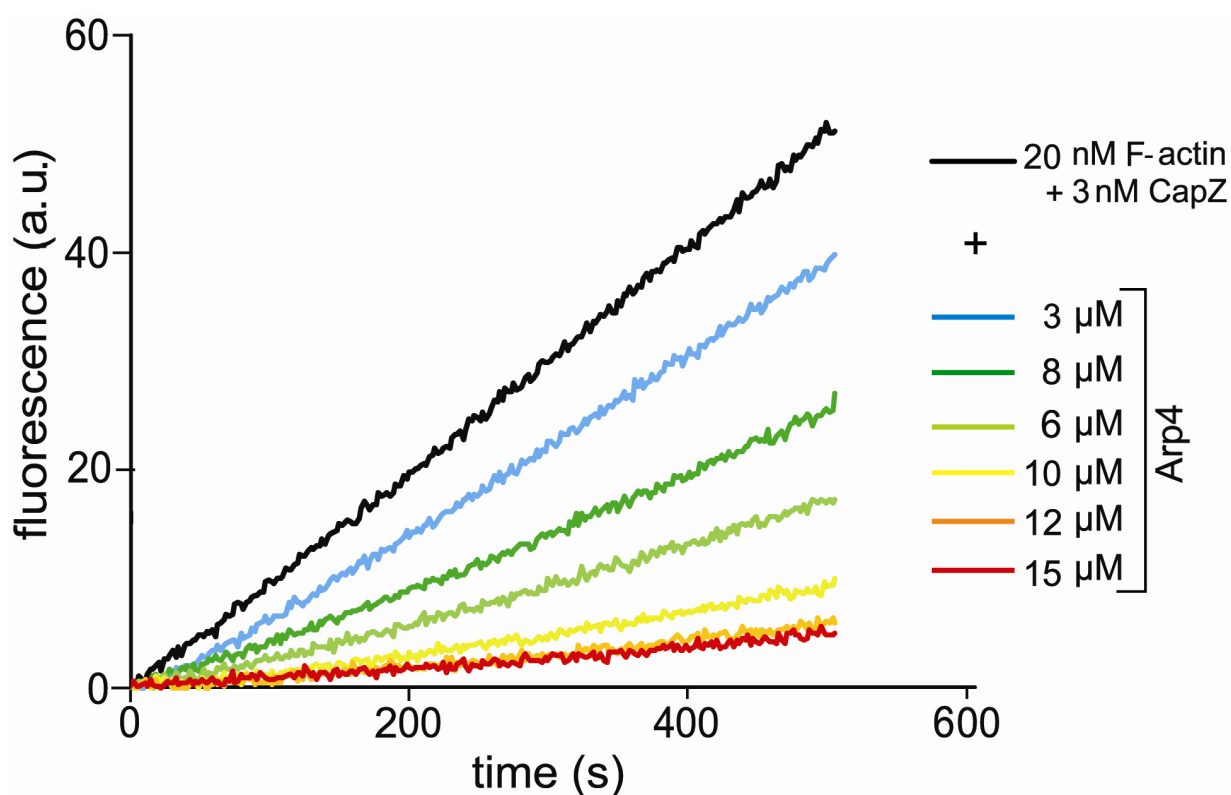


Figure 43: Effect of Arp4 on pointed end elongation

Actin filaments capped at the barbed end by CapZ were used in polymerization assays to measure pointed end elongation. Increasing amounts of Arp4 inhibit pointed end elongation.

3.7.3 Arp4 depolymerizes actin filaments

The effect of Arp4 on existing actin filaments was investigated as well. To this end, preformed, pyrene labeled actin filaments both with free and CapZ capped ends were incubated with Arp4 and fluorescence was monitored (actin depolymerization assays were performed in collaboration with Dennis Breitsprecher from the group of Jan Faix at Hannover Medical School, Germany).

Surprisingly, the addition of 10 μM Arp4 to 2 μM F-actin with free barbed ends showed a strong effect, triggering an immediate, rapid disassembly of actin filaments indicated by the rapid loss of pyrene fluorescence. The initial rate of this disassembly reaction was comparable to that of LatrunculinA (LatA)-mediated F-actin disassembly which was used as a control (see Figure 44).

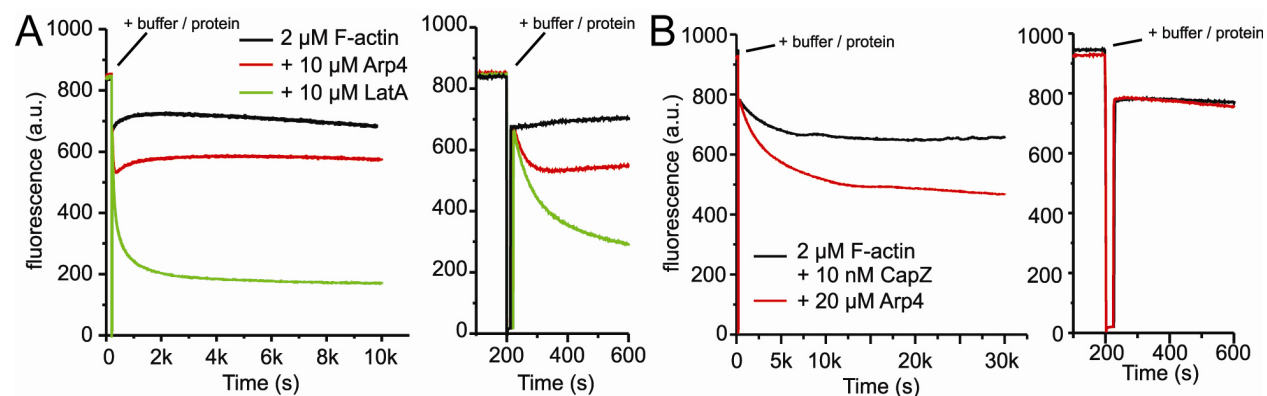


Figure 44: Depolymerization of actin filaments by Arp4

A) Time-course of the effects of Arp4 on the G-/F-actin equilibrium. Pyrene fluorescence of F-actin was detected for 200 s. Subsequently, KMEI buffer alone or supplemented with Arp4 or LatA was added, and the decrease in fluorescence was followed for 10,000 s. The smaller timescale highlights fast, instant depolymerization upon addition of Arp4 (right).

B) Effect of Arp4 on the G-/F-actin equilibrium when barbed ends are capped. The experiments were performed as in (A) with the exception that CapZ was added. The smaller timescale illustrates that rapid Arp4-mediated F-actin disassembly is abolished when barbed ends were capped (right).

LatA was shown to depolymerize F-actin completely by binding to the pointed end of monomers with nM affinities and therefore preventing both re-incorporation into the filament, and nucleotide exchange (Coue et al, 1987; Yarmola et al, 2000). In contrast to LatA, Arp4-mediated F-actin disassembly was not complete, but stopped after ~ 100 s. Subsequently, the G-/F-actin equilibrium was slowly restored, suggesting that Arp4-binding to the barbed end of the monomer does not inhibit its re-incorporation into the filament, consistent with the findings above that Arp4 does not efficiently sequester monomers under these conditions.

According, to the finding that Arp4 binds to the barbed ends of actin monomers (see section 3.7.2) the rapid Arp4-mediated disassembly was inhibited when using F-actin with CapZ-capped barbed ends. In this case, Arp4 rather depolymerized F-actin more slowly and, most importantly, sequestered monomers, as it inhibits the addition of actin monomers to the free pointed ends of the filaments (see Figure 44). This nicely corroborates the results from the critical concentration analysis (see Figure 42).

3.7.4 Effects of Arp4 on the equilibrium of G- and F-actin depends on the nucleotide state

Keeping in mind the results from the previous section it is interesting to ask why Arp4 rapidly depolymerized uncapped F-actin only to some extent and not completely? Since pre-polymerized F-actin is composed of ADP-actin, it could be possible that Arp4 efficiently removes ADP-actin from the barbed end, but still allows exchange of ADP to ATP in the bound actin monomer. As ATP is still present in the buffer the newly formed ATP-actin could be reincorporated into the barbed end of the filament leading to the observed equilibrium. In order to test this hypothesis, equivalent depolymerization experiments were performed in KMEI/Mg-exchange buffer containing ADP instead of ATP. ATP was removed entirely from the mixture by adding hexokinase and glucose prior to the experiment. As expected, Arp4 now completely disassembles actin filaments, resulting in a depolymerization rate comparable to LatA-mediated filament disassembly (see Figure 45).

To further verify the increased preference of Arp4 to ADP- compared to ATP-actin, pyrene polymerization assays equivalent to Figure 38 were performed but this time with monomeric Mg^{2+} -ADP-actin (see Figure 45). They showed that the inhibitory effect of Arp4 on the polymerization of ADP-actin was markedly enhanced when compared to ATP-actin. Most strikingly, addition of ATP during the polymerization process released the strong inhibition of ADP-actin polymerization by Arp4 and led to enhanced polymerization, supporting that Arp4-binding to the monomer does not interfere with nucleotide exchange and suggesting that the affinity of Arp4 for ADP-actin is much higher than for ATP-actin.

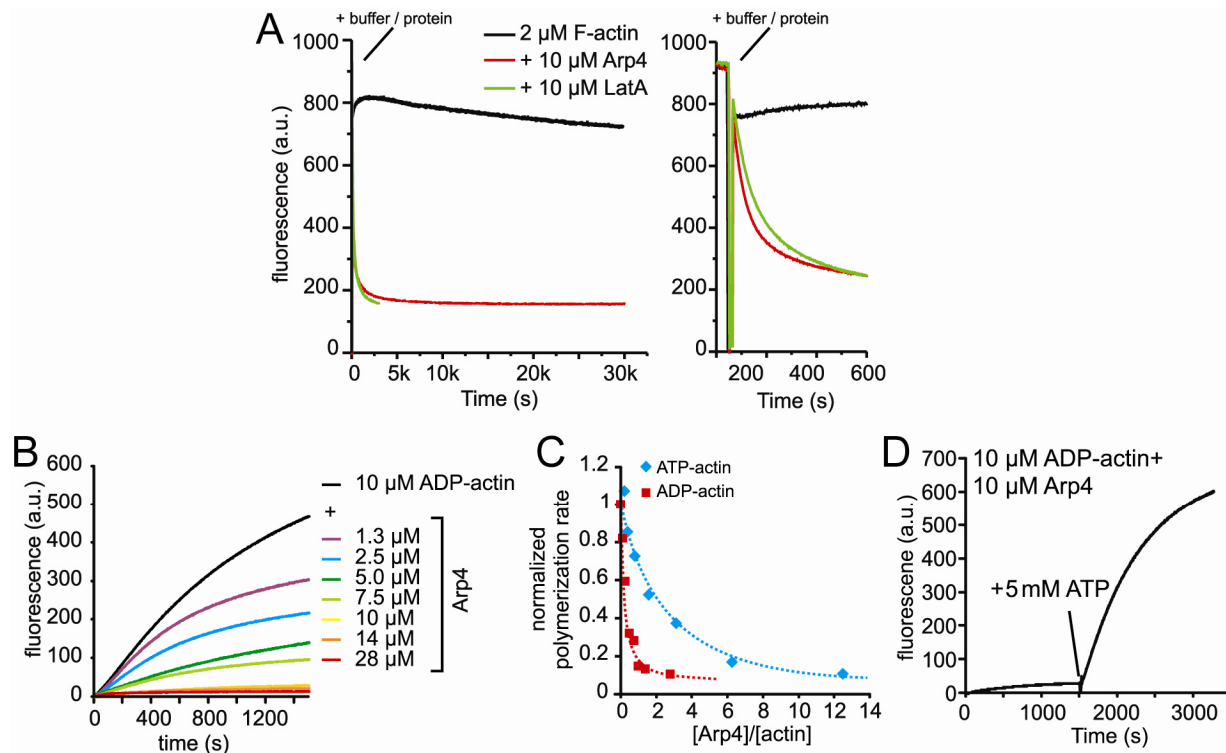


Figure 45: Arp4 activities are dependent on the nucleotide state of actin

A) Effect of Arp4 on the F-/G-actin equilibrium in the absence of ATP. The experiment was performed as in Figure 44. Buffers contained ADP instead of ATP. Residual ATP was removed by adding hexokinase and glucose prior to the experiments. The smaller timescale highlights immediate and complete depolymerization of ADP-actin by Arp4 (right).

B) ADP-actin assembly assay. Mg^{2+} -ADP-actin was polymerized in the presence of the Arp4 concentrations indicated. A strong inhibition of the polymerization of ADP-actin by Arp4 can be observed (compare Figure 38).

C) Normalized polymerization rates derived from B and Figure 38 are shown for comparison. The inhibition of actin assembly by Arp4 is much more efficient for ADP-actin.

D) Addition of ATP to Arp4-inhibited ADP- Mg^{2+} -actin polymerization restored actin assembly.

These data indicate that Arp4 primarily binds ADP-actin via a barbed end interaction, and that this interaction does not interfere with nucleotide exchange. Interestingly, profilin also stimulates the exchange of ADP to ATP in actin to further bolster the pool of polymerization competent actin (Witke, 2004).

3.7.5 Arp8 does not inhibit actin polymerization but sequesters ADP-actin

Since Arp8 is also part of the complex containing Arp4, actin and the HSA domain of the INO80 protein, it was tested whether Arp8 also affects actin dynamics. In contrast to Arp4 however, Arp8 did not affect the initial polymerization kinetics of ATP-actin as judged by pyrene assays (see Figure 46). The results of the pyrene assays were further confirmed by TIRF microscopy. After quantification of the elongation rates and filament lengths it could be observed that Arp8 has no effect on both (see Figure 46).

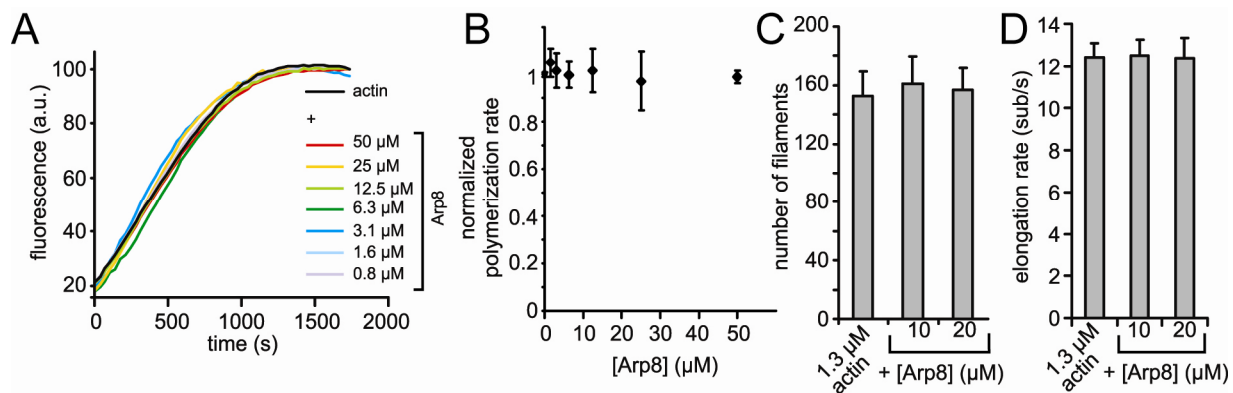


Figure 46: Arp8 does not affect actin polymerization

A) Pyrene assays of actin polymerization in the presence of Arp8. ATP-actin was polymerized with the Arp8 concentrations indicated, and the increase in pyrene fluorescence was detected over time. Arp8 did not markedly change the polymerization behavior of actin.

B) Normalized polymerization rates derived from three independent measurements equivalent to A show no inhibition of polymerization by Arp8.

C) Numbers of filaments in the presence and absence of Arp8, as determined by TIRF microscopy.

D) Filament elongation rates in the presence and absence of Arp8, as determined by TIRF microscopy. Arp8 has no influence on both parameters. The assay was performed as described in Figure 41.

Unexpectedly, and in marked contrast to Arp4, Arp8 efficiently sequestered actin monomers at steady state. This was assessed by fluorescence measurements of pyrene assays after 16 h which showed a marked decrease in fluorescence dependent on the Arp8 concentration and confirmed by high-speed sedimentation analyses (see Figure 47).

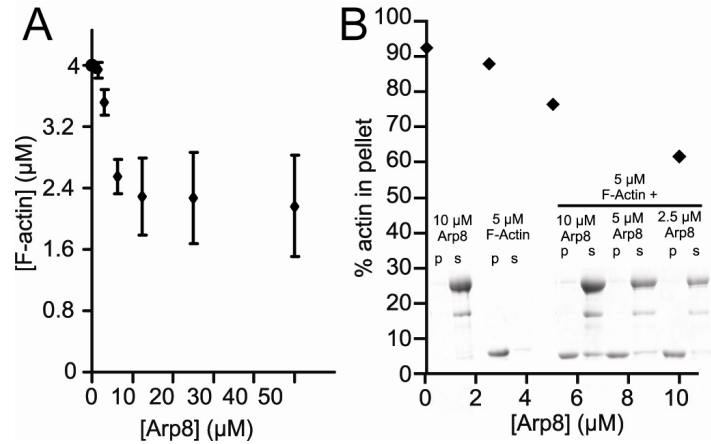


Figure 47: Arp8 sequesters actin monomers

A) Steady-state F-actin fluorescence is decreased, dependent on the Arp8 concentration, indicating that Arp8 sequesters actin monomers (experiments were performed equivalent to Figure 46).

B) Co-sedimentation assays of Mg^{2+} -ATP-actin polymerized in the presence of the indicated Arp8 concentrations also show that Arp8 sequesters actin monomers since increasing amounts of actin are found in the supernatant dependent on the Arp8 concentration. The experiment also shows that Arp8 does not bind to actin filaments.

Consistent, with the result that Arp8 sequesters monomers, it shifted the critical concentration of both, capped and uncapped filaments to about $1.3 \mu\text{M}$ (see Figure 48). From this the apparent K_D for the actin Arp8 interaction can be calculated to about $16.5 \mu\text{M}$ (Hertzog & Carrier, 2005).

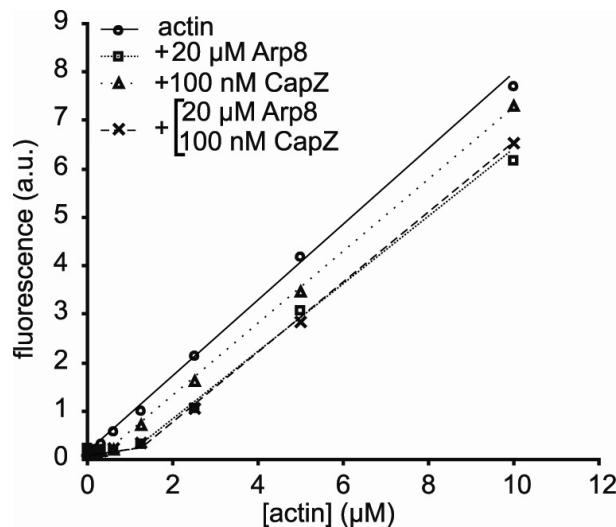


Figure 48: Effect of Arp8 on the critical concentration of actin polymerization

Critical concentration plot of F-actin in the presence and absence of Arp8 and CapZ. Conditions are as in Figure 42. Note that the change in critical concentration does not depend on the presence of CapZ. $C_{\text{crit}(\text{free})}$ and $C_{\text{crit}(\text{capped})}$ are both shifted to $1.3 \mu\text{M}$ corresponding to a K_D of the Arp8-G-actin interaction of $\sim 16.5 \mu\text{M}$.

These results show that Arp8 binds and sequesters actin monomers in a manner that prevents their re-incorporation into either end of the filament. Furthermore, they indicate that Arp8 does not specifically interact with the barbed end of actin monomers.

SPR experiments to verify the direct interaction of Arp8 with actin indicate that it indeed specifically binds to actin (see Figure 49). Due to problems with unspecific binding to the reference channels of the chips however it was not possible to determine a K_D .

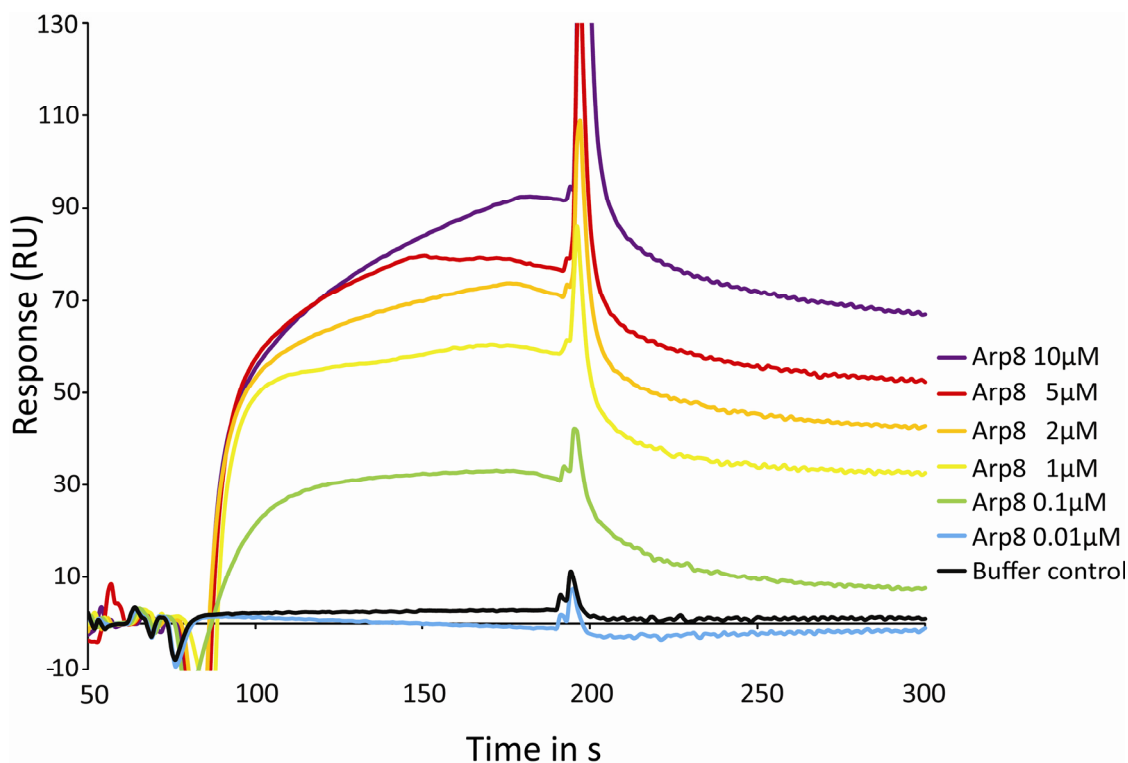


Figure 49: Surface plasmon resonance data of Arp8 binding to actin

Arp8 was passed over a sensor chip containing immobilized actin in a concentration range of 0.01-10 μM . Change in surface plasmon resonance was measured and the sensograms are depicted.

As Arp8 is able to sequester actin monomers it was expected that like Arp4 it would also be able to depolymerize existing actin filaments. Indeed, the analysis of the kinetics of Arp8-mediated disassembly of F-actin revealed some striking effects. While no obvious sequestration of monomers was observed immediately after Arp8 addition, F-actin depolymerized after a lag-phase of approximately 2500 s with very slow kinetics (see Figure 50A). This is in line with the observation that Arp8 does not influence the initial rate of actin polymerization (monitored in a time frame of about 1800 s; see Figure 46) but does sequester monomers once steady state is reached (see Figure 47).

Similar to Arp4, the conversion of ATP to ADP in the reaction mixture by adding hexokinase and glucose prior to the experiment changes the behavior of Arp8 towards actin. The presence of ADP instead of ATP resulted in loss of the lag-phase of the depolymerization reaction, leading to instant depolymerization of F-actin (see Figure 50A).

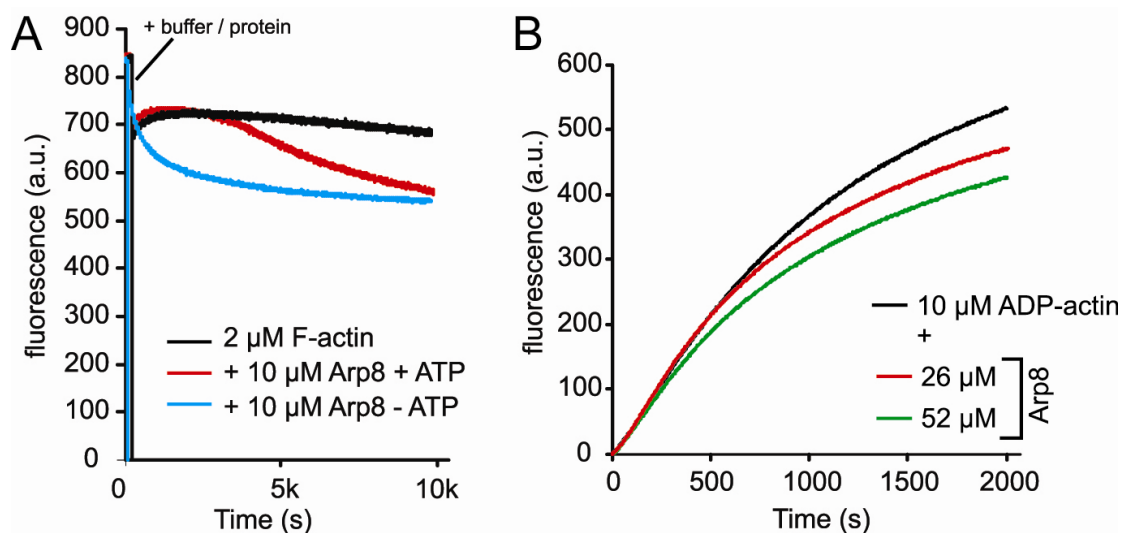


Figure 50: Actin filament depolymerization by Arp8 and the nucleotide state of actin

A) Arp8 depolymerizes F-actin in the presence of ATP with very slow kinetics (red curve). Conditions are as in Figure 44. Note that removal of ATP from the reaction mixture led to a loss of the pronounced lag-phase of Arp8-mediated F-actin disassembly (blue curve).

B) ADP-actin assembly assay. Mg^{2+} -ADP-actin was polymerized in the presence of the Arp8 concentrations indicated. The amount of F-actin was reduced with increasing amounts of Arp8.

However, the kinetics of the Arp8 mediated depolymerization were still significantly slower compared to Arp4 mediated depolymerization of ADP-actin filaments in the absence of ATP (see Figure 45). On top of that the depolymerization reaction was not complete, even after 10,000 s which is in line with a rather low affinity of Arp8 to ADP-actin monomers.

Consistent with very slow binding kinetics of Arp8 to ADP-actin, no reduction in the initial polymerization rate of ADP-actin in the presence of Arp8 using pyrene assays was detected (see Figure 50B). Instead the amount of F-actin was reduced with increasing amounts of Arp8, an effect that is not observed in the presence of ATP (see Figure 46). Thus, it is probable that Arp8 like Arp4 binds preferentially to ADP-actin but with slow kinetics. This binding occurs in a region of the monomer that is not involved in interactions with the barbed end of the filament, possibly the side of an actin monomer.

3.7.6 Arp4 and Arp8 synergistically inhibit actin polymerization

The hypothesis that Arp8 and Arp4 might interact with distinct regions of the actin monomer and the findings that both proteins affect the G-/F-actin equilibrium differently suggested to investigate whether they act in concert during actin monomer binding. Therefore, pyrene assays with ATP-actin in the presence of a constant concentration of Arp4 were performed. The Arp4 concentration was chosen to only slightly inhibit actin polymerization. To this reaction, different amounts of Arp8 were added to see if Arp8 modifies the inhibiting effect of Arp4. Indeed, Arp8 enhanced the inhibitory effect of Arp4 on actin polymerization in a concentration dependent manner by as much as 3-fold (see Figure 51). Analysis of the polymerization reaction by TIRF-microscopy additionally showed that excess amounts of Arp8 enhanced the inhibitory effect of Arp4 on both, filament nucleation and elongation, resulting in a reduction of growing filaments by ~75% and a reduction in the filament elongation rate by ~25% (see Figure 51).

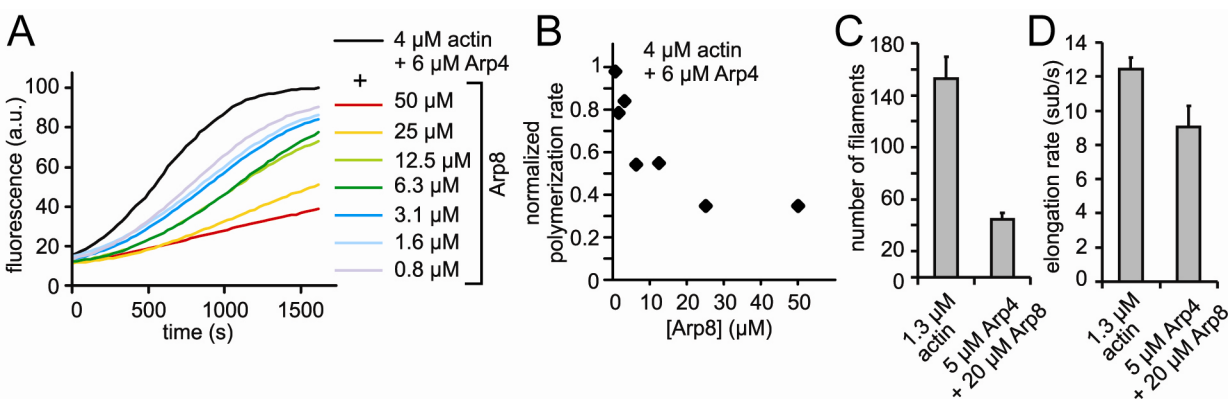


Figure 51: Concerted influence of Arp4 and Arp8 on actin polymerization

A) Pyrene assays of actin polymerization. Mg^{2+} -ATP-actin was polymerized by addition of KMEI buffer in the presence of 6 μM Arp4 and the Arp8 concentrations indicated.

B) Arp8 enhances Arp4-mediated inhibition of polymerization. Polymerization rates were obtained from A and normalized to the slope of the assembly of Mg^{2+} -ATP-actin in presence of 6 μM Arp4.

C) Numbers of filaments in the presence and absence of Arp4 and Arp8, as determined by TIRF microscopy.

D) Filament elongation rates in the presence and absence of Arp4 and Arp8, as determined by TIRF microscopy. Arp8 increases the inhibiting effect of Arp4 (compare Figure 41).

Analysis of the effect of both proteins on actin sequestration by measuring the steady state fluorescence of pyrene assays and performing spin down assays with F-actin also revealed that both proteins modify each other's activities. Specifically, Arp4 enhanced actin monomer

sequestration by Arp8, leading to a reduction of F-actin by ~75% after 16 h incubation with both proteins as assessed by steady state pyrene fluorescence measurements. Sedimentation analyses revealed a ~50% reduction of F-actin after 5 h incubation with Arp4 and Arp8 and show that both proteins together do not bind to actin filaments (see Figure 52).

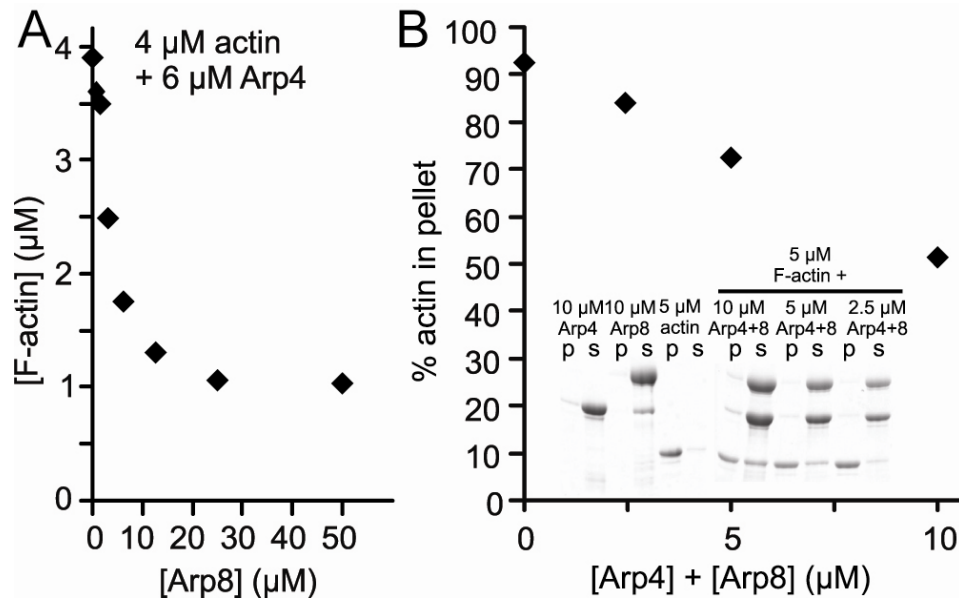


Figure 52: Sequestering of actin monomers by Arp4 and Arp8

A) Steady state F-actin fluorescence experiments indicate that Arp4 increases Arp8-mediated sequestering of monomers.

B) Co-sedimentation assays of actin polymerized in the presence of the Arp4 and Arp8 concentrations indicated. The sequestration effect of Arp8 is more pronounced in the presence of Arp4 (compare to Figure 47).

A more detailed analysis of the combined effects of Arp4 and Arp8 on monomer sequestration was monitored in a depolymerization assay after Arp4 and Arp8 addition. This assay revealed that the effects of both proteins, namely instantaneous, fast depolymerization by Arp4 and slow depolymerization by Arp8, seem to add up in a non cooperative way to achieve an enhanced actin sequestration activity (see Figure 53).

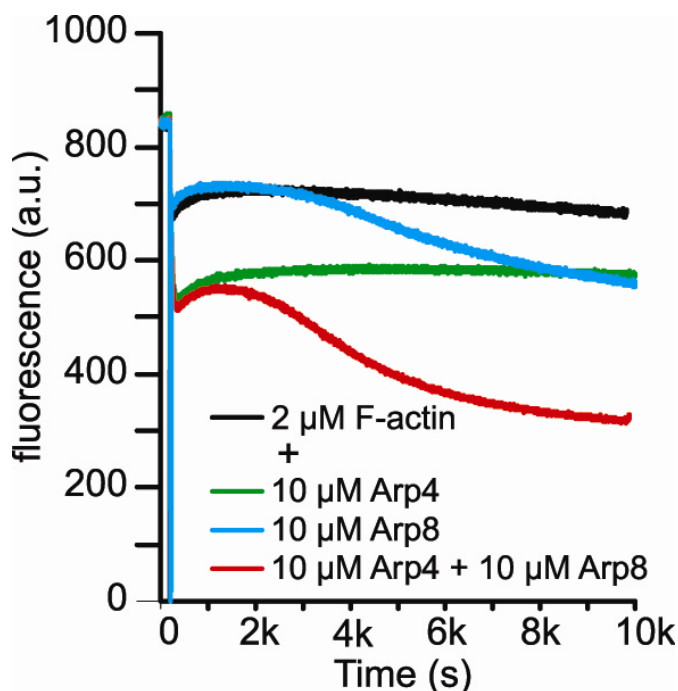


Figure 53: Additive depolymerization of actin filaments by Arp4 and Arp8

Combined effects of Arp4 and Arp8 on the F-/G-actin equilibrium (red curve) suggest an additive and sequential effect of fast depolymerization by Arp4 (green curve) and slow depolymerization by Arp8 (blue curve).

Thus, it is likely that both proteins efficiently bind to and sequester monomeric ADP-actin in a synergistic fashion, leading to a stronger reduction of filamentous actin if both proteins are present.

3.7.7 Model for the actin-Arp4 interaction

Since the biochemical analyses of Arp4 strongly suggested a direct binding of Arp4 to the barbed end of the actin monomer, the contacts of the Arp4 molecules in the asymmetric unit of the crystal structure were analyzed more closely to evaluate whether Arp4 could mediate barbed end interactions despite its altered surface patterns compared to actin. The asymmetric unit is comprised of two “dimers” of Arp4. The two Arp4 molecules within each “dimer” contact each other over a surface area of roughly 1550 \AA^2 per monomer which corresponds to the largest interacting surface found in the crystal packing. Within each of the two similar Arp4 “dimers”, a helix (residues 462-468 of Arp4) is inserted into the hydrophobic cleft at the barbed end of its binding partner and vice versa (see Figure 54).

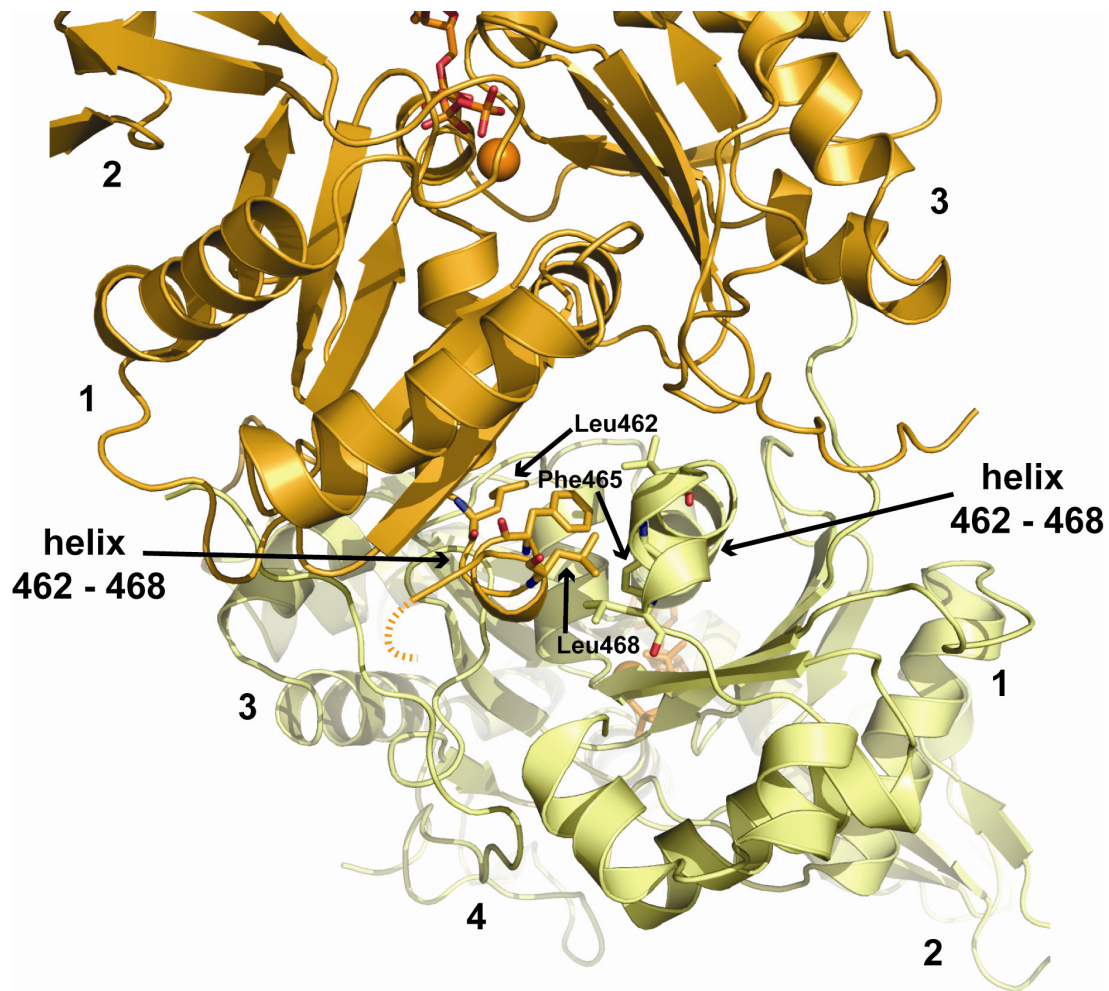


Figure 54: Arp4 “dimer” interface in the asymmetric unit of the crystal

One of the two Arp4 “dimers” found in the asymmetric unit of the crystal (yellow and orange), subdomains are labeled. Two helices (462-468) are reciprocally inserted into the hydrophobic grooves of the corresponding molecule. Hydrophobic residues within those helices are depicted in sticks and labeled. Residues 472-489 of the orange Arp4 molecule are omitted for clarity; their position is indicated by the dashed line.

This data is reminiscent of the interactions of gelsolin, or the first WH2 domain of ciboulot, with the barbed end of actin (Hertzog et al, 2004). Especially, an overlay of the ciboulot-actin complex with the Arp4 “dimer” reveals a very similar positioning of the interacting helices, although the two helices have reversed directionality, resulting in a similar positioning of hydrophobic residues compared to the Arp4 “dimer” interactions (see Figure 55).

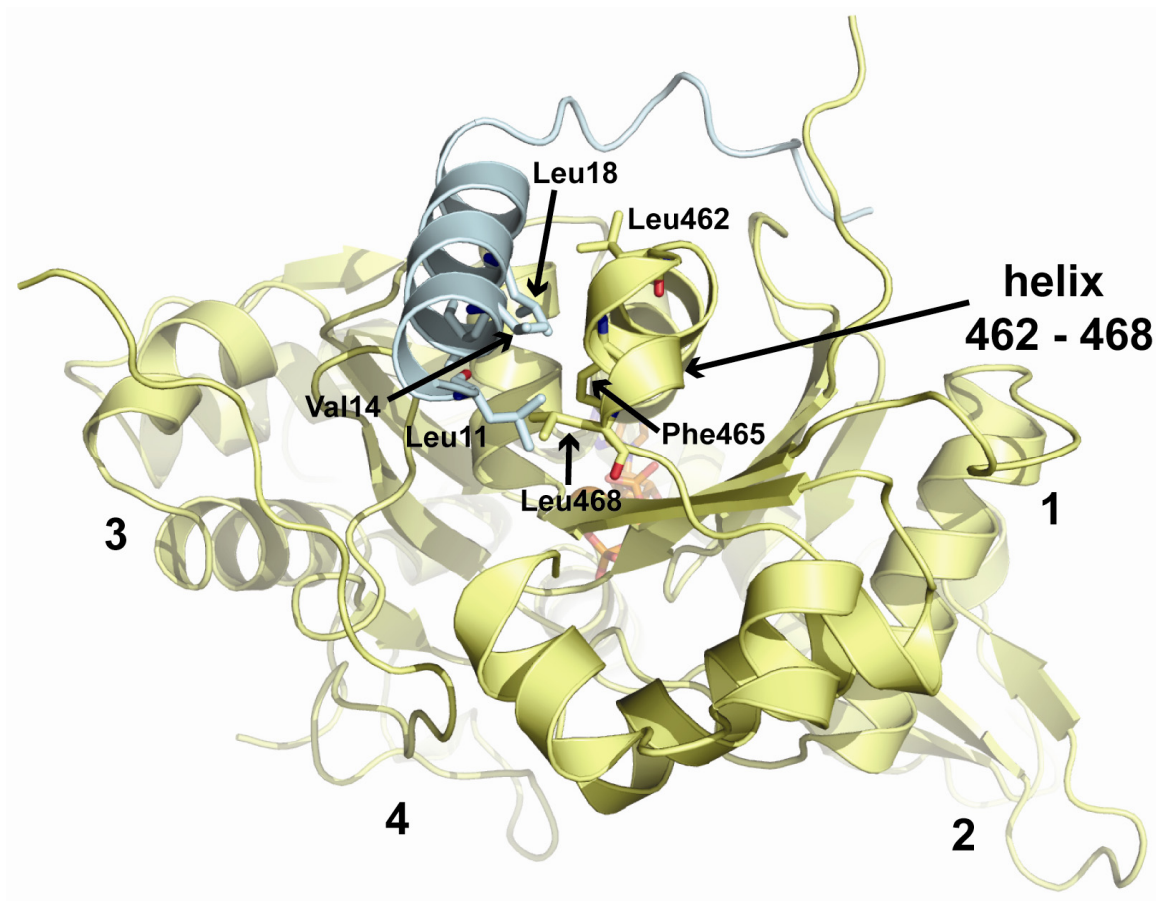


Figure 55: Interaction of ciboulot with actin

Overlay of Arp4 (yellow) with the first WH2 domain of ciboulot bound to actin (pdb 1SQK, cyan). Actin from the ciboulot:actin complex was superimposed with Arp4 and then omitted for clarity. Interestingly the interacting helix of ciboulot coincides nicely with the position of the Arp4 helix 462-468 of the “dimer” binding partner (see Figure 54), showing a similar spacing of hydrophobic residues (represented in sticks and labeled).

This raises the possibility that the Arp4:Arp4 barbed end “dimer” in the asymmetric unit represents the assembly of the actin:Arp4 interaction. Indeed, an overlay of the actin structure with one Arp4 subunit in the dimer of the asymmetric unit reveals that the helix 349-355 in actin is ideally suited to take over the place of its Arp4 counterpart providing the same spacing of hydrophobic residues (see Figure 56).

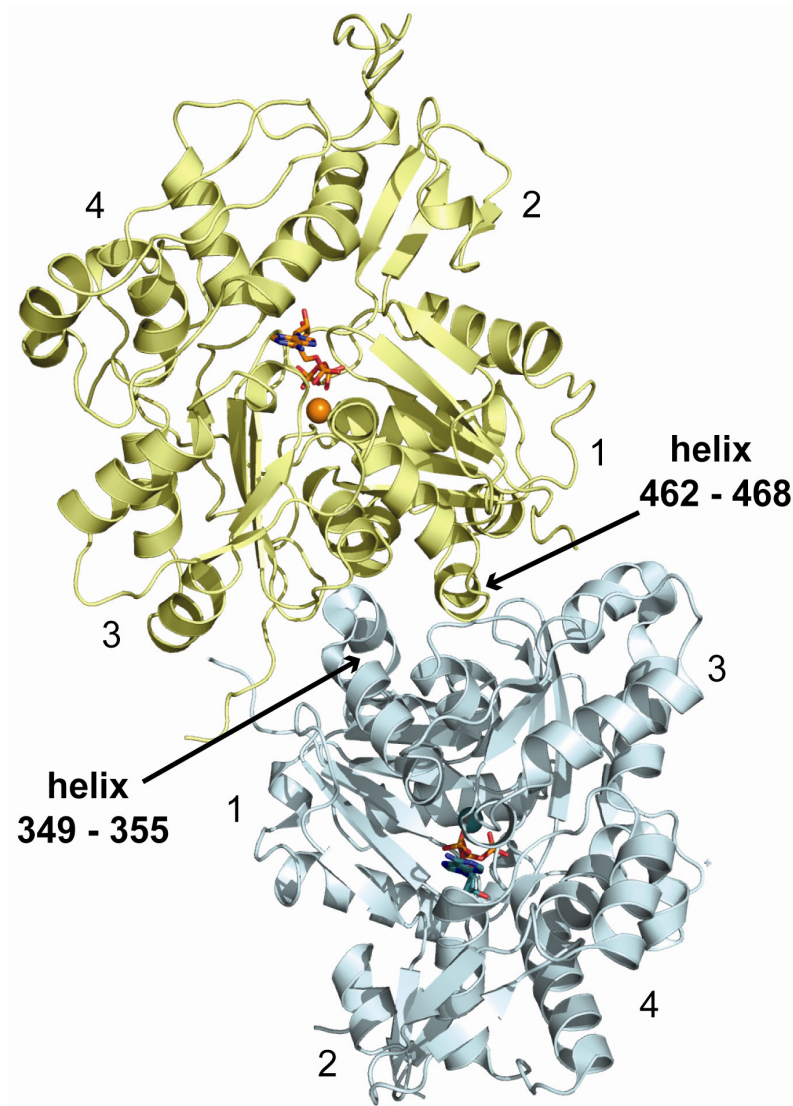


Figure 56: Proposed interface between actin and Arp4

Model of an Arp4 (yellow) actin (cyan) complex. Actin was superimposed with the orange Arp4 in Figure 54. Helix 349-355 of actin coincides with Arp4 helix 462-468 and shows virtually identical spacing of hydrophobic residues.

If this unconventional barbed to barbed interaction really occurs *in vivo* and is functionally relevant remains to be tested. It is worth noting however that an anti-parallel actin-actin dimer that displays barbed to barbed end interaction, as proposed here, has indeed previously been observed and could be a first intermediate in the nucleation process of actin filaments (Millonig et al, 1988). The structure of this dimer has been solved and clearly demonstrates the barbed to barbed arrangement of two actin monomers albeit the molecular contacts being slightly different than proposed for the Arp4 actin interaction (Bubb et al, 2002).

4. Discussion

Chromatin remodeling complexes are large multi subunit protein assemblies. It is thus intrinsically difficult to study them by conventional structural methods. X-ray crystallography and electron microscopy are usually hampered by the flexibility and heterogeneity of the studied species, whereas NMR spectroscopy is restricted by the large size of the complexes. Accordingly, structural insights into the molecular details of these protein machines is scarce as is the mechanistic understanding of the underlying remodeling processes which is usually dependent on the knowledge of atomic details.

The best way to deal with these difficulties is to use a hybrid approach combining structural information from different techniques. Electron microscopy and SAXS experiments can generate low resolution structural information about the entire chromatin remodeling complex, or larger sub-fragments of the complex. SAXS can also be useful in dealing with structural flexibility of the remodeler, since it allows the study of flexible molecules in solution, albeit these data must be analyzed with care. NMR and X-ray crystallography can be used to obtain high resolution structures of smaller individual subunits, or even single domains of proteins. The entire data can then be integrated into one hybrid model of the complex allowing for a more detailed picture of its molecular architecture. Examples where this approach has been successful are the structures of the nuclear pore complex (Brohawn et al, 2009), or RNA Polymerase I (Kuhn et al, 2007). If possible, the model can be further verified by using biochemical methods like cross linking approaches coupled with mass spectrometric analysis to verify molecular contacts (Leitner et al, 2010) or mutational studies to identify functionally important sites *in vivo*.

The approach of this study to elucidate the functional architecture of the INO80 chromatin remodeling complex was quite similar. While the main focus was to solve crystal structures of single INO80 components this was supplemented by EM studies of the entire complex and SAXS studies on single components and subcomplexes.

As this project was the first to establish structural work on the INO80 complex in the laboratory, many basic problems had to be solved in order to allow subsequent structural studies on this chromatin remodeler.

4.1 Structure and function of the INO80 complex

The initial focus of the work was to establish expression and purification protocols for individual INO80 components. The efforts of many structural genomics consortia working on the expression and purification of thousands of different proteins with the ultimate goal of structure determination have shown that one major bottleneck of the structure determination pipeline is to obtain soluble protein (Graslund et al, 2008). Of over 8000 archaeal and 58000 bacterial targets that were cloned in a decade of research only 36 and 30 % respectively could be purified in the end. For eukaryotic proteins this number drops even further as from over 42000 cloned targets only 19 percent could be purified (Graslund et al, 2008). This illustrates some of the difficulties in obtaining soluble protein but does not take into account that many proteins whose structure determination is of interest in present times are even more challenging than the proteins contained in the sample mentioned above. Those proteins are often large in size, contain intrinsically unstructured regions or are part of protein complexes which makes the purification even harder.

In the case of this study several isolated INO80 components could be purified with very nice yield, stability and homogeneity. Among those were Arp4, Arp8 and Ies5. Others could only be purified with marginal yields, were prone to degradation, or displayed a tendency to aggregate. Nevertheless, it was possible at least to obtain Arp5, Ies4, Ies6 and Nhp10 in a soluble form. The other INO80 subunits were either not expressed, insolubly expressed, or not stable enough for purification on their own.

As mentioned, the function of most INO80 subunits is unknown and, with the exception of the INO80 protein itself, the Rvb1-Rvb2 complex and possibly the actin related proteins 4, 5 and 8 they do not possess any enzymatic activity that has been identified yet. Thus, it is difficult to perform any functional assays with individual purified components. The main focus was therefore their structural characterization, which proved to be difficult as well, as only isolated Arp4 yielded diffraction quality crystals, despite extensive screening efforts. Several factors have to be taken into account when trying to improve the crystallization properties of the INO80 subunits. The main focus should be to optimize the sample quality to obtain more stable and homogeneous proteins. Although one can try to vary the purification buffers by changing pH, or adding detergents the more promising approach is probably to alter the expression constructs. This could be done by probing the protein fold via limited proteolysis thus identifying core

structural elements which are unperturbed by proteases. The potentially flexible and unstructured parts could then be removed from the protein. This is a well established approach in structural biology and has also been used in this study on Arp4, Arp8 and the Rvb1-Rvb2 complex (data not shown). However it was only successful in identifying a stable construct of Arp8 lacking the first 244 amino acids. The lack of structure for this part was already obvious from sequence alignments with actin (see Figure 24). Nevertheless, this approach should be intensified in the future to further reduce the size of already soluble subunits and to obtain more stable entities.

Another obvious point to consider is the fact that most of the INO80 subunits do not occur in isolation *in vivo* but always associated with their respective interaction partners of the complex. It is therefore quite conceivable that unstructured or hydrophobic parts of the proteins get structured or masked upon binding to their respective interaction partner. The expression of subcomplexes of several proteins is thus a promising strategy to overcome solubility and stability problems of single INO80 components.

In this study, complexes composed of Nhp10-Ies5, Nhp10-Ies3-Ies5, Arp5-Ies6 and Rvb1-Rvb2 could be purified with relatively good yields and purity obtaining fairly homogeneous samples. With the successful purification of those complexes new interactions between Nhp10 and Ies5 as well as Arp5 and Ies6 were discovered for the first time. This leads to a revised view of the INO80 complex architecture compared to the current state of knowledge in the literature (see Figure 57 and compare Figure 3).

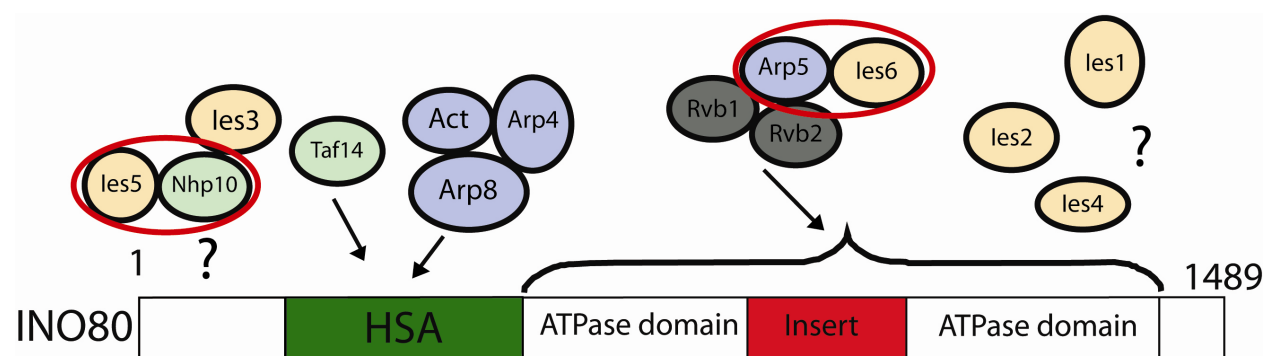


Figure 57: Revised architecture of the INO80 complex

Compared to the current view of the INO80 architecture (see Figure 3) an updated version illustrating the interactions between Arp5 and Ies6 as well as Nhp10 and Ies5 (highlighted in red) is depicted.

Furthermore, the initially aggregating or insoluble proteins Nhp10 and Ies3 respectively could be stabilized and integrated into better behaving protein complexes proving the feasibility of this approach. Nevertheless, those complexes still do not behave ideally as indicated by their elution from gel filtration and their behavior in SAXS experiments. In both cases the experimentally determined molecular weights of the complexes are substantially larger than the expected molecular weights of stoichiometric 1:1(:1) complexes (see Table 9).

Table 9: Experimentally determined molecular masses of INO80 subcomplexes

Protein complex	Theoretical molecular mass of a 1:1(:1) complex	Molecular mass determined by gel filtration	Molecular mass determined by SAXS
Nhp10-Ies5	39 kDa	116 kDa	n.d.
Nhp10-Ies3-Ies5	67 kDa	270 kDa	114 kDa
Arp5-Ies6	89 kDa	170 kDa	141 kDa

Although it might be possible that the complexes are larger than just simple 1:1(:1) assemblies it is more likely that the experimentally determined masses are increased due to unfolded protein parts or a very elongated shape of the complexes. Especially, that the molecular masses determined from gel filtration and SAXS are so divergent argues that this is not an effect based on real differences in molecular weight. The Kratky plots of Nhp10-Ies3-Ies5 and Arp5-Ies6 (see Figure 19) also indicate that these complexes are not completely folded. However, this is not surprising considering that with the INO80 protein itself at least one interaction partner is still missing in the respective complexes. One focus of future work should therefore be to characterize the specific INO80 domains that recruit those subcomplexes into the entire remodeler. Adding the accordant INO80 constructs to the subcomplex could then further stabilize it and improve the sample quality for crystallization.

The Rvb1-Rvb2 complex could also be purified with very nice yield but did not form a single uniform species as indicated by the elution profile from gel filtration (see Figure 21). So far the exact assembly state of Rvb1-Rvb2 is not completely clear, as different studies suggest the proteins to be able to form monomers, homo- or hetero-hexamers, and double hexamers (Jha & Dutta, 2009). When checked on a Coomassie gel after gel filtration both the “6mer” and “12mer”

species contain Rvb1 and Rvb2 respectively. This is an indication that the Rvb proteins form heterohexameric rings as opposed to homohexamers only containing one of the two proteins. It is also possible however, that homohexameric rings of Rvb1 and Rvb2 respectively co-elute from the size exclusion column.

Although both species could be crystallized the crystals did not diffract well enough to solve the structure. As both Rvb proteins belong to the AAA+ family of ATPases it might be worthwhile to screen different nucleotide states of the complex for crystallization. This could lead to the formation of a more homogeneous sample were each subunit is bound to the same nucleotide, instead of a possible mixture obtained after purification. So far, this approach has only been tried by incubating the protein complex with ADP prior to crystallization. Although crystals could be obtained, it was not possible to identify suitable crystals with better diffraction than the original crystals (see Figure 22). Other nucleotides to test in the future are non-hydrolysable ATP analogs or ATP hydrolysis transition state mimics.

Although chromatin remodelers are seemingly ideal targets for electron microscopic studies due to their size the structure reconstruction is usually faced with a lot of problems. Difficulties in sample preparation, low stability of the complexes, heterogeneity of the preparations and a lack of reference structures make it a daunting challenge to create EM structures of remodelers. Nevertheless, there are examples in recent years, where low resolution structures of chromatin remodelers have been obtained. Among those are the ACF complex (Racki et al, 2009) the RSC complex bound to a nucleosome (Chaban et al, 2008) or the yeast SWI/SNF complex (Smith et al, 2003). Indeed, the micrographs obtained from INO80 samples in this study also revealed a problem with sample homogeneity as different species could be identified in the preparations (see Figure 10). This makes it impossible, especially when lacking a reference structure to identify the actual particles of the INO80 holo-complex and to reconstruct a three dimensional representation of the complex. One possibility to overcome the problem of sample instability and heterogeneity could be to bind the INO80 complex to its substrate the nucleosome. This could help to stabilize the complex in a distinct conformation and prevent it from falling apart. In order to do this, one needs to obtain nucleosomes in a highly pure and defined state. Furthermore, the binding of INO80 to different nucleosome species has to be characterized so that a suitable substrate can be identified which binds to the complex in a defined and stable manner.

4.2 An unexpected role for the actin related proteins Arp4 and Arp8

Nuclear Arps are components of several chromatin remodeling complexes often together with actin itself. Their exact function in those complexes however is largely unknown (Dion et al, 2010). Mutational studies have shown that deletion of Arp8 from INO80 abolishes INO80's ATPase and chromatin remodeling activity (Shen et al, 2003) and deletions of Arp7 and Arp9 from RSC reduce the ATPase activity of the complex (Szerlong et al, 2003). Moreover, Arps seem to have structural roles within chromatin remodelers, as the deletion of Arp6 from SWR1 leads to a dissociation of the complex into two functional modules (Wu et al, 2005). Finally, a role in binding to histones, specifically phosphorylated H2A has been shown for Arp4 (Galarneau et al, 2000; Morrison et al, 2004; van Attikum et al, 2004).

A more speculative role of Arps is the participation in the long range organization of chromatin. The knockdown of mammalian Arp4 (Baf53) for example leads to an increase in chromosome territory size (Lee et al, 2007), whereas Arp6 seems to be involved in the recruitment of genomic loci to the nuclear pores, a process important for the establishment of long term transcriptional memory (Tan-Wong et al, 2009; Yoshida et al, 2010). Furthermore, the presence of certain forms of filamentous actin in the nucleus gives rise to the possibility that nuclear Arps participate in the regulation of nuclear actin dynamics (Dion et al, 2010; Gieni & Hendzel, 2009).

To help reveal the structures and functions of nuclear actin related proteins in chromatin remodeling enzymes, the first structure of a nuclear Arp, namely Arp4 and its functional interaction with Arp8 and actin were determined. The combined effect of Arp4 and Arp8 on actin dynamics was of special interest, as Arp4, Arp8 and actin together with the HSA domain of the INO80 protein form a submodule in the INO80 chromatin remodeler (Szerlong et al, 2008).

The structure of Arp4 is highly related to actin, exhibiting the actin fold as the core element of the molecule. Like actin it contains four subdomains centered around a nucleotide binding cleft where ATP was found to be bound. In comparison to actin, Arp4 contains several loop insertions and deletions at important sites of the structure. The resulting differences in the surface properties of Arp4 likely have consequences in terms of protein-protein interactions that Arp4 can undergo with actin and classical actin binding proteins. While an interaction with ADP-G-actin exists, Arp4 does not form filaments and the position of the loop insertions and deletions make it unlikely that Arp4 forms complexes with regulatory actin binding proteins like profilin. Especially, the capability of Arp4 to form actin like filaments is diminished, as the insertions sit

at sites where actin protomers form contacts according to the current model of F-actin (see Figure 35 - 37) (Oda et al, 2009). Thus it seems like Arp4 on the one hand is suited to interact with actin while at the same time preventing it from forming polymers explaining how actin is held in a discrete monomeric state within chromatin remodeling complexes.

In contrast to actin, Arp4 seems to form a stable complex with ATP displaying little if not lacking ATP hydrolysis in solution. This lack is emphasized by the fact that the ATP bound state of Arp4 is stable for the time span of two to three weeks, which is needed for purification and crystal growth of the protein. Again this feature of the molecule can be nicely explained by the crystal structure, as Arp4 has a more shielded ATP binding site with several divergent residues compared to actin (see Figure 34). As mentioned, actin uses ATP hydrolysis as a built in timing mechanism to discriminate freshly polymerized ATP-actin filaments from older ADP-actin filaments that can subsequently be depolymerized (Campellone & Welch, 2010). It is interesting to note that a 40,000 fold stimulation of ATP hydrolysis activity occurs once actin is incorporated into the filament (Blanchoin & Pollard, 2002).

It is thus conceivable, that the ATP hydrolysis activity of actin related proteins is stimulated once they are integrated into protein complexes like chromatin remodelers for example. Arp4 might show ATP hydrolysis as a part of the Arp4-Arp8-actin HSA domain complex and the ATP/ADP binding and ATP hydrolysis properties of the three proteins could be reciprocally influenced by each other within the INO80 complex. It could further be possible that the ATP hydrolysis rate of the actin related proteins is responsive to the remodeling activity of the entire INO80 complex. Although this is highly speculative and needs to be addressed by future experiments this could provide a mechanism to couple the chromatin remodeling activity of INO80 to an activity in regulating nuclear actin turnover. This opens the possibility for dynamic regulation of actin binding and actin polymerization depending on the nucleotide state of the three proteins. For instance, by controlling the nucleotide state of Arps, such as by allosteric regulation of their ATP-hydrolysis activity, other components of the remodeler could control the interaction with actin or vice versa interaction with actin and alteration of the nucleotide state could impact on the activity of the chromatin remodeler.

Although the insights gained from the structural study of Arp4 allow explaining certain properties of the protein they do not answer the questions about the function of Arp4 in the nucleus, especially in the context of chromatin remodeling complexes. Keeping in mind that

Arp4 is an actin related protein, several assays were performed to test whether it has the capability to influence actin and its properties *in vitro*. Interestingly, Arp4 reduces the initial speed of actin filament assembly as determined by pyrene actin polymerization assays. It does so likely by inhibiting filament nucleation as judged from TIRF microscopy which shows that Arp4 most notably reduces the amount of newly formed actin filaments. On top of that, it has the remarkable property to rapidly depolymerize pre-existing actin filaments. The combined data of assays performed together with ATP- or ADP-actin and filaments having free or blocked barbed ends suggest that Arp4 performs its action by preferably interacting with ADP-G-actin via the barbed end. The direct interaction of Arp4 with actin was further verified by surface plasmon resonance experiments.

The inhibition of actin nucleation by Arp4 is strikingly reminiscent of profilin, a cytosolic protein that helps to regulate the structure and dynamics of actin filaments and promotes ADP to ATP exchange in G-actin (Witke, 2004). The notion that Arp4 seems to possess characteristics of a well known actin binding protein opens the possibility that it might have functions in regulating the properties of nuclear actin in the context of chromatin structure and dynamics possibly in connection with other Arps. A role of nuclear Arps in regulating some form of nuclear actin turnover is not completely unexpected, as the functionally best understood Arps are those of the cytoplasmic Arp2/3 complex which is most prominently involved in branching of cytoplasmic actin filaments (Pollard, 2007).

Like the Arp2/3 complex, Arp4 might require additional partners to perform its full activity. Indeed, in the INO80 complex Arp4 is found to be associated with Arp8 and both proteins are integrated into the complex by the INO80p HSA domain (Szerlong et al, 2008). Consequently, isolated Arp8 was also tested for its effect on actin dynamics *in vitro* and found to have distinctly different influences compared to Arp4. First, it does not reduce the rate of actin polymerization as observed by pyrene assays but it sequesters actin monomers as seen in sedimentation experiments with filamentous actin. Second, it interacts with a region of actin different from the barbed end and has the capability to slowly depolymerize actin filaments. The direct interaction of Arp8 and actin was verified by surface plasmon resonance. Like Arp4, Arp8 displays a preference to interact with ADP-actin compared to ATP-actin. The properties of Arp8 and its influence on actin dynamics are unique in the field of actin binding proteins and have not been previously reported.

More interesting than the isolated effect of both proteins is their concerted effect on actin dynamics as they are always part of a subcomplex within the INO80 remodeler. Indeed, both proteins seem to reinforce each other's effects and act synergistically on actin. Specifically, Arp8 which has no effect on the initial speed of actin polymerization on its own strengthens the inhibiting effect of Arp4 on polymerization. This leads to a more complete inhibition of actin polymerization with both proteins present. On the other hand the depolymerizing effects of both proteins namely the fast depolymerization of Arp4 and the slower depolymerization of Arp8 appear to be additive which again leads to a reinforcement of both individual effects in the end.

As a result, both proteins together are effective in stabilizing monomeric actin possibly leading to the formation of a trimeric complex which subsequently can be incorporated into the INO80 complex with the help of the HSA domain.

It is tempting to speculate that this conserved HSA, Arp4, Arp8 and actin complex within the INO80 complex could form a platform to specifically regulate nuclear actin at the sites of INO80 chromatin remodeling activity, such as Arp2/3 regulates cytoplasmic actin nucleation at barbed end branch points. In support of this, the BAF complex, a chromatin remodeler that contains Arp4 and actin as well binds to pointed ends of filaments *in vitro* in the presence of phosphatidyl inositol 4-5 bisphosphate and stabilizes actin filaments (Rando et al, 2002).

With a model of the Arp4-actin interaction in hand it is possible to infer a likely arrangement of all four proteins within the tetrameric Arp8-Arp4-actin-HSA domain complex found in the INO80 remodeler. The biochemical data suggest that Arp8 sequesters actin by binding to a region of actin distinct from the barbed end. This gives rise to a possible model of the complex where actin is bound by Arp8 and Arp4 simultaneously with the help of the HSA domain in a way that masks actin's barbed end by Arp4 but exposes its pointed end (see Figure 58).

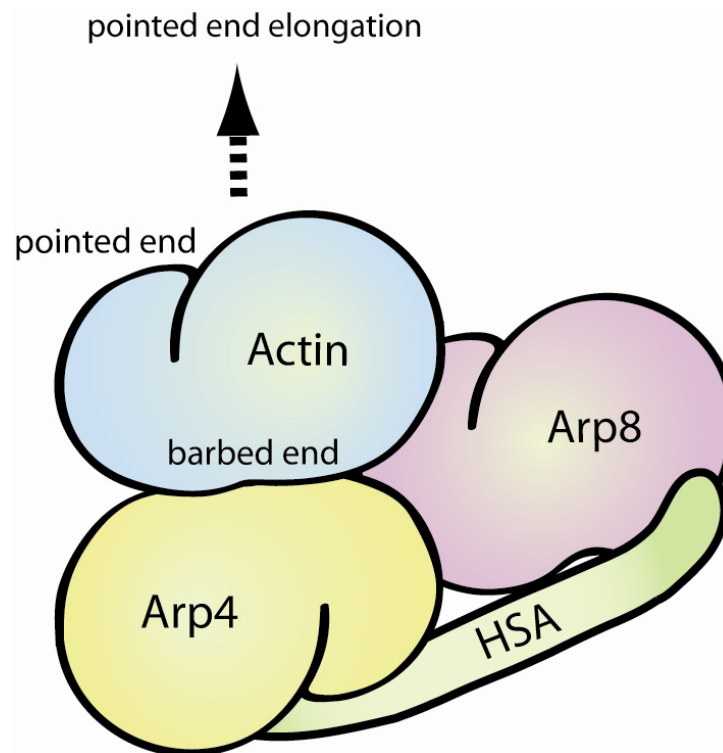


Figure 58: Schematic model of the Arp8-Arp4-actin-HSA domain complex

Model of the Arp4-Arp8-actin-HSA complex. The model satisfies the biochemical data as Arp4 and actin interact via their barbed ends and Arp8 binds to actin neither via the barbed nor the pointed end. The HSA domain most likely acts as a scaffold to organize and stabilize the complex.

In this model the pointed end of actin is accessible for the addition of further actin monomers. Hence, the subcomplex might provide an ordered starting point for the addition of further actin molecules, thus promoting pointed end growth of the filament. A first set of experiments performed with recombinantly purified Arp4-Arp8-actin-HSA complex indeed shows that the complex has a profound impact on actin filament formation. Specifically, it seems to be able to stimulate the formation of new actin filaments while stabilizing already existing filaments (Christian Gerhold, personal communication). The exact role and catalytic functions of this INO80 subcomplex however remain to be further characterized.

Even though the presence of actin and especially polymeric actin in the nucleus is still a controversial issue, it appears to be widely accepted now that actin has important functions in the nucleus (Gieni & Hendzel, 2009; Jockusch et al, 2006). It has been proposed for example that nuclear actin, nuclear myosin and perhaps nuclear Arps are involved in long-range organization of nuclei (Dion et al, 2010). Little is known however, about the regulation of nuclear actin and

the reason for the absence of classical phalloidin stainable F-actin in the nucleus, despite the fact that nuclear actin can be found in monomeric, oligomeric and polymeric forms (McDonald et al, 2006).

The biochemical data of Arp4 and Arp8 suggest how they help to stabilize monomeric actin in modifying complexes by specifically sequestering ADP-G-actin. Although it is possible that Arp4 has only structural roles or functions in core histone binding within chromatin remodelers (Galarneau et al, 2000), such functions do not readily explain why Arp4 coexists with actin in all complexes it is found (Dion et al, 2010). Furthermore, the Arp4-actin pair is present in many different complexes that modify chromatin, but not in other DNA associated machineries. Arp4 is an essential gene in yeast and humans and thus hard to study as knockouts are not informative. Interestingly however, knockdown of mammalian Arp4 (BAF53) increases chromosome territory size and deletion of Arp8 in yeast leads to an abnormally increased cell volume and irregular, elongated cell morphology compared to wild type together with unusually elongated buds (Hibbs et al, 2007; Watanabe et al, 2009). These observations are consistent with a possible role of Arp4 and Arp8 in actin metabolism.

An exciting function of Arp4 and Arp8 suggested by the biochemical data and supported by hints from the literature could therefore be the regulation of actin metabolism and dynamics specifically in the context of chromatin remodeling. Once the Arps are assembled within the INO80 complex they could gain a function in stimulating the formation of actin filaments which are subsequently important for the large scale movement of chromatin. If this assumption holds true it does not only clarify the function of nuclear Arps within chromatin remodeling complexes but also creates a link between nuclear actin dynamics and chromatin remodeling.

It will be interesting to study the role of ATP hydrolysis of Arp4 and Arp8 in the light of these new findings as well as previous data that show that the ATP binding and hydrolysis function of Arp4 can regulate interaction with the other remodeler subunits *in vitro* (Sunada et al, 2005). Additionally, the impact of nuclear actin on chromatin structure and dynamics can now be tested by exclusive and fold preserving disruption and modulation of the Arp4-actin pair. Due to its many functions and myriad interactions, actin is a notoriously difficult protein to study by genetic means and mutagenesis. The structural and biochemical results obtained for Arp4 and Arp8 together with the testable interaction model with ADP-G-actin monomers now open the door to probe the function of nuclear Arps and actin in more detail.

5. Summary

The INO80 complex is a chromatin remodeler involved in diverse nuclear processes like transcriptional regulation, replication fork progression, checkpoint regulation and DNA double strand break repair. In the yeast *S. cerevisiae* the complex consists of 15 subunits with a total molecular mass of about 1.2 MDa. Knowledge about the atomic structure and molecular architecture of the entire complex is scarce. Similarly, an understanding for the roles of the individual subunits of the complex is mostly lacking. Especially the function of actin and the actin related proteins Arp4 and Arp8 which are found as monomeric components of INO80 and other chromatin remodelers is poorly understood.

The goal of this study was to elucidate the functional architecture of the INO80 complex by using a hybrid methods approach. Different structural techniques such as X-ray crystallography, small angle X-ray scattering (SAXS) and electron microscopy (EM) were combined to achieve this goal. Additionally, various functional assays to study the biochemical properties of the actin related proteins and their interaction with actin were employed.

In a set of primary experiments expression and purification protocols for seven individual INO80 components, namely Arp4, Arp5, Arp8, Ies4, Ies5, Ies6 and Nhp10 could be established. Additionally, four subcomplexes containing more than one protein, namely Rvb1-Rvb2, Nhp10-Ies5, Nhp10-Ies5-Ies3 and Arp5-Ies6 were purified. Thereby two previously unknown interactions between the INO80 subunits Nhp10 and Ies5, as well as Arp5 and Ies6 could be identified. Subsequently, the newly identified complexes of Nhp10-Ies5-Ies3 and Arp5-Ies6 were studied with SAXS to obtain low resolution solution structures of both. On top of that the entire INO80 complex was purified endogenously from *S. cerevisiae* and studied by EM. Unfortunately, a three dimensional reconstruction of the remodeler could not be created. Crystallization attempts on all purified INO80 components were successful for the complex of Rvb1-Rvb2 and the actin related protein Arp4. Whereas the structure of Rvb1-Rvb2 could not be solved due to limited diffraction an atomic structure of ATP bound Arp4 at 3.4 Å resolution was obtained.

Remarkably, Arp4 does not form filaments despite its high similarity to conventional actin. The lack of polymerization is confirmed by the SAXS structure of isolated Arp4 which indicates it to be monomeric and can be nicely explained on the basis of the crystal structure. Several loop insertions and deletions at positions which are crucial for contact formation within the actin

filament, especially at the pointed end of the molecule, prevent Arp4 to engage in filament like interactions. Furthermore, the crystal structure of Arp4 reveals an ATP molecule to be constitutively bound to the protein. The lack of ATPase activity of Arp4 in contrast to actin can be explained with the help of the crystal structure as well. Several residues in the nucleotide clamping loops of Arp4 are divergent from actin leading to a tighter closure and better shielding of the phosphate moieties of the bound ATP from the environment.

Most interestingly, Arp4 dramatically influences actin polymerization kinetics. Different fluorescence assays and *in vitro* TIRF microscopy were used to show that Arp4 is able to inhibit actin polymerization and to depolymerize actin filaments most likely by complex formation with monomeric ADP-actin via the barbed end. Its ability to inhibit actin filament nucleation without sequestering actin while still allowing ADP to ATP exchange within actin resembles the actin binding protein profilin.

Arp8 was confirmed by SAXS measurements to be monomeric as well. It is able to sequester actin monomers and to slowly depolymerize actin filaments. Consistent with the formation of a discrete Arp4-Arp8-actin complex within the INO80 remodeler the effects of Arp4 on actin polymerization are further stimulated by Arp8. As both proteins reciprocally enhance their individual effects on actin it is likely that they help to maintain actin in a defined monomeric state within the INO80 chromatin remodeler.

The data further suggest a possible assembly between actin and Arp4 via their barbed ends and a model how the Arp4-Arp8-actin complex is integrated into the INO80 chromatin remodeler.

Taken together, the findings represent a remarkable advancement in the understanding of nuclear actin related proteins and nuclear actin biochemistry in general. Most excitingly, they indicate a link between chromatin remodeling and nuclear actin dynamics possibly giving chromatin remodeling complexes a role in the actin mediated large scale movement of chromatin.

6. References

- Adams PD, Afonine PV, Bunkoczi G, Chen VB, Davis IW, Echols N, Headd JJ, Hung LW, Kapral GJ, Grosse-Kunstleve RW, McCoy AJ, Moriarty NW, Oeffner R, Read RJ, Richardson DC, Richardson JS, Terwilliger TC, Zwart PH (2010) PHENIX: a comprehensive Python-based system for macromolecular structure solution. *Acta Crystallogr D Biol Crystallogr* **66**(Pt 2): 213-221
- Altschuler GM, Klug DR, Willison KR (2005) Unfolding energetics of G-alpha-actin: a discrete intermediate can be re-folded to the native state by CCT. *J Mol Biol* **353**(2): 385-396
- Aoyama N, Oka A, Kitayama K, Kurumizaka H, Harata M (2008) The actin-related protein hArap8 accumulates on the mitotic chromosomes and functions in chromosome alignment. *Exp Cell Res* **314**(4): 859-868
- Bao Y, Shen X (2007) INO80 subfamily of chromatin remodeling complexes. *Mutat Res* **618**(1-2): 18-29
- Barron-Casella EA, Torres MA, Scherer SW, Heng HH, Tsui LC, Casella JF (1995) Sequence analysis and chromosomal localization of human Cap Z. Conserved residues within the actin-binding domain may link Cap Z to gelsolin/severin and profilin protein families. *J Biol Chem* **270**(37): 21472-21479
- Berger I, Fitzgerald DJ, Richmond TJ (2004) Baculovirus expression system for heterologous multiprotein complexes. *Nat Biotechnol* **22**(12): 1583-1587
- Bergfors TM (2009) *Protein crystallization*, La Jolla, Calif.: International University Line.
- Blanchoin L, Pollard TD (2002) Hydrolysis of ATP by polymerized actin depends on the bound divalent cation but not profilin. *Biochemistry* **41**(2): 597-602
- Bohnsack MT, Stuken T, Kuhn C, Cordes VC, Gorlich D (2006) A selective block of nuclear actin export stabilizes the giant nuclei of *Xenopus* oocytes. *Nat Cell Biol* **8**(3): 257-263
- Bonder EM, Fishkind DJ, Mooseker MS (1983) Direct measurement of critical concentrations and assembly rate constants at the two ends of an actin filament. *Cell* **34**(2): 491-501
- Breitsprecher D, Kiesewetter AK, Linkner J, Faix J (2009) Analysis of actin assembly by in vitro TIRF microscopy. *Methods Mol Biol* **571**: 401-415
- Breitsprecher D, Kiesewetter AK, Linkner J, Urbanke C, Resch GP, Small JV, Faix J (2008) Clustering of VASP actively drives processive, WH2 domain-mediated actin filament elongation. *EMBO J* **27**(22): 2943-2954
- Brohawn SG, Partridge JR, Whittle JR, Schwartz TU (2009) The nuclear pore complex has entered the atomic age. *Structure* **17**(9): 1156-1168
- Bubb MR, Govindasamy L, Yarmola EG, Vorobiev SM, Almo SC, Somasundaram T, Chapman MS, Agbandje-McKenna M, McKenna R (2002) Polylysine induces an antiparallel actin dimer that nucleates filament assembly: crystal structure at 3.5-A resolution. *J Biol Chem* **277**(23): 20999-21006

- Campellone KG, Welch MD (2010) A nucleator arms race: cellular control of actin assembly. *Nat Rev Mol Cell Biol* **11**(4): 237-251
- Campos EI, Reinberg D (2009) Histones: annotating chromatin. *Annu Rev Genet* **43**: 559-599
- Carey M, Li B, Workman JL (2006) RSC exploits histone acetylation to abrogate the nucleosomal block to RNA polymerase II elongation. *Mol Cell* **24**(3): 481-487
- Chaban Y, Ezeokonkwo C, Chung WH, Zhang F, Kornberg RD, Maier-Davis B, Lorch Y, Asturias FJ (2008) Structure of a RSC-nucleosome complex and insights into chromatin remodeling. *Nat Struct Mol Biol* **15**(12): 1272-1277
- Chuang CH, Carpenter AE, Fuchsova B, Johnson T, de Lanerolle P, Belmont AS (2006) Long-range directional movement of an interphase chromosome site. *Curr Biol* **16**(8): 825-831
- Clapier CR, Cairns BR (2009) The biology of chromatin remodeling complexes. *Annu Rev Biochem* **78**: 273-304
- Conaway RC, Conaway JW (2009) The INO80 chromatin remodeling complex in transcription, replication and repair. *Trends Biochem Sci* **34**(2): 71-77
- Corona DF, Tamkun JW (2004) Multiple roles for ISWI in transcription, chromosome organization and DNA replication. *Biochim Biophys Acta* **1677**(1-3): 113-119
- Coue M, Brenner SL, Spector I, Korn ED (1987) Inhibition of actin polymerization by latrunculin A. *FEBS Lett* **213**(2): 316-318
- Dion V, Shimada K, Gasser SM (2010) Actin-related proteins in the nucleus: life beyond chromatin remodelers. *Curr Opin Cell Biol* **22**: 1-9
- Dominguez R (2004) Actin-binding proteins--a unifying hypothesis. *Trends Biochem Sci* **29**(11): 572-578
- Dominguez R (2009) Actin filament nucleation and elongation factors--structure-function relationships. *Crit Rev Biochem Mol Biol* **44**(6): 351-366
- Drenth J, Mesters J (2007) *Principles of protein x-ray crystallography*, 3rd edn. New York: Springer.
- Durr H, Korner C, Muller M, Hickmann V, Hopfner KP (2005) X-ray structures of the Sulfolobus solfataricus SWI2/SNF2 ATPase core and its complex with DNA. *Cell* **121**(3): 363-373
- Ebbert R, Birkmann A, Schuller HJ (1999) The product of the SNF2/SWI2 paralogue INO80 of Saccharomyces cerevisiae required for efficient expression of various yeast structural genes is part of a high-molecular-weight protein complex. *Mol Microbiol* **32**(4): 741-751
- Eberharter A, Becker PB (2004) ATP-dependent nucleosome remodelling: factors and functions. *J Cell Sci* **117**(Pt 17): 3707-3711

- Emsley P, Cowtan K (2004) Coot: model-building tools for molecular graphics. *Acta Crystallogr D Biol Crystallogr* **60**(Pt 12 Pt 1): 2126-2132
- Felsenfeld G, Groudine M (2003) Controlling the double helix. *Nature* **421**(6921): 448-453
- Flanagan JF, Peterson CL (1999) A role for the yeast SWI/SNF complex in DNA replication. *Nucleic Acids Res* **27**(9): 2022-2028
- Franke WW (2004) Actin's many actions start at the genes. *Nat Cell Biol* **6**(11): 1013-1014
- Fukui Y, Katsumaru H (1979) Nuclear actin bundles in Amoeba, Dictyostelium and human HeLa cells induced by dimethyl sulfoxide. *Exp Cell Res* **120**(2): 451-455
- Galarneau L, Nourani A, Boudreault AA, Zhang Y, Heliot L, Allard S, Savard J, Lane WS, Stillman DJ, Cote J (2000) Multiple links between the NuA4 histone acetyltransferase complex and epigenetic control of transcription. *Mol Cell* **5**(6): 927-937
- Galkin VE, VanLoock MS, Orlova A, Egelman EH (2002) A new internal mode in F-actin helps explain the remarkable evolutionary conservation of actin's sequence and structure. *Curr Biol* **12**(7): 570-575
- Gasteiger E, Gattiker A, Hoogland C, Ivanyi I, Appel RD, Bairoch A (2003) ExPASy: The proteomics server for in-depth protein knowledge and analysis. *Nucleic Acids Res* **31**(13): 3784-3788
- Georgieva M, Harata M, Miloshev G (2008) The nuclear actin-related protein Act3p/Arp4 influences yeast cell shape and bulk chromatin organization. *J Cell Biochem* **104**(1): 59-67
- Gieni RS, Hendzel MJ (2009) Actin dynamics and functions in the interphase nucleus: moving toward an understanding of nuclear polymeric actin. *Biochem Cell Biol* **87**(1): 283-306
- Golemis E, Adams PD (2005) *Protein-protein interactions : a molecular cloning manual*, 2nd edn. Cold Spring Harbor, N.Y.: Cold Spring Harbor Laboratory Press.
- Gonsior SM, Platz S, Buchmeier S, Scheer U, Jockusch BM, Hinssen H (1999) Conformational difference between nuclear and cytoplasmic actin as detected by a monoclonal antibody. *J Cell Sci* **112** (Pt 6): 797-809
- Graslund S, Nordlund P, Weigelt J, Hallberg BM, Bray J, Gileadi O, Knapp S, Oppermann U, Arrowsmith C, Hui R, Ming J, dhe-Paganon S, Park HW, Savchenko A, Yee A, Edwards A, Vincentelli R, Cambillau C, Kim R, Kim SH et al (2008) Protein production and purification. *Nat Methods* **5**(2): 135-146
- Gribun A, Cheung KL, Huen J, Ortega J, Houry WA (2008) Yeast Rvb1 and Rvb2 are ATP-dependent DNA helicases that form a heterohexameric complex. *J Mol Biol* **376**(5): 1320-1333
- Hanahan D (1983) Studies on transformation of Escherichia coli with plasmids. *J Mol Biol* **166**(4): 557-580
- Harata M, Karwan A, Wintersberger U (1994) An essential gene of Saccharomyces cerevisiae coding for an actin-related protein. *Proc Natl Acad Sci U S A* **91**(17): 8258-8262

Harata M, Oma Y, Mizuno S, Jiang YW, Stillman DJ, Wintersberger U (1999) The nuclear actin-related protein of *Saccharomyces cerevisiae*, Act3p/Arp4, interacts with core histones. *Mol Biol Cell* **10**(8): 2595-2605

Hertzog M, Carlier MF (2005) Functional characterization of proteins regulating actin assembly. *Curr Protoc Cell Biol* **Chapter 13**: Unit 13 16

Hertzog M, van Heijenoort C, Didry D, Gaudier M, Coutant J, Gigant B, Didelot G, Preat T, Knossow M, Guittet E, Carlier MF (2004) The beta-thymosin/WH2 domain; structural basis for the switch from inhibition to promotion of actin assembly. *Cell* **117**(5): 611-623

Hibbs MA, Hess DC, Myers CL, Huttenhower C, Li K, Troyanskaya OG (2007) Exploring the functional landscape of gene expression: directed search of large microarray compendia. *Bioinformatics* **23**(20): 2692-2699

Hofmann W, Reichart B, Ewald A, Muller E, Schmitt I, Stauber RH, Lottspeich F, Jockusch BM, Scheer U, Hauber J, Dabauvalle MC (2001) Cofactor requirements for nuclear export of Rev response element (RRE)- and constitutive transport element (CTE)-containing retroviral RNAs. An unexpected role for actin. *J Cell Biol* **152**(5): 895-910

Holmes KC, Popp D, Gebhard W, Kabsch W (1990) Atomic model of the actin filament. *Nature* **347**(6288): 44-49

Horn PJ, Peterson CL (2002) Molecular biology. Chromatin higher order folding--wrapping up transcription. *Science* **297**(5588): 1824-1827

Iwasa M, Maeda K, Narita A, Maeda Y, Oda T (2008) Dual roles of Gln137 of actin revealed by recombinant human cardiac muscle alpha-actin mutants. *J Biol Chem* **283**(30): 21045-21053

Jha S, Dutta A (2009) RVB1/RVB2: running rings around molecular biology. *Mol Cell* **34**(5): 521-533

Jin J, Cai Y, Yao T, Gottschalk AJ, Florens L, Swanson SK, Gutierrez JL, Coleman MK, Workman JL, Mushegian A, Washburn MP, Conaway RC, Conaway JW (2005) A mammalian chromatin remodeling complex with similarities to the yeast INO80 complex. *J Biol Chem* **280**(50): 41207-41212

Jockusch BM, Schoenenberger CA, Stetefeld J, Aebi U (2006) Tracking down the different forms of nuclear actin. *Trends Cell Biol* **16**(8): 391-396

Jonsson ZO, Jha S, Wohlschlegel JA, Dutta A (2004) Rvb1p/Rvb2p recruit Arp5p and assemble a functional Ino80 chromatin remodeling complex. *Mol Cell* **16**(3): 465-477

Kabsch W (1993) Automatic processing of rotation diffraction data from crystals of initially unknown symmetry and cell constants. *Journal of Applied Crystallography* **26**(6): 795-800

Kabsch W, Mannherz HG, Suck D, Pai EF, Holmes KC (1990) Atomic structure of the actin:DNase I complex. *Nature* **347**(6288): 37-44

- Kiefersauer R, Than ME, Dobbek H, Gremer L, Melero M, Strobl S, Dias JM, Soulimane T, Huber R (2000) A novel free-mounting system for protein crystals: transformation and improvement of diffraction power by accurately controlled humidity changes. *Journal of Applied Crystallography* **33**(5): 1223-1230
- Kim Y, Quartey P, Li H, Volkart L, Hatzos C, Chang C, Nocek B, Cuff M, Osipiuk J, Tan K, Fan Y, Bigelow L, Maltseva N, Wu R, Borovilos M, Duggan E, Zhou M, Binkowski TA, Zhang RG, Joachimiak A (2008) Large-scale evaluation of protein reductive methylation for improving protein crystallization. *Nat Methods* **5**(10): 853-854
- Kinner A, Wu W, Staudt C, Iliakis G (2008) Gamma-H2AX in recognition and signaling of DNA double-strand breaks in the context of chromatin. *Nucleic Acids Res* **36**(17): 5678-5694
- Klymenko T, Papp B, Fischle W, Kocher T, Schelder M, Fritsch C, Wild B, Wilm M, Muller J (2006) A Polycomb group protein complex with sequence-specific DNA-binding and selective methyl-lysine-binding activities. *Genes Dev* **20**(9): 1110-1122
- Koch MH, Vachette P, Svergun DI (2003) Small-angle scattering: a view on the properties, structures and structural changes of biological macromolecules in solution. *Q Rev Biophys* **36**(2): 147-227
- Konarev PV, Petoukhov MV, Volkov VV, Svergun DI (2006) ATSAS 2.1, a program package for small-angle scattering data analysis. *Journal of Applied Crystallography* **39**: 277-286
- Korenbaum E, Nordberg P, Bjorkegren-Sjogren C, Schutt CE, Lindberg U, Karlsson R (1998) The role of profilin in actin polymerization and nucleotide exchange. *Biochemistry* **37**(26): 9274-9283
- Krauss SW, Chen C, Penman S, Heald R (2003) Nuclear actin and protein 4.1: essential interactions during nuclear assembly in vitro. *Proc Natl Acad Sci U S A* **100**(19): 10752-10757
- Krogan NJ, Keogh MC, Datta N, Sawa C, Ryan OW, Ding H, Haw RA, Pootoolal J, Tong A, Canadien V, Richards DP, Wu X, Emili A, Hughes TR, Buratowski S, Greenblatt JF (2003) A Snf2 family ATPase complex required for recruitment of the histone H2A variant Htz1. *Mol Cell* **12**(6): 1565-1576
- Kuhn CD, Geiger SR, Baumli S, Gartmann M, Gerber J, Jennebach S, Mielke T, Tschochner H, Beckmann R, Cramer P (2007) Functional architecture of RNA polymerase I. *Cell* **131**(7): 1260-1272
- Kukalev A, Nord Y, Palmberg C, Bergman T, Percipalle P (2005) Actin and hnRNP U cooperate for productive transcription by RNA polymerase II. *Nat Struct Mol Biol* **12**(3): 238-244
- Lane NJ (1969) Intranuclear fibrillar bodies in actinomycin D-treated oocytes. *J Cell Biol* **40**(1): 286-291
- Laskowski RA (2009) PDBsum new things. *Nucleic Acids Res* **37**(Database issue): D355-359
- Laskowski RA, MacArthur MW, Moss DS, Thornton JM (1993) PROCHECK: a program to check the stereochemical quality of protein structures. *Journal of Applied Crystallography* **26**(2): 283-291
- Lee K, Kang MJ, Kwon SJ, Kwon YK, Kim KW, Lim JH, Kwon H (2007) Expansion of chromosome territories with chromatin decompaction in BAF53-depleted interphase cells. *Mol Biol Cell* **18**(10): 4013-4023

- Leitner A, Walzthoeni T, Kahraman A, Herzog F, Rinner O, Beck M, Aebersold R (2010) Probing native protein structures by chemical cross-linking, mass spectrometry, and bioinformatics. *Mol Cell Proteomics* **9**(8): 1634-1649
- Llorca O (2007) Electron microscopy reconstructions of DNA repair complexes. *Curr Opin Struct Biol* **17**(2): 215-220
- Luger K (2003) Structure and dynamic behavior of nucleosomes. *Curr Opin Genet Dev* **13**(2): 127-135
- Lusser A, Kadonaga JT (2003) Chromatin remodeling by ATP-dependent molecular machines. *Bioessays* **25**(12): 1192-1200
- Machesky LM, Atkinson SJ, Ampe C, Vandekerckhove J, Pollard TD (1994) Purification of a cortical complex containing two unconventional actins from *Acanthamoeba* by affinity chromatography on profilin-agarose. *J Cell Biol* **127**(1): 107-115
- Maier VK, Chioda M, Rhodes D, Becker PB (2008) ACF catalyses chromatosome movements in chromatin fibres. *EMBO J* **27**(6): 817-826
- Marfella CG, Imbalzano AN (2007) The Chd family of chromatin remodelers. *Mutat Res* **618**(1-2): 30-40
- Martin AC, Welch MD, Drubin DG (2006) Arp2/3 ATP hydrolysis-catalysed branch dissociation is critical for endocytic force generation. *Nat Cell Biol* **8**(8): 826-833
- Matias PM, Gorynia S, Donner P, Carrondo MA (2006) Crystal structure of the human AAA+ protein RuvBL1. *J Biol Chem* **281**(50): 38918-38929
- McCoy AJ, Grosse-Kunstleve RW, Adams PD, Winn MD, Storoni LC, Read RJ (2007) Phaser crystallographic software. *J Appl Crystallogr* **40**(Pt 4): 658-674
- McDonald D, Carrero G, Andrin C, de Vries G, Hendzel MJ (2006) Nucleoplasmic beta-actin exists in a dynamic equilibrium between low-mobility polymeric species and rapidly diffusing populations. *J Cell Biol* **172**(4): 541-552
- Milankov K, De Boni U (1993) Cytochemical localization of actin and myosin aggregates in interphase nuclei in situ. *Exp Cell Res* **209**(2): 189-199
- Millonig R, Salvo H, Aebi U (1988) Probing actin polymerization by intermolecular cross-linking. *J Cell Biol* **106**(3): 785-796
- Miralles F, Visa N (2006) Actin in transcription and transcription regulation. *Curr Opin Cell Biol* **18**(3): 261-266
- Mizuguchi G, Shen X, Landry J, Wu WH, Sen S, Wu C (2004) ATP-driven exchange of histone H2AZ variant catalyzed by SWR1 chromatin remodeling complex. *Science* **303**(5656): 343-348
- Mohrmann L, Verrijzer CP (2005) Composition and functional specificity of SWI2/SNF2 class chromatin remodeling complexes. *Biochim Biophys Acta* **1681**(2-3): 59-73

- Morrison AJ, Highland J, Krogan NJ, Arbel-Eden A, Greenblatt JF, Haber JE, Shen X (2004) INO80 and gamma-H2AX interaction links ATP-dependent chromatin remodeling to DNA damage repair. *Cell* **119**(6): 767-775
- Morrison AJ, Kim JA, Person MD, Highland J, Xiao J, Wehr TS, Hensley S, Bao Y, Shen J, Collins SR, Weissman JS, Delrow J, Krogan NJ, Haber JE, Shen X (2007) Mec1/Tel1 phosphorylation of the INO80 chromatin remodeling complex influences DNA damage checkpoint responses. *Cell* **130**(3): 499-511
- Muller J, Oma Y, Vallar L, Friederich E, Poch O, Winsor B (2005) Sequence and comparative genomic analysis of actin-related proteins. *Mol Biol Cell* **16**(12): 5736-5748
- Murawska M, Kunert N, van Vugt J, Langst G, Kremmer E, Logie C, Brehm A (2008) dCHD3, a novel ATP-dependent chromatin remodeler associated with sites of active transcription. *Mol Cell Biol* **28**(8): 2745-2757
- Narlikar GJ, Fan HY, Kingston RE (2002) Cooperation between complexes that regulate chromatin structure and transcription. *Cell* **108**(4): 475-487
- Nolen BJ, Pollard TD (2007) Insights into the influence of nucleotides on actin family proteins from seven structures of Arp2/3 complex. *Mol Cell* **26**(3): 449-457
- Oda T, Iwasa M, Aihara T, Maeda Y, Narita A (2009) The nature of the globular- to fibrous-actin transition. *Nature* **457**(7228): 441-445
- Ogiwara H, Enomoto T, Seki M (2007) The INO80 chromatin remodeling complex functions in sister chromatid cohesion. *Cell Cycle* **6**(9): 1090-1095
- Papamichos-Chronakis M, Peterson CL (2008) The Ino80 chromatin-remodeling enzyme regulates replisome function and stability. *Nat Struct Mol Biol* **15**(4): 338-345
- Papamichos-Chronakis M, Watanabe S, Rando OJ, Peterson CL (2011) Global regulation of H2A.Z localization by the INO80 chromatin-remodeling enzyme is essential for genome integrity. *Cell* **144**(2): 200-213
- Paul AS, Pollard TD (2009) Review of the mechanism of processive actin filament elongation by formins. *Cell Motil Cytoskeleton* **66**(8): 606-617
- Paulsen M, Ferguson-Smith AC (2001) DNA methylation in genomic imprinting, development, and disease. *J Pathol* **195**(1): 97-110
- Pendleton A, Pope B, Weeds A, Koffer A (2003) Latrunculin B or ATP depletion induces cofilin-dependent translocation of actin into nuclei of mast cells. *J Biol Chem* **278**(16): 14394-14400
- Pettersen EF, Goddard TD, Huang CC, Couch GS, Greenblatt DM, Meng EC, Ferrin TE (2004) UCSF Chimera--a visualization system for exploratory research and analysis. *J Comput Chem* **25**(13): 1605-1612

- Poch O, Winsor B (1997) Who's who among the *Saccharomyces cerevisiae* actin-related proteins? A classification and nomenclature proposal for a large family. *Yeast* **13**(11): 1053-1058
- Pollard TD (2007) Regulation of actin filament assembly by Arp2/3 complex and formins. *Annu Rev Biophys Biomol Struct* **36**: 451-477
- Puri T, Wendler P, Sigala B, Saibil H, Tsaneva IR (2007) Dodecameric structure and ATPase activity of the human TIP48/TIP49 complex. *J Mol Biol* **366**(1): 179-192
- Putnam CD, Hammel M, Hura GL, Tainer JA (2007) X-ray solution scattering (SAXS) combined with crystallography and computation: defining accurate macromolecular structures, conformations and assemblies in solution. *Q Rev Biophys* **40**(3): 191-285
- Racki LR, Narlikar GJ (2008) ATP-dependent chromatin remodeling enzymes: two heads are not better, just different. *Curr Opin Genet Dev* **18**(2): 137-144
- Racki LR, Yang JG, Naber N, Partensky PD, Acevedo A, Purcell TJ, Cooke R, Cheng Y, Narlikar GJ (2009) The chromatin remodeller ACF acts as a dimeric motor to space nucleosomes. *Nature* **462**(7276): 1016-1021
- Rando OJ, Zhao K, Janmey P, Crabtree GR (2002) Phosphatidylinositol-dependent actin filament binding by the SWI/SNF-like BAF chromatin remodeling complex. *Proc Natl Acad Sci U S A* **99**(5): 2824-2829
- Ray S, Grove A (2009) The yeast high mobility group protein HMO2, a subunit of the chromatin-remodeling complex INO80, binds DNA ends. *Nucleic Acids Res* **37**(19): 6389-6399
- Reisler E, Egelman EH (2007) Actin structure and function: what we still do not understand. *J Biol Chem* **282**(50): 36133-36137
- Rhodes G (2006) *Crystallography made crystal clear : a guide for users of macromolecular models*, 3rd edn. Amsterdam ; Boston: Elsevier/Academic Press.
- Rickard JE, Sheterline P (1986) Cytoplasmic concentrations of inorganic phosphate affect the critical concentration for assembly of actin in the presence of cytochalasin D or ADP. *J Mol Biol* **191**(2): 273-280
- Rould MA, Wan Q, Joel PB, Lowey S, Trybus KM (2006) Crystal structures of expressed non-polymerizable monomeric actin in the ADP and ATP states. *J Biol Chem* **281**(42): 31909-31919
- Sambrook J, Russell DW, Laboratory. CSH (2001) *Molecular cloning : a laboratory manual / Joseph Sambrook, David W. Russell*, 3rd. ed. edn. Cold Spring Harbor, N.Y. :: Cold Spring Harbor Laboratory.
- Schleicher M, Jockusch BM (2008) Actin: its cumbersome pilgrimage through cellular compartments. *Histochem Cell Biol* **129**(6): 695-704
- Schoenenberger CA, Buchmeier S, Boerries M, Sutterlin R, Aebi U, Jockusch BM (2005) Conformation-specific antibodies reveal distinct actin structures in the nucleus and the cytoplasm. *J Struct Biol* **152**(3): 157-168

- Sept D, McCammon JA (2001) Thermodynamics and kinetics of actin filament nucleation. *Biophys J* **81**(2): 667-674
- Shen X (2004) Preparation and analysis of the INO80 complex. *Methods Enzymol* **377**: 401-412
- Shen X, Mizuguchi G, Hamiche A, Wu C (2000) A chromatin remodelling complex involved in transcription and DNA processing. *Nature* **406**(6795): 541-544
- Shen X, Ranallo R, Choi E, Wu C (2003) Involvement of actin-related proteins in ATP-dependent chromatin remodeling. *Mol Cell* **12**(1): 147-155
- Shvetsov A, Musib R, Phillips M, Rubenstein PA, Reisler E (2002) Locking the hydrophobic loop 262-274 to G-actin surface by a disulfide bridge prevents filament formation. *Biochemistry* **41**(35): 10787-10793
- Smith CL, Horowitz-Scherer R, Flanagan JF, Woodcock CL, Peterson CL (2003) Structural analysis of the yeast SWI/SNF chromatin remodeling complex. *Nat Struct Biol* **10**(2): 141-145
- Stein N (2008) CHAINSAW: a program for mutating pdb files used as templates in molecular replacement. *Journal of Applied Crystallography* **41**(3): 641-643
- Sugiyama T, Cam HP, Sugiyama R, Noma K, Zofall M, Kobayashi R, Grewal SI (2007) SHREC, an effector complex for heterochromatic transcriptional silencing. *Cell* **128**(3): 491-504
- Sunada R, Gorzer I, Oma Y, Yoshida T, Suka N, Wintersberger U, Harata M (2005) The nuclear actin-related protein Act3p/Arp4p is involved in the dynamics of chromatin-modulating complexes. *Yeast* **22**(10): 753-768
- Svergun D, Barberato C, Koch MHJ (1995) CRY SOL - A program to evaluate x-ray solution scattering of biological macromolecules from atomic coordinates. *J Appl Crystallogr* **28**: 768-773
- Szerlong H, Hinata K, Viswanathan R, Erdjument-Bromage H, Tempst P, Cairns BR (2008) The HSA domain binds nuclear actin-related proteins to regulate chromatin-remodeling ATPases. *Nat Struct Mol Biol* **15**(5): 469-476
- Szerlong H, Saha A, Cairns BR (2003) The nuclear actin-related proteins Arp7 and Arp9: a dimeric module that cooperates with architectural proteins for chromatin remodeling. *EMBO J* **22**(12): 3175-3187
- Tan-Wong SM, Wijayatilake HD, Proudfoot NJ (2009) Gene loops function to maintain transcriptional memory through interaction with the nuclear pore complex. *Genes Dev* **23**(22): 2610-2624
- Thoma NH, Czyzewski BK, Alexeev AA, Mazin AV, Kowalczykowski SC, Pavletich NP (2005) Structure of the SWI2/SNF2 chromatin-remodeling domain of eukaryotic Rad54. *Nat Struct Mol Biol* **12**(4): 350-356
- Torreira E, Jha S, Lopez-Blanco JR, Arias-Palomo E, Chacon P, Canas C, Ayora S, Dutta A, Llorca O (2008) Architecture of the pontin/reptin complex, essential in the assembly of several macromolecular complexes. *Structure* **16**(10): 1511-1520

- Tsukuda T, Fleming AB, Nickoloff JA, Osley MA (2005) Chromatin remodelling at a DNA double-strand break site in *Saccharomyces cerevisiae*. *Nature* **438**(7066): 379-383
- van Attikum H, Fritsch O, Hohn B, Gasser SM (2004) Recruitment of the INO80 complex by H2A phosphorylation links ATP-dependent chromatin remodeling with DNA double-strand break repair. *Cell* **119**(6): 777-788
- van Attikum H, Gasser SM (2009) Crosstalk between histone modifications during the DNA damage response. *Trends Cell Biol* **19**(5): 207-217
- Vidanes GM, Bonilla CY, Toczyski DP (2005) Complicated tails: histone modifications and the DNA damage response. *Cell* **121**(7): 973-976
- Visegrady B, Lorinczy D, Hild G, Somogyi B, Nyitrai M (2005) A simple model for the cooperative stabilisation of actin filaments by phalloidin and jasplakinolide. *FEBS Lett* **579**(1): 6-10
- Volkov VV, Svergun DI (2003) Uniqueness of ab initio shape determination in small-angle scattering. *J Appl Crystallogr* **36**: 860-864
- Vorobiev S, Strokopytov B, Drubin DG, Frieden C, Ono S, Condeelis J, Rubenstein PA, Almo SC (2003) The structure of nonvertebrate actin: implications for the ATP hydrolytic mechanism. *Proc Natl Acad Sci U S A* **100**(10): 5760-5765
- Watanabe M, Watanabe D, Nogami S, Morishita S, Ohya Y (2009) Comprehensive and quantitative analysis of yeast deletion mutants defective in apical and isotropic bud growth. *Curr Genet* **55**(4): 365-380
- Welch MD, Drubin DG (1994) A nuclear protein with sequence similarity to proteins implicated in human acute leukemias is important for cellular morphogenesis and actin cytoskeletal function in *Saccharomyces cerevisiae*. *Mol Biol Cell* **5**(6): 617-632
- Welch WJ, Suhan JP (1985) Morphological study of the mammalian stress response: characterization of changes in cytoplasmic organelles, cytoskeleton, and nucleoli, and appearance of intranuclear actin filaments in rat fibroblasts after heat-shock treatment. *J Cell Biol* **101**(4): 1198-1211
- Witke W (2004) The role of profilin complexes in cell motility and other cellular processes. *Trends Cell Biol* **14**(8): 461-469
- Wriggers W, Chacon P (2001) Using Situs for the registration of protein structures with low-resolution bead models from X-ray solution scattering. *J Appl Crystallogr* **34**: 773-776
- Wu WH, Alami S, Luk E, Wu CH, Sen S, Mizuguchi G, Wei D, Wu C (2005) Swc2 is a widely conserved H2AZ-binding module essential for ATP-dependent histone exchange. *Nat Struct Mol Biol* **12**(12): 1064-1071
- Wu X, Yoo Y, Okuhama NN, Tucker PW, Liu G, Guan JL (2006) Regulation of RNA-polymerase-II-dependent transcription by N-WASP and its nuclear-binding partners. *Nat Cell Biol* **8**(7): 756-763

- Xu D, Bai J, Duan Q, Costa M, Dai W (2009) Covalent modifications of histones during mitosis and meiosis. *Cell Cycle* **8**(22): 3688-3694
- Yarmola EG, Somasundaram T, Boring TA, Spector I, Bubb MR (2000) Actin-latrunculin A structure and function. Differential modulation of actin-binding protein function by latrunculin A. *J Biol Chem* **275**(36): 28120-28127
- Ye J, Zhao J, Hoffmann-Rohrer U, Grummt I (2008) Nuclear myosin I acts in concert with polymeric actin to drive RNA polymerase I transcription. *Genes Dev* **22**(3): 322-330
- Yoo Y, Wu X, Guan JL (2007) A novel role of the actin-nucleating Arp2/3 complex in the regulation of RNA polymerase II-dependent transcription. *J Biol Chem* **282**(10): 7616-7623
- Yoshida T, Shimada K, Oma Y, Kalck V, Akimura K, Taddei A, Iwahashi H, Kugou K, Ohta K, Gasser SM, Harata M (2010) Actin-related protein Arp6 influences H2A.Z-dependent and -independent gene expression and links ribosomal protein genes to nuclear pores. *PLoS Genet* **6**(4): e1000910
- Yu EY, Steinberg-Neifach O, Dandjinou AT, Kang F, Morrison AJ, Shen X, Lue NF (2007) Regulation of telomere structure and functions by subunits of the INO80 chromatin remodeling complex. *Mol Cell Biol* **27**(16): 5639-5649
- Zhang H, Richardson DO, Roberts DN, Utley R, Erdjument-Bromage H, Tempst P, Cote J, Cairns BR (2004) The Yaf9 component of the SWR1 and NuA4 complexes is required for proper gene expression, histone H4 acetylation, and Htz1 replacement near telomeres. *Mol Cell Biol* **24**(21): 9424-9436
- Zhao K, Wang W, Rando OJ, Xue Y, Swiderek K, Kuo A, Crabtree GR (1998) Rapid and phosphoinositol-dependent binding of the SWI/SNF-like BAF complex to chromatin after T lymphocyte receptor signaling. *Cell* **95**(5): 625-636

7. Appendix

7.1 Expression and purification trials of INO80 complex components

Table 10: Survey of all expression and purification efforts concerning the INO80 complex

INO80 Subunit	Expression host	Soluble	Purified	Aggregation	Stable	Crystal screen	Crystals
yINO80	<i>E. coli</i> Insect cells	no	no	n.d.	n.d.	no	no
yArp4	Insect cells	yes	yes	no	yes	yes	yes
yArp5	Insect cells	yes	yes	no	no	yes	no
yArp8	Insect cells	yes	yes	no	yes	yes	yes*
yIes1	<i>E. coli</i>	no	no	n.d.	n.d.	no	no
yIes2	<i>E. coli</i>	yes	yes	yes	no	no	no
yIes3	<i>E. coli</i> Insect cells	no	no	n.d.	n.d.	no	no
yIes4	<i>E. coli</i>	yes	yes	yes	yes	no	no
yIes5	<i>E. coli</i>	yes	yes	no	yes	yes	no
yIes6	<i>E. coli</i>	yes	yes	no	no	no	no
yNhp10	<i>E. coli</i>	yes	yes	yes	yes	yes	no
yRvb1 yRvb2	<i>E. coli</i>	yes	yes	no	yes	yes	yes
yNhp10 yIes5	<i>E. coli</i>	yes	yes	no	yes	yes	no
yNhp10 yIes3 yIes5	Insect cells	yes	yes	no	yes	yes	no
hArp5 hIes6	Insect cells	yes	yes	no	yes	yes	no

* Arp8 crystals were obtained by Christian Gerhold

7.2 Abbreviations

Å	Ångström (=10 ⁻¹⁰ m)
aa	Amino acid
ACF	ATP-utilizing chromatin assembly and remodeling factor
ADP	Adenosine di-phosphate
Arp	Actin related protein
ATP	Adenosine tri-phosphate
β-ME	β-Mercapto ethanol
bp	Base pair(s)
BSA	Bovine serum albumin
ca.	Circa
CapZ	Capping protein muscle Z-line
DMSO	Dimethyl sulfoxide
DNA	Deoxyribonucleic acid
dsDNA	Double stranded DNA
DSB	Double strand break
<i>Eco / E.coli</i>	<i>Escherichia coli</i>
EDTA	Ethylenediaminetetraacetic acid
e.g.	<i>Exempli gratia</i> (for example)
EM	Electron microscopy
F-actin	Filamentous-actin
G-actin	Globular-actin
HR	Homologous recombination
HMG-1	High mobility group-1
Ies	INO80 subunit

IEX	<u>I</u> on <u>e</u> xchange chromatography
INO80	<u>I</u> nositol requiring mutant <u>80</u>
kb	<u>K</u> ilo <u>b</u> ase pair(s)
KMEI	<u>K</u> Cl, <u>M</u> gCl ₂ , <u>E</u> GTA, <u>i</u> midazole buffer
LatA	<u>L</u> atrunculin <u>A</u>
LB	<u>L</u> uria- <u>B</u> ertani
M	<u>M</u> olar
MMR	<u>M</u> ismatch <u>r</u> epair
MR	<u>M</u> olecular <u>r</u> eplacement
MS	<u>M</u> ass spectrometry
NCBI	<u>N</u> ational <u>C</u> enter for <u>B</u> io <u>t</u> echnology <u>I</u> nformation
n.d.	<u>N</u> ot <u>d</u> etermined
NER	<u>N</u> ucleotide <u>e</u> xcision <u>r</u> epair
NHEJ	<u>N</u> on- <u>h</u> omologous <u>e</u> nd- <u>j</u> oining
Nhp10	<u>N</u> on <u>h</u> istone protein <u>10</u>
NMR	<u>N</u> uclear <u>m</u> agnetic <u>r</u> esonance spectroscopy
NuA4	<u>N</u> ucleosome <u>a</u> cetyltransferase of histone H4
o/n	<u>O</u> ver <u>n</u> ight
PAGE	<u>P</u> oly <u>a</u> crylamide gel <u>e</u> lectrophoresis
PCR	<u>P</u> olymerase <u>c</u> hain <u>r</u> epair
pdb	<u>P</u> rotein <u>D</u> ata <u>B</u> ank
PEG	<u>P</u> oly <u>e</u> thylene glycol
pI	<u>I</u> soelectric point
PMSF	<u>P</u> henyl <u>m</u> ethyl <u>s</u> ulfonyl <u>f</u> luorid
RNA	<u>R</u> ibonucleic acid

RSC	<u>R</u> emodels the <u>S</u> tructure of <u>C</u> hromatin
Rvb	<u>R</u> uv <u>B</u> like
<i>S. cerevisiae</i>	<u>S</u> accharomyces <u>c</u> erevisiae
SAD	<u>S</u> ingle-wavelength <u>a</u> nomalous <u>d</u> iffraction
SDS	<u>S</u> odium <u>d</u> odecyl <u>s</u> ulfate
SMC	<u>S</u> tructural <u>m</u> aintenance of <u>c</u> hromosomes protein
SPR	<u>S</u> urface <u>p</u> lasmon <u>r</u> esonance
ssDNA	<u>S</u> ingle <u>s</u> tranded DNA
SWR1	<u>S</u> wi2/ <u>S</u> nf2 <u>r</u> elated 1
SWI/SNF	<u>S</u> witching/ <u>S</u> ucrose <u>n</u> on <u>f</u> ermenting
Taf14	<u>T</u> ranscription <u>f</u> actor 14
TB	<u>T</u> ris- <u>b</u> orate
TF	<u>T</u> ranscription <u>f</u> actor
v	<u>V</u> olume
w	<u>W</u> eight
w/o	<u>W</u> ithout
wt	<u>W</u> ild-type
YEATS	<u>Y</u> af9, <u>E</u> NL, <u>A</u> F9, <u>T</u> af14, <u>S</u> as5
YPD	<u>Y</u> east extract <u>p</u> eptone <u>d</u> extrose

8. Curriculum Vitae

Personal details

Name	Sebastian Fenn
Date of birth	June 13, 1982
Place of birth	Fürth (Bavaria), Germany
Nationality	German
Marital status	single

Education

1988 – 1992	Grundschule in Cadolzburg, Germany
07/1992 – 06/2002	Dietrich-Bonhoeffer Gymnasium Oberasbach, Germany

Academic Training

10/2002 – 01/2007	Studies of Biochemistry (Diploma) at the University of Bayreuth, Germany
04/2006 – 11/2006	Diploma thesis in the group of Prof Thomas James, University of California San Francisco, USA - “Structural investigation of human poly(c)-binding protein 2”
04/2005 – 03/2007	Scholarship from the German National Academic Foundation
since 04/2007	PhD thesis in the group of Prof. Dr. Karl-Peter Hopfner, Gene Center, Department of Biochemistry, University of Munich, Germany
12/2007 – 04/2010	PhD fellowship of the Boehringer Ingelheim Fonds

9. Acknowledgements

I would like to thank everybody who has contributed to the successful completion of this work.

First and foremost I am indebted to my supervisor Prof. Karl-Peter Hopfner for giving me the opportunity to work on this challenging project and for providing an extremely positive and supportive environment and the freedom that allowed me to grow as a person and as a scientist.

The whole Hopfner group and all its current and former members deserve particular gratitude for the friendly and most enjoyable working atmosphere in the lab. Special thanks to my fellow INO80 companions Brigitte Keßler, Christian Gerhold, Kristina Lakomek, Alessandro Tosi and Gregor Witte for all the help and advice and for sharing the highs and many lows of research. Furthermore I would like to thank my bachelor student Andreas Lange and all other members of the Hopfner lab who have supported me with guidance, expertise or hands on help.

Dennis Breitsprecher and Jan Faix from Hannover Medical School provided an invaluable collaboration that helped to expand several interesting aspects of this work, thank you very much for that.

I am grateful to the Boehringer Ingelheim Fonds for the financial and personal support, the nice atmosphere during the workshops and the opportunity to meet lots of interesting people.

Nadja, you helped me in more ways than I can mention and I can't express how happy I am to share my life with you. I am looking forward to see our little family grow in the future.

Zuletzt möchte mich von ganzem Herzen bei meinen Eltern und meiner Familie bedanken, die mich stets unterstützt und ermutigt haben.

My apologies to all other whom I have not mentioned by name – my gratitude is with you as well.